BIOENGINEERED IMMUNE ORGANOIDS FOR CONTROLLING B CELL DEVELOPMENT

A Dissertation

Presented to the Faculty of the Graduate School

of Cornell University

In Partial Fulfillment of the Requirements for the Degree of

Doctor of Philosophy

by

Alberto Purwada

August 2017

BIOENGINEERED IMMUNE ORGANOIDS FOR CONTROLLING B CELL DEVELOPMENT

Alberto Purwada

Cornell University 2017

The humoral arm of the adaptive immune system works by producing antigen-specific antibody to clear pathogens from the extracellular spaces in the body. The humoral immunity requires the germinal center (GC) reaction to enable the formation of antibody-secreting cells and the production of antibodies that can bind the target antigen and trigger the appropriate immune responses. GC is a microanatomical structure in the B cell follicle that transiently arises from lymphocyte proliferation over the course of humoral immune response. While *in vivo* models have provided us with new insights regarding the GC reaction, there is a lack of *ex vivo* systems that can be utilized to model the GC process. Existing techniques do not fully recapitulate the lymphoid niche or require implantation into live animal models. It is thus challenging to assess the specific signals that control GC reaction, analyze the heterogeneous GC B cell population, and understand the decision-making process that determines GC B cell fate.

In order to address these limitations, we have developed immune organoids to recapitulate key GC characteristics and control B cell activation in culture. We first analyzed the techniques that have been used to engineer B cell phenotype (Chapter 1). Inspired by the role of integrin in cell microenvironment, we utilized the gelatin matrix to enhance GC-like B cell expansion in culture (Chapter 2). We next showed that *ex vivo* GC-like B cells were comparable to *in vivo* GC B cells and could be used to study the GC cell cycle regulation (Chapter 3). We then used the modular immune organoid to assess the role of integrin ligand specificity in modulating GC-like B cell phenotype (Chapter 4). Finally, we demonstrated that B Cell Receptor (BCR) stimulation could induce ASC differentiation and facilitate the enrichment of antigen-specific GC-like B cells in the presence of a negative selection pressure (Chapter 5).

Having described the works done to develop an improved B cell culture system, we concluded this dissertation with a reflection on the research journey and some suggestions regarding the next key steps to continue this project (Chapter 6). In the long term, we believe that the immune organoid platform could be used to obtain mechanistic insights about the adaptive immune system generation, understand the decision-making process in GC reaction, model lymphoid transformations that trigger certain diseases, and identify therapeutic agents that can interact with the immune system.

BIOGRAPHICAL SKETCH

Alberto Purwada was born in Jakarta, Indonesia. After graduating high school, he entered Boston University in 2009. He started his research experience by working on tissue engineering, stem cells, and microfluidics. During his undergraduate years, he was granted the Kenneth R. Lutchen Distinguished Fellowship to work on research projects that can utilize engineering skills and scientific knowledge to positively impact society. Alberto graduated *summa cum laude* with a Bachelor of Science in Biomedical Engineering in 2013 and then started his doctoral study in Biomedical Engineering at Cornell University in the same year. Under the mentorship of Prof. Ankur Singh, Alberto pursued his research in studying the role of immune cell microenvironment in controlling B cell activation and differentiation. During his graduate education, he was awarded the Howard Hughes Medical Institute Med-into-Grad Fellowship to work on research projects that can benefit from clinical mentorship and potentially impact clinical practice. He has completed the required academic coursework to major in Biomedical Engineering and minor in both Biochemical Engineering and Molecular Biology.

No man is an island, entire of itself. Every man is a piece of the continent, a part of the main. Over the past few years, I have realized that each scientific discovery is only possible with the help of others. While running experiments may seem like a solitary experience, every piece of data is made possible with guidance from the advisor, help from committee members, collaboration with research colleagues, perseverance from self, encouragement from family members, and support from friends.

I want to thank them for their tremendous support throughout this journey.

ACKNOWLEDGMENTS

This work was performed at Cornell University and supported by a dissertation committee consisting of Prof. Ankur Singh (graduate advisor, Mechanical and Aerospace Engineering), Prof. David Putnam (Biomedical Engineering), Prof. Avery August (Microbiology and Immunology), and Prof. Robert Weiss (Biological and Biomedical Sciences). Many thanks to them for taking the time to attend my exams, review my presentations, ask insightful questions, and discuss the important elements of this project.

I would like to especially thank my advisor Prof. Ankur Singh for his guidance and support in making the work described here possible. Being the first Ph.D. student in his lab, I was able to benefit from having as many discussions as needed and being able to develop new projects together. I am grateful to have participated in every aspect of this project including idea development, experiment design, data analysis, and manuscript preparation. These experiences have enabled me to better appreciate scientific discoveries. I cannot imagine spending these past years with another mentor or academic environment.

I would like to thank my research colleagues for making the Singh Lab a great place to work over the last few years. I truly appreciated having them to create a positive atmosphere, discuss research projects, and have a great time. I would also like to thank my family and friends for the constant love and support. I cannot thank them enough for what they have done throughout my time completing this research.

This project has been financially supported by numerous funding agencies: the National Science Foundation CAREER Award DMR-1554275, the National Institutes of Health 1R21CA185236-01, the Cornell University and Weill Cornell Medical College Seed Grant Program, and the Howard Hughes Medical Institute Med-into-Grad Fellowship (HHMI 56006761). Unless otherwise noted, all procedures (experiment setup, data collection, and analysis) were done by Alberto Purwada. Detailed acknowledgement and author contributions were provided at the end of each chapter.

TABLE OF CONTENTS

LIST OF FIGURES

LIST OF ABBREVIATIONS

Abbreviations	Descriptions
GC	Germinal center
PEG	Polyethylene glycol
PEG-MAL	Polyethylene glycol with maleimide functionalization
BCR	B cell receptor
CPM	Counts per million
MFI	Median fluorescence intensity
SRBC	Sheep red blood cells
CD40L	CD40 ligand
DTT	Dithiothreitol (non-degradable crosslinker)
VPM	GCRDVPMSMRGGDRCG peptide (degradable crosslinker)
RGD	GRGDSPC peptide
REDV	GREDVGC peptide
HEPES	4-(2-hydroxyethyl)-1-piperazineethanesulfonic acid
Ab	Antibody
Ag	Antigen
OVA	Ovalbumin (carrier protein)
NP	4-hydroxy-3-nitrophenylacetyl (hapten)
Ig	Immunoglobulin
FDC	Follicular dendritic cells
Tfh cells	Follicular T helper cells
ECM	Extracellular matrix
MHC	Major histocompatibility complex
SiNP	Silicate nanoparticles
IHC	Immunohistochemistry
IF	Immunofluorescence
GCB	Germinal center B cells
NB	Naïve B cells
KO	Knockout
PBS	Phosphate-buffered saline
ASC	Antibody-secreting cells (e.g. plasmablasts and plasma cells)
FACS	Fluorescence-activated cell sorting
P/S	Penicillin/Streptomycin
FBS	Fetal bovine serum
DMEM	Dulbecco's Modified Eagle Medium
RPMI	Roswell Park Memorial Institute Medium
BCL6	B cell lymphoma 6
EZH2	Enhancer of zeste homolog 2
IRF4	Interferon regulatory factor 4
BLIMP1	B lymphocyte induced maturation protein 1

CHAPTER 1

Introduction to Humoral Immunity and B Cell Engineering Approaches

1.1. Abstract

Germinal center (GC) reaction occurs during the humoral immune response generation to ensure the secretion of antibodies capable of binding target antigens with specificity, affinity, and capability to elicit the appropriate immune responses. While numerous insights regarding GC reaction have been gained using animal models, there are several challenges associated with *in vivo* systems. Here we review various techniques that have been demonstrated to control B cell phenotype in cell culture system, analyze the motivations behind each approach, describe the techniques, and discuss several considerations for their implementation in B cell research. These methods include soluble factors, stromal cells, synthetic platforms, and biomaterials integration. By classifying these techniques based on the length scale of their interaction with B cells, this chapter aims to summarize the key elements of *ex vivo* B cell studies, gain inspiration from relevant fields, and propose research directions. By accomplishing these goals, we hope that this chapter can introduce the relevance of rationally designed B cell culture platform with tunable signal presentation to assist with immunology research and therapeutics development.

1.2. Introduction

The adaptive immune system enables the body to respond against specific invading pathogens. This function is exerted by both cellular and humoral arms of the immune system. As opposed to the cellular immunity that targets infected or mutated cells, humoral immunity specifically protects the extracellular spaces via the secretion of immunoglobulin molecules (also referred to as antibodies) by B cells that can bind the surface molecules of a foreign substance with high specificity and affinity. Such binding is also

capable of generating the appropriate immune responses: neutralization, opsonization, or complement activation. In order to work properly, an antibody requires the following three key traits: specificity, affinity, and functionality.

It is important to understand how the aforementioned three critical traits are gained by B cells during their development process. Specificity results from several mechanisms. Early during B cell development, V(D)J recombination occurs to facilitate the rearrangement of numerous gene segments and this process allows the generation of various immunoglobulin genes. Later during the humoral immune response, somatic hypermutation occurs in the form of single point mutations (along with insertions and deletions) to further modify the rearranged immunoglobulin genes. Upon translation, these diverse immunoglobulin genes can give rise to a broad range of immunoglobulin molecules capable of binding many molecular targets. Affinity results from the repeated rounds of Darwinian-like selection that picks high-affinity B cell clones. Functionality comes from class switch recombination (CSR) that controls the antibody effector function. Studies performed over the past decades have demonstrated that the germinal center (GC) reaction is responsible for inducing somatic hypermutation, selection, and CSR. This indicates the importance of GC in ensuring the generation of an effective humoral immunity.

First reported back in 1884, GC is frequently defined as a microanatomical structure containing proliferating lymphocytes in the lymph node B cell follicles, appearing transiently following immunization, and consisting of two cellular compartments that can be distinguished with imaging techniques [1-3]. While the GC reaction is very complex, the prevailing view suggests that GC reaction is formed after naïve B cells encountering their corresponding exogenous antigens in the follicle, interacting with follicular T helper (Tfh) cells in the interfollicular region, start proliferating in the follicle, experiencing somatic hypermutation to rearrange immunoglobulin variable region genes, and then undergoing affinity-based selection via interaction with follicular dendritic cell (FDC) and Tfh cells [2-4]. The GC reaction dynamics can also be understood from the visual schematic provided to accompany this

chapter (Figure 1-1). The schematic can be used not only to see GC progression over time, but also the decision making made by GC B cells following the selection process. While there are general agreements regarding its constituent components and functional outcomes, numerous models have been proposed to describe the GC reaction dynamics [1, 3]. New insights have been generated regarding the migration across GC zones, the role of Tfh cells in selecting high-affinity B cell clones, and the factors that sustain GC reaction over time [3]. This situation indicates that GC has been known to play an important role in mounting an antigen-specific humoral immune response and yet GC reaction still appears as a black box with researchers learning new things about it all the time.

The aforementioned insights pertaining to GC reaction in humoral immunity and the broader immune system have been generated mostly from *in vivo* systems with few validations using *in vitro* models, which makes sense considering the complexity of a single immune reaction that involves numerous cell types and signaling molecules over varying time and length scales. While the animal models have facilitated such fundamental discoveries, *in vivo* systems are faced with several inherent challenges: high cost, long turnaround time, and low experimental throughput. The inherent complexity of an animal model can also make it difficult to identify the critical building blocks necessary to recapitulate an immune reaction outside of animal models or even modulate it by changing the relevant design parameters. In contrast, there is no reliable *in vitro* systems that can capture such complexity because existing techniques have typically relied on co-culturing B cells with stromal cells on a tissue culture plate in the presence of certain soluble growth factors added exogenously at certain time points during the cell culture period. This situation has suggested the necessity of an artificial culture system that replicates the simplicity of *in vitro* approaches and reproduces the key attributes of *in vivo* models.

We hypothesized that such goal can be achieved with a rationally designed tool to model the B cell development process. But we have to first understand the critical design parameters for reproducing humoral immune response in the test tubes. These elements can be identified from animal studies and

further demonstrated using *in vitro* approaches. We then have to figure out the bioengineering techniques that can modulate cell phenotype and pick the ones that can be adapted in studying B cells. Considering the recent proliferation of new insights regarding GC reaction, the aforementioned techniques can be used to further understand the factors that control GC kinetics during its initiation, maintenance, and termination phases. The first step toward achieving this goal is to assess what techniques have been shown to reasonably control B cell activation.

This introduction chapter is written to answer such question by first describing what factors have been identified as important for B cell activation process from *in vivo* studies, then showcasing how such findings have inspired approaches to generate specific B cell phenotypes *in vitro*, and finally proposing what considerations are needed to further B cell engineering effort in the future. Due to the complexity of B cell development, this chapter plans on analyzing the relevant factors based on the length scale of each interaction. This classification will help us determine the appropriate bioengineering techniques based on the length scale because the physical dimension is one of the main levers in designing bioengineered systems. As various studies have suggested that the average murine B cell diameter is approximately 4-6 micron with a possible increase in the range of 7-10 micron following activation, such number will be used a baseline for the length scale (medium) and summarize published findings using this conceptual framework. This chapter will also draw inspirations from other immune engineering techniques and biomaterials-based approaches to provide future perspectives on B cell engineering.

1.3. Small-scale Approach to B Cell Engineering

The small-scale approach is defined by the use of synthetic or biological molecules with a diameter smaller than 5 nm, thus making these particles smaller than B cells. This method typically works by interaction with a specific marker on the cell surface and/or triggering a particular intracellular process

within the cell itself. Considering the length scale of said interaction, this technique generally consists of adding the soluble factors exogenously into the cell culture system.

1.3.1. Antigen Physical Modification

B cell activation is initiated following an engagement between a specific antigen and its corresponding B Cell Receptor (BCR) to stimulate subsequent B cell proliferation and differentiation [5]. While the protocol appears to be straightforward and similar across publications, the results can vary because antigenic stimulation depends on the antigen characteristics that include size, molecular weight, and form upon entering lymphoid organs (i.e. individual particles or immune complexes) [5]. With this perspective on the relationship between antigen and immune response, several research studies have been focused on engineering the physical characteristics of an antigen to modulate the resulting immune response.

Modifying the physical characteristics of an antigen can be done in several ways. Paus et al. modulated the strength of BCR-antigen binding by using sheep red blood cells (SRBCs) conjugates of a series of recombinant hen egg lysozyme (HEL) proteins that bind the corresponding BCR with varying affinities [6]. The resulting data suggested that lower antigen affinity resulted in normal GC reaction but impaired extrafollicular plasma cell response, although the latter could be improved by increasing epitope density and vice versa. Peptide ligands with varying affinity have also been prepared via phage display and the resulting data suggested that BCR affinity could modulate several BCR activation metrics [7]. Similar studies on epitope density have been done as exemplified by the use of virus-like particles with a varying surface amount of peptide D2 to increase antigen-specific IgG antibody production and the utilization of a fusion protein bearing varying amount of M2e epitopes to induce the generation of antibodies with greater antigen binding strength [8, 9]. The antigen can also be combined with particles to modulate the subsequent immune response. Based on the idea that BCR crosslinking is facilitated by structurally repetitive antigens (i.e. the multivalent display of an antigen can enhance humoral response), Moon et al.

designed a unique class of lipid-based nanoparticles with recombinant *Plasmodium vivax* circumsporozoite VMP001 antigens presented on the surface and also encapsulated inside it and this platform enhanced GC B cell number and frequency [10].

This antigen modification approach can be done to systematically investigate how the nature of an antigen influences the corresponding humoral immune response. Nevertheless, there are several challenges here: the need for animal models for investigating the immune reaction against a particular antigen, the requirement of genetic engineering to modify antigen affinity, and the lack of comprehensive understanding of the role of varying materials (and their specific modifications) toward the B cell activation and differentiation events.

1.3.2. Viral Genes Delivery

Epstein-Barr virus (EBV) has the unique capability of immortalizing B cells. In this process, EBV infection results in the constitutive expression of several viral genes (EBNAs and LMPs) and such gene expression pattern, in turn, hijacks the cellular pathways for physiological B cell activation process [11].

There are several ways to achieve B cell immortalization with EBV viral genes. The standard protocol generally consists of co-incubating mononuclear cells with virus suspension in culture for 3-5 weeks until transformed cells can be observed under phase-contrast microscopy [12]. The introduction of specific viral genes can also be achieved with the development of a plasmid carrying several EBV genes in E. coli and the introduction of this recombinant vector into primary B cells for immortalization [13]. This approach enables the use of defined parts of EBV genome and the potential co-delivery of additional genes to further modify the immortalized B cells. Despite the relatively simple process, the use of EBV to generate constitutively activated B cells can have several challenges: the possibility of viral particles being released [14], the generation of B cells with abnormal phenotypes such as lacking surface

immunoglobulin or inactivated immunoglobulin genes [15], and the adoption of tumor-like cell phenotype [11].

1.3.3. Soluble Factors

Although soluble factors are generally used to supplement other stimulatory techniques and activation with soluble ligands have been found to be quite inefficient, it is important to recognize the ability of soluble biomolecules in controlling the B cell activation and/or differentiation process *in vitro*. Following engagement with the CD40 ligand, isotype switching has been known to be inducible with cytokine presence and controllable based on cytokine type [16, 17]. BAFF has been shown to preferentially promote the survival of murine B cells from the spleen, but not those from the peripheral blood or lymph node [18]. The use of immunoglobulin (Ig) antibody capable of crosslinking with BCR to mimic antigen-specific interaction has also been exogenously added to activate B cells in culture, although some researchers have reported the importance of immobilizing IgM on a surface as soluble Ig antibody has less potency than its immobilized counterpart [19-21] While CD40 receptor on B cell surface can be targeted for activation, published works have described the importance of CD40 ligand (CD40L) to be membrane-bound and/or presented in trimeric format as further explained in the section on stromal cells below. Complicating things further, a particular stimulatory signal can also be stimulating apoptosis or promoting survival depending on multiple factors (i.e. signal strength) [22]. While the addition of soluble factors is the simplest way of modulating B cell phenotype *ex vivo*, it is still challenging to determine the right signal presentation format and understand the unclear results seen in the literature.

1.4. Medium-scale Approach to B Cell Engineering

This approach is defined as the engineering of B cells at the cellular level via tools that are within the ballpark of B cell diameter, which is assumed to be around 5 nm, and engagement with multiple cellular

markers on the cell surface. Ensuring signal presentation at the cellular level can present more technical challenges when compared to the simple addition of soluble factors because B cells have to receive multiple signals targeted toward several receptors and/or sustained interactions at a short distance. Researchers can achieve this with the use of stromal cells, artificial cells, or patterned scaffold with single cell patterning.

1.4.1. Immune Cells

Several reviews have discussed the importance of CD4+ Tfh cells in initiating the differentiation of activated B cells into GC B cells, controlling the resulting GC reaction, and providing survival signals [1, 23]. These findings have arisen from the critical need for several key signals found in Tfh cells and the negative effects seen in GC reaction when those signals are absent. Further studies have suggested additional roles that include selecting high-affinity B cells via transient contacts and thus promoting the expansion of B cells expressing high levels of peptide bound to MHC Class II [24, 25].

While most studies have utilized animal models to showcase the role of Tfh cells during GC reaction, some *in vitro* experiments have been performed to understand the specific signals that are important in said process. Lahvis et al. demonstrated that activated CD4+ T cells could improve the upregulation of PNA marker on the surface of B cells in culture via CD40-CD40L interaction and increase the expression of other activation markers, but the latter could only be achieved with either activated CD8+ T cells or cytokine combinations alone [26]. Huang et al. suggested that the cell-cell contact between activated CD4+ human T cells and naïve human B cells could enhance the percentage of somatic mutations in both IgM and IgG transcripts but such outcome could not be achieved with the soluble trimeric CD40L addition [27]. Zan et al. further showed that BCR crosslinking and cell-cell contact with activated CD4+ T Cells, which was based on CD40L and CD28 presentation, were required for *in vitro* somatic hypermutation induction [28]. Despite the important roles of Tfh cells in B cell culture, there are several

challenges faced by this approach: the need to obtain differentiated Tfh cells, the requirement to have multiple cells types in the same culture, and the lack of comprehensive understanding about the precise signal presentation to GC B cells. Additional signals have been found to maintain the adhesive interaction between T and B cells [29]. Nevertheless, more studies are needed to better understand Tfh differentiation protocol and characterize the resulting cells from phenotypic and functional perspectives [30-32].

From current reviews on GC reaction, FDC network has been shown to permeate throughout the GC light zone (LZ) compartment, retain intact antigen in the form of immune complexes for an extended period, generate various biological signals, and facilitate the GC selection process based on antigen affinity [1, 33]. Kosco et al. showed that co-culturing FDCs with B cells and T cells resulted in the formation of large cellular aggregates and increased B cell proliferation [34]. Several studies suggested that FDCs containing immune complexes could mediate *in vitro* somatic hypermutation process [35, 36]. The molecular basis of such adhesion between B cells and FDCs has been shown to require ICAM-1 and VCAM-1 on FDCs and LFA-1 and VLA-4 on B cells [37-39]. But it can be challenging to include the FDC component because of the small number of FDC in the lymphoid tissues, the sensitivity of FDC population to stresses *in vitro*, and the technical complexities of protocols currently available in the literature [40, 41].

1.4.2. Stromal Cells

Signals critical for B cell development process are mostly physically presented or secreted with precise spatiotemporal considerations. This concept can be illustrated by the CD40L signal, which is presented by Tfh cells and has been identified as a critical driver for GC induction because GC will fail to form if the CD40L-CD40 interaction is blocked [42, 43]. While the use of relevant immune cells can facilitate the introduction of relevant biological signals, such approach can be troublesome because primary immune cells have to be harvested prior to each experiment, these cells can be prone to apoptosis in the absence of

stimulatory signals, activation protocol may have to be carried out for certain ligands to be expressed, and signal presentation can be unstable/variable across batches.

Going with the same example, a simple addition of soluble recombinant CD40L does not yield the same reaction efficiency because CD40L is biologically active in its trimeric form [44, 45]. CD40L, along with few other B cell stimulatory signals, has also been shown to require membrane-bound (instead of soluble) presentation to be effective in its functionality. With this concept in mind, several culture methods to activate and/or differentiate B cells have been developed with the use of CD40L-presenting stromal cells. Pound et al. utilized CD32-transfected L cells, which were in turn conjugated with CD40 monoclonal antibody due to the binding capability between CD32 and the Fc region of IgG antibodies, to stimulate DNA synthesis in cultured human GC B cells [46]. Arpin et al. implemented a combination of CD40L-transfected L cells and several cytokines to induce the differentiation of human GC B cells into cells resembling either plasma cells or memory B cells [47]. Nojima et al. engineered fibroblasts to present CD40L and secrete BAFF for improving B cell proliferation, isotype switch, and induction of GC phenotype [48]. The resulting stromal cell line is called 40LB and it has been shown to mediate selective expansion of antigen-specific B cells by presenting antigen and Fas ligand, as CD40L-activated GC-like B cells are prone to Fas-dependent cell death unless the BCR is ligated [49]. While stromal cells enable the easy introduction of critical signals from relevant immune cells, there are several potential issues: the need to genetically engineer the stromal cells and the potential cross-reaction with other signals.

1.4.3. Synthetic System

As researchers have identified important signals in the interaction between B cells and their neighboring cells, several synthetic systems have been developed in order to study B cell in a more controlled environment with the combination of substrates or patterns and conjugated biomolecules. The culture

condition can be designed to recreate physiological conditions based on the known building blocks and/or systematically investigate the role of various design parameters.

The use of patterning to ensure the placement of B cells at specific spots within an array has been demonstrated in several studies. As B cells are non-adherent or weakly adherent, B cell patterning requires the combination of microscale pattern of interest and surface-conjugated antibody targeted against a particular marker on B cell surface. This can be contrasted with the patterning of adherent cells that typically require only physical wells with treated surface or protein spots containing bioadhesive ligands. These two methods are not mutually exclusive, however, since the use of physical microwells can strengthen the anchoring of B cells to scaffold surface and prevent disturbance from various mechanical agitations (e.g. mixing, washing, etc.). While this approach is typically done to showcase the feasibility of anchoring non-adherent cells on a 2D surface and identifying a rare cell population, the resulting platform can be used in certain applications that have been demonstrated in other cell types. Some examples include identification of therapeutic molecules, analysis of single-cell behaviors, and investigate the spatial presentation of biologically relevant signals.

Patterning can be applied in various ways that include microarray chip containing microscale cell chambers [50, 51], patterned polymer spots [52, 53], or a combination of both [54]. Kim et al. demonstrated that spatial B cell configurations could be achieved by combining patterned biotinylated spots with streptavidin and biotin-functionalized anti-CD44 antibody [52]. This paper interestingly noted the importance of maintaining antibody orientation to improve array fill rate (as compared to the surface-adsorbed antibody with random orientations). Vasconcellos et al. showed that patterned substrates could bind B cells via CD44-mediated interaction (with hyaluronic acid as the top layer) or electrostatic interaction (with chitosan as the top layer), although the former appeared stronger as demonstrated by the high number of cells from chitosan group released with the introduction of soluble HA and the high resistance in the HA group against flow-induced detachment [55]. Another work from Kim and

colleagues also demonstrated the possibility of combining lymphocytes and patterned scaffold to prepare an array of cells for biosensing [51]. In the aforementioned paper, the detection of a certain peptide was conducted by having B cells to capture the peptide and present it via the peptide-MHC complex to the neighboring T cells. There are three interesting approaches performed in this work, namely: the combination of physical microwells and anti-CD44 antibody to pattern and anchor lymphocytes, the use of calcium-binding fluorochrome to visualize the binding between TCR on T cells and the peptide-MHC complex, and the ability to demonstrate dose-dependent response toward the added peptide analyte. While interesting, patterning has mostly been done for single-cell analysis and has yet to be used to study the mechanistic role of signal density.

Another application of patterning is to investigate the antigen extraction process by B cells. Antigen extraction occurs following the encounter between B cells and APCs at some point before or during the GC reaction, where B cells process the antigen to be presented as peptide-MHC complex to CD40L-presenting Tfh cells. Since this synapse formation is a transient event, it can be challenging to understand the molecular building blocks that regulate the said interaction. Researchers have studied the interaction between BCR and antigen leading to the internalization process with a synthetic platform, specifically by incubating B cells with antigen presented on a planar surface [56-59]. The resulting findings have indicated that, among other things, cellular antigen extraction machinery depends on B cell activation state and antigen extraction is controlled by several physical properties (e.g. membrane flexibility, antigen affinity, and antigen tethering strength). In addition to antigen extraction, antigen-induced B cell activation has also been shown to depend on the stiffness of antigen-presenting substrate as indicated by the greater expression of BCR and the phosphorylated form of BCR target proteins - pSyk, and pTyr [60]. These studies have demonstrated the role of physical environment in modulating B cell phenotypes.

Single cell patterning is a fascinating technique because of the defined signal presentation targeted toward single B cells, the separation between individual B cells to decouple same cell interactions, and the high

throughput experimentation capability. Nevertheless, there are several technical challenges facing this method that include ensuring that relevant signals are presented, generating consistently uniform patterns across experiments, reducing the number of individual spots occupied by either zero or more than one cells, and avoiding mechanical disturbance that can easily alter the patterned cell population.

1.5. Large-scale Approach to B Cell Engineering

This approach is defined as the engineering of B cells with tools targeted at the level of B cell population, generally by encapsulating numerous B cells inside a matrix and culturing them in 3D. Such method can be contrasted with culturing B cells on a planar scaffold in the presence of other signals, which is covered in the previous section on medium-scale approach, since each spot or well is designed to target individual B cells. While large-scale B cell engineering is interesting, such technique is still challenging to implement due to the lack of scaffold characterization data. We have yet to understand how scaffold type, mechanics, and matrix proteins can influence B cell phenotype, activation, and differentiation.

1.5.1. Antibody Production

A published work from Suematsu and Watanabe showcased the formation of lymphoid organoid following the implantation of a sponge-like collagenous scaffold containing chemokine-producing lymphoid stromal cells and activated DCs into mice [61]. Looking at the organoids formed in the transplanted construct, the researchers demonstrated the formation of B cell zones - with proliferating cells and differentiated plasma cells - and T cell zones and the vascularization of this scaffold. It is interesting to note following transplantation and immunization in normal mice, the scaffold could be re-transplanted in Severe combined immunodeficiency (SCID) mice and provide them with antigen-specific antibody production after immunization. The collagen sponge was found to have a 1 mm thickness, heterogeneous pore shape, and pore size ranging from 50 to 300 μm. Another work done by the same

group showcased that the lymphoid organoid in SCID mice could generate antibody response 4 weeks after transplantation, antibody-secreting cells migrated from the scaffold to the spleen of SCID mice to facilitate high IgG1 antibody production, and GC-like CD38+ B cells increase in frequency following the second round of immunization [62].

1.5.2. Analyte Detection

The use of a similar collagen-based matrix was shown by Banerjee et al. to facilitate the construction of biosensor for detecting the presence of pathogenic bacteria and/or bacterial toxin [63]. Collagen type 1 gel was used to encapsulate B cells for the purpose of entrapping non-adherent cells and capturing cells of different size because collagen pore size is tunable. After preparing the construct to have a thickness in the range of 30 to 50 μm when dispensed in 48- or 96-well plate, the researchers demonstrated that reduction in B cell viability could be detected as a function of bacteria/toxin presence, amount, and incubation time. While the detection described in this work was non-specific, Rider et al. have demonstrated that bacterial-specific detection capability could be imparted on B cells by genetically engineering them to express BCR specific for a particular pathogen and emit light following BCR binding with high speed, specificity, and sensitivity [64].

1.5.3. Cell Expansion

In order to mimic the tissue niche, biomaterials have been investigated in other immune-related bioengineering studies. While these reports were not exclusively focused on B cells, they could elucidate our understanding regarding the role of microenvironment and B cell functions in the body. In one example, *in vitro* bone marrow was fabricated with inverted colloidal crystal geometry for expanding CD34+ hematopoietic stem cells (HSCs) with B cell differentiation [65]. This approach was fascinating because of the nanocomposite surface made from negatively charged silicate nanoparticles and positively

charged PDDA to facilitate cell adhesion, the high percentage of cells expressing B cell surface markers (e.g. CD40 and immunoglobulin molecules) when compared to the control plate, and the high amount of IgM secreted by B cell-like population in response to bacterial LPS exposure – also when compared to the control plate. In another study, scaffold-based CD34+ HSC expansion was successfully done with fibronectin-immobilized 3D polyethylene terephthalate (PET) matrix although no difference in CD19+ was seen among matrix protein type or when compared to the control plate [66].

1.5.4. Cell Culture Condition

Changing cell culture condition represents B cell engineering at the macro level because such technique influences the way cells interact with their environment, specifically from the perspective of nutrient and gas exchanges. This concept was illustrated by Abbott et al. in activating B cells via anti-CD40 and anti-IgM in hypoxic (1% O_2) condition [67]. Inspired by the observation that hypoxic areas were observed in splenic GCs, the hypoxic condition was found to result in greater GL7 surface marker expression, accelerated class switch kinetics from IgM to IgG1 at early time points, and increased amount of differentiation into the CD138+ ASC phenotype. While limited studies have been done to investigate the role of hypoxia in B cells, published works have also suggested that oxygen availability could control CXCR4 expression in B cells and other cell types [68, 69].

1.6. Inspirations from Other Immune Engineering Techniques

While this chapter attempts to cover important topics pertaining to B cell engineering approaches, additional conceptual and technical insights can be obtained from related research areas. We will look into published studies on early B cell development, T cell engineering, and relevant biomedical engineering innovations.

1.6.1. B Cell Generation from Stem Cells

As B cells are generated from hematopoietic stem cells (HSCs) in the bone marrow, there are numerous protocols that have been developed to recapitulate this process in the laboratory. The approaches typically require the co-culture of stem cells with OP9 stromal cells in the presence of soluble recombinant factors that generally include FLT3 ligand (FLT3L) and other cytokines [70-75]. Following a combinatorial presentation of biomolecules, validation of the resulting B cells is carried out by looking at the cell phenotype and the response following stimulation with LPS. Interestingly, several protocols have also looked at the role of ligand density in controlling B cell development process. The Notch ligand Delta1 (DL1) was shown to facilitate differentiation into the B cell lineage only at lower density and the resulting cell population can form CD19+ early B cell precursor after exposure to classical B cell differentiation protocol, while the higher density of said ligand inhibits this B cell lineage induction process [76]. The examples listed above show the importance of presenting biological signals via stromal cells and soluble factors, while ligand density can drastically control the resulting cellular response.

1.6.2. T Cell Generation and Activation

While this chapter has been focused mainly on B cell engineering techniques, the study of immune cell microenvironment and the implementation of biomaterials-based engineering techniques are more commonly seen in the context of T cell generation (from stem cells) and activation process. We will look into T cell works for conceptual insights and technical ideas.

The use of DL1-presenting stromal cells to generate early T cell population *in vitro* has been reported in several publications [77-80]. The use of DL1-presenting OP9 stromal cells became widespread because of its simplicity in comparison to the traditional T cell generation protocols like fetal thymic organ cultures (FTOCs) or reaggregate thymic organ cultures (RTOCs). These approaches require the culture of

hematopoietic progenitor cells and thymic stromal cells as 3D cellular constructs because thymic stromal cells fail to maintain DL-1 expression in 2D monolayer format and therefore lose the ability to induce T cell differentiation in such setting [81]. Such finding suggested the importance of 3D architecture in facilitating T cell differentiation within the thymic microenvironment.

Realization regarding the role of cell microenvironment resulted in the gradual use of biomaterials-based approaches in T cell generation protocols. While DL1-presenting stromal cells represent a robust way of forming T cells, it can be difficult to understand the role of ligand density and engineered ligand represents a possible approach to study this issue. The use of immobilized ligand was first demonstrated by Dallas et al. in two ways. First of all, DL-1 ligand density level determines whether murine Lin- Sca+ Kit- (LSK) cells decides to enter the T cell differentiation pathway exclusively for forming Thy1+ CD25+ early T cell precursors [76]. Secondly, culturing murine LSK cells with increasing density of immobilized DL1 showcased that the group with the highest density produced the highest number of CD44+ CD25+ DN2 early T cell progenitor population [82]. It is also importing to note that DL1 is immobilized because such presentation provides greater potency than the soluble one as reported by Varnum-Finney et al., further suggesting that ligand stabilization can determine its function [83]. These approaches suggest the importance of engineered signal and presentation style in controlling T cell differentiation events.

Since 3D cell microenvironment is one focus area of biomaterials research and has been demonstrated to be important in the thymic microenvironment, 3D matrix utilization in T cell research has also been demonstrated in several publications. The focus on 3D format was also demonstrated by Marshall et al. with the use of a highly porous tantalum-based 3D matrix to generate CD4+ and CD8+ T cells from matrix-encapsulated thymus fragments encapsulated. This tantalum-based system was previously studied by Poznansky et al. in the form of matrix seeded with murine thymic stroma for the generation of mature functional CD3+ T cells from bone marrow (BM)-derived hematopoietic progenitor cells [84]. Combining 3D scaffold and stromal-free system, Lee et al. developed a 3D inverted colloidal crystal

scaffolds coated with immobilized engineered DL1 notch ligand for culturing CD34 hematopoietic stromal cells [85]. The data suggested that the resulting cell population maintained HSC marker CD117 expression and exhibited T cell lineage commitment - as indicated by the TCR alpha and CD3 expression, although no CD4+ and/or CD8+ T cell were observed there. But we have yet to fully understand the mechanistic role of 3D architecture toward T cell differentiation and rational design can be challenging without a comprehensive understanding of the relationship between scaffold design parameters and T cell phenotype.

In addition to the 3D scaffold, ligand-presenting beads represented another biomaterials-based technique for immune cell engineering. This concept was demonstrated by Lin et al. to solve the challenge of generating mature functional T cells *in vitro* specifically by co-culturing mouse embryonic stem cell (ES) cells or immature DP T cells with MHC Class I tetramers [86]. With the idea that T cell maturation requires interaction between TCR and MHC molecules, this approach was conducted and resulted in the generation of antigen-specific CD8+ T cells from the precursor cell population. In another work, Taqvi et al. added DLL4-presenting beads into ES cells being cultured with OP9 stromal cells to direct the differentiation toward T cell lineage as indicated by Thy1.2 cell surface marker expression [87].

The beads-based approach has been further applied in the context of *in vitro* T cell activation. *In vitro* T cell activation and expansion has generally been carried out by stimulating the TCR complex and the co-stimulatory molecules. The conventional approach involves the use of immobilized antibodies against CD3 and CD28 as demonstrated by Levine et al. with beads presenting both signals to expand polyclonal CD4+ T cells [88]. Immobilized signal appeared to be important because soluble anti-CD28 antibody does not work as well for long term T cell proliferation and this phenomenon was found to occur due to CD28 downregulation with soluble signal [89]. The importance of immobilized signal presentation was further demonstrated by Tham et al. with latex microspheres providing peptide-MHC complex (pMHC) in the presence of either bead-bound B7-1 and B7-2 recombinant proteins or soluble ones, as the former

resulted in superior cell proliferation and IL-2 secretion in contrast to the latter [90]. While activation can be carried out with either pMHC or anti-CD3 antibody, Oelke et al. showed that pMHC facilitated antigen-specific expansion while CD3 resulted in decreased antigen specificity [91]. In addition to studies on signal presentation format, the role of signal density has also been explored in T cell activation. Matic et al. observed that increased anti-CD3 antibody density alone upregulated CD69 expression, while greater anti-CD3 antibody density with the anti-CD28 antibody produced greater T cell expansion and IL-2 secretion [92]. Despite the versatility of such beads-based approach, a more comprehensive niche recapitulation will require the reconstitution of biomimetic microarchitecture and other signals.

These surface-bound activation signals can then be combined with 3D scaffold functionalized with important biomolecules to further engineer the system, as shown by Stephan et al. with the scaffold containing GFOGER collagen-mimicking peptide and stimulatory beads as T cell delivery platform for cancer therapy [93]. Motivated by lymphocytes known to typically move along collagen fibers, the use of GFOGER resulted in a greater migration velocity similar to the one seen in lymphoid organs and more cells migrating out in response to IP-10 inflammatory cytokine. Just like methods employed to augment T cell differentiation, three approaches appear to be as important for improving T cell activation in culture: signal immobilization, ligand density, and 3D scaffold utilization. It is possible that similar biomaterials-based approaches can also be used in the context of B cell engineering.

1.7. Conclusions and Perspectives

As described here, several approaches are available to control B cell development and GC reaction in the cell culture system. The strategies can be very different depending on the length scale of interaction with B cells, ranging from the simple addition of soluble factors into the development of biomaterials-based scaffold presenting relevant signals. For such artificial systems, the most important considerations consist of whether the relevant signal is presented and if the important cellular events can be recapitulated.

The main challenges of developing a B cell culture system consist of determining if the generated B cells are functionally comparable to the ones generated in animal models, maintaining B cell viability throughout the culture period without triggering diseased/transformed phenotypes, and ensuring the ability to respond appropriately toward specific stimulatory signals. Illustrating the difficulty of recapitulating GC phenotype, standard *ex vivo* B cell stimulation protocols frequently induce lymphoid transformations - as indicated by the expression of genes that typically characterize ABC DLBCL [94] - and fail to upregulate BCL6 expression [95]. While we have learned the transcriptional program for GC reaction maintenance and the signals that are required to enable ASC differentiation (Figure 1-2), we have yet to determine if such program exists in *ex vivo* B cell culture models and whether they can reconstitute such response toward those signals.

An additional challenge is to provide the relevant biological signals for controlling *ex vivo* GC reaction. Since most B cell studies are done with animal models, there is a lack of information regarding the microenvironmental cues needed to recapitulate the B cell activation process. This situation is compounded by the lack of information on the interaction between relevant matrix proteins and B cell phenotype in culture. While transplanted collagen-based scaffold has been reported to produce organoids with physiologically GC characteristics such as B cell clusters with actively proliferating B cells (Figure 1-3), we have yet to understand if and how the scaffold drives the cell cluster formation.

Despite the limited knowledge so far, there are several promising directions for B cell engineering. Biomaterials research has been focused toward understanding the extracellular matrix (ECM) since ECM has been known to modulate various cell behaviors with integrin molecules mediating cell-matrix interactions. Integrin ligands have also been observed to mediate the interactions between B cells and other immune cells as described earlier in this chapter [37-39]. ECM proteins that act as integrin ligands have also been found in the secondary lymphoid tissues [96, 97]. It is therefore exciting to investigate the

role of ECM proteins and/or integrin ligands in controlling B cell activation or other processes in the context of lymphoid tissue microenvironment. Natural polymers can be used to directly implement ECM component and one example is to utilize gelatin for cell encapsulation due to its wide use in 3D cell culture [98-101]. It is also possible to utilize synthetic matrix that can be functionalized with integrin ligands as demonstrated by Phelps et al. with the use of 4-arm maleimide-functionalized polyethylene glycol (PEG) and thiolated adhesive peptide [102, 103]. Despite the flexibility of such synthetic systems, we will have to first identify the integrin ligands that are present and relevant for B cell processes before presenting them in culture. We also need to investigate the role of matrix proteins, 3D microarchitecture, and ligand density.

While biomaterials-based technologies are rarely used to study immune cells, biomaterials have been becoming increasingly popular in other research areas due to the ability to integrate cell culture dimension (2D vs. 3D) and design parameters (e.g. signal tethering, chemical gradients, and cell patterning) to recapitulate cell microenvironment. There are also inspirations that can be gained from biomaterials utilized to modulate immune activation and regulation in animal models. Material parameters (e.g. type, size, shape, structure, and functionalization) can also impart specific functionalities (e.g. targeting and controlled release) on nanoparticle-based vaccines [104, 105]. By identifying key signals and optimizing signal presentation format, we can design a more physiologically relevant B cell culture platform. We thus plan on studying *ex vivo* B cell development process and assessing the role of various microenvironment signals. This project will be done to generate a B cell culture system that replicates the simplicity of *ex vivo* approaches and reproduces the key attributes of *in vivo* models. We hope that a successful development of such technology will enable us to model the GC reaction for understanding the key factors that regulate GC kinetics, tracking the fate of GC B cell, and learning the decision making process that happens in GC.

1.8. Figures

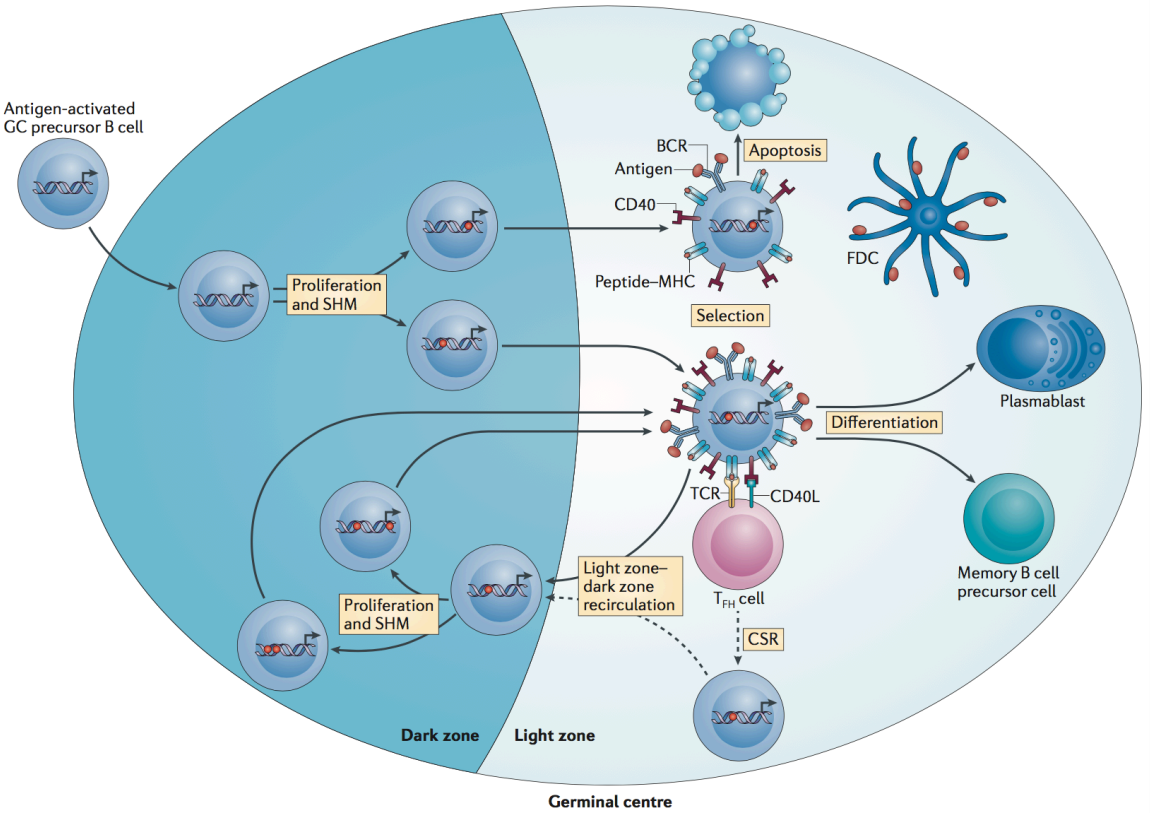

Figure 1-1: Schematic of GC Reaction Dynamics
Activated B cells initiate GC formation by first undergoing massive proliferation and experiencing somatic hypermutation (SHM) in the dark zone compartment. Dark zone GC B cells then migrate into the light zone compartment to undergo the affinity-based selection process and class switching (CSR). During selection, GC B cells can decide to undergo apoptosis, cycle back into the dark zone, or terminally differentiate toward ASC or memory B cell fates. Adapted by permission from Macmillan Publishers Ltd: Nature Reviews Immunology [3], copyright 2015.

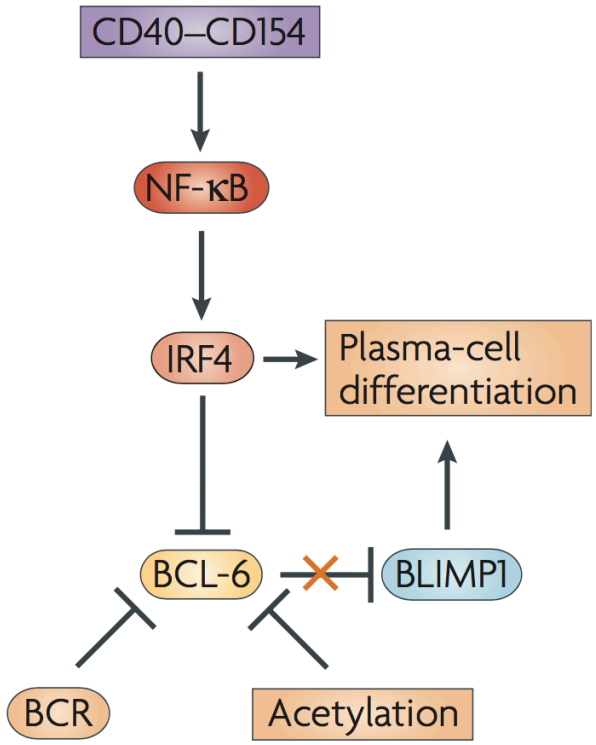

Figure 1-2: Schematic of GC Transcriptional Maintenance Program
GC maintenance is enabled by BCL6 by transcriptionally repressing differentiation toward ASC pathway. BCL6 repression by CD40 and/or BCR stimulations will result in the initiation of ASC differentiation program via IRF4 and BLIMP1 induction. Adapted by permission from Macmillan Publishers Ltd: Nature Reviews Immunology [4], copyright 2008.

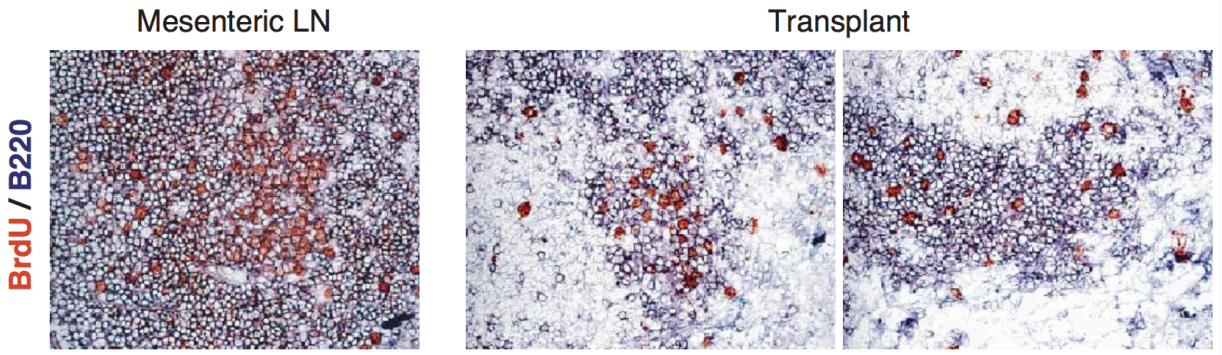

Figure 1-3: Proliferating B Cell Clusters in Lymph Nodes and Organoids
Comparison between mesenteric lymph nodes - as a representative secondary lymphoid organ - and the transplanted organoids based on the formation of B cell clusters containing proliferating B cells in the centers. Tissue sections were stained by double staining with B220 (purple) and BrdU (red). B220 was used to visualize the B cell populations. BrdU was delivered intraperitoneally at 1 hour before tissue harvesting and used to stain actively proliferating cells. Adapted by permission from Macmillan Publishers Ltd: Nature Biotechnology [61], copyright 2004.

CHAPTER 2

Ex vivo Engineered Immune Organoids for Controlled Germinal Center Reaction

2.1. Abstract

Realizing the limitations of existing *ex vivo* B cell culture systems, we were inspired to study the role of lymphoid microenvironment with a focus on integrin signaling. We developed a biomaterials-based immune organoid to model GC reaction by integrating 40LB stromal cells and gelatin scaffold reinforced with silicate nanoparticle. We first determined the optimal composition for this artificial lymphoid niche based on mechanical properties and stromal cell characteristics. We then demonstrated the ability of our immune organoids to produce B cell clusters, sustain B cell number in culture, and enhance the expansion of GC-like B cells. We also noted the importance of RGD motif from the gelatin matrix in maintaining B cell number in the absence of 40LB stromal support. These results suggest the importance of capturing the lymphoid microenvironment in the development of an immune organoid.

2.2. Introduction

Following up on our goal to develop an improved *ex vivo* B cell culture system, we utilized a 40LB stromal cell line for GC phenotype induction in B cells [48]. Since 40LB stromal cells were fibroblasts that had been engineered to present membrane-bound CD40 ligand (CD40L) and secrete BAFF, these cells could represent the relevant immune cells (Tfh cells and FDCs) and be expanded easily in culture. B

The content of this chapter has been published as Purwada, Alberto, Manish K. Jaiswal, Haelee Ahn, Takuya Nojima, Daisuke Kitamura, Akhilesh K. Gaharwar, Leandro Cerchietti, and Ankur Singh. "Ex vivo engineered immune organoids for controlled germinal center reactions." *Biomaterials* 63 (2015): 24-34. The detailed methodology has been published as Purwada, Alberto, and Ankur Singh. "Immuno-engineered organoids for regulating the kinetics of B-cell development and antibody production." *Nature protocols* 12, no. 1 (2017): 168-182.

cells activated by this method were also found to proliferate extensively, experience isotype class switch following soluble IL-4 cytokine addition, and exhibit the expression of relevant GC markers: GL7, Fas, PNA, $CD38^{low}$, and BCL6. These characteristics suggest that such stromal-driven approach represents several improvements from conventional activation protocols and therefore warrant further study.

Inspired by the stromal-driven B cell activation method, we initiated a pilot study by co-culturing 40LB stromal cells with primary naïve B cells in the presence of soluble IL-4 and varied stromal density that ranged from 20,000 to 60,000 cells per sample. Our result interestingly showed that the total number of CD19+ B cells were significantly reduced in culture between initial time point (day 0) and analysis time (day 4) with no clear difference between any of the 40LB seeding densities (Figure 2-1). From this finding, we used the 20,000 40LB seeding density for further comparison. With this inability to induce extensive cell proliferation in culture, we hypothesized that it would be important to recapitulate certain aspect of the lymphoid microenvironment to ensure optimal *ex vivo* B cell activation process.

Recent studies have suggested that the ECM component of lymphoid tissues can modulate B cell phenotype. After learning that B cells express various integrin subunits (e.g. αv, β3, α4, and β1), Song et al. showed that marginal zone (MZ) and follicular (FO) B cells bind laminin α5 in an RGD-dependent manner and knocking out laminin α5 will result in increased apoptosis of MZ B cells based on the TUNEL assay readout [96]. The researchers also showcased how laminin α5 can synergize with BAFF in producing a high number of MZ B cells. Wang et al. then mentioned the upregulation of both αv and β3 chains on GC B cells (vs. follicular B cells) such that this cell population can adhere strongly to vitronectin [97]. Interestingly, knocking out integrin β3 will result in overrepresentation in the splenic GC compartment. While it was not known at the moment if RGD-mediated binding to the microenvironment via αvβ3 integrins could improve GC B cell number in culture, cell adhesion process has been linked to cell survival in several cases and this motivates us to investigate this hypothesis further.

We took the first step in this line of reasoning by examining a genome-wide gene expression analysis previously published by Dominguez et al. and currently stored in the National Institute of Health (NIH) repository to understand the integrin gene expression level in both follicular naïve and GC B cells (Figure 2-1) [106]. Counts per million (CPM) was used as the quantification metric because it represented the number of counts scaled by the number of fragments sequenced times one million such that we could normalize the library size in each sample. The gene expression level for integrin subunits α2, α5, and α6 were found to be low in both B cell populations. The α4 integrin subunit, on the other hand, was highly expressed in total naïve B cells with 317 CPM and then reduced to 67 CPM following differentiation into GC B cells. While the β1 integrin subunits had an expression level of 36 CPM in naïve B cells, the value went up to 81 CPM in GC B cells. We then examined the expression of both αv and β3 integrin genes. Their values appeared to be unchanged during B cell differentiation with 22-24 CPM for αv and 48-50 for β3. These studies indicated that while the gene expression of α4 and β1 integrin subunits varied during differentiation, the gene expression of αv and β3 integrin subunits was kept constant.

Despite the gene expression trend obtained by RNA sequencing, it would be important to validate such finding based on the expression of integrin subunits on B cell surface because there can be numerous post-translational modifications that occur following transcription. We determined the cell surface expression of integrin subunits by immunizing mice with sheep red blood cells (SRBC) such that GC developed over 8 days period and harvesting the spleen for flow cytometry analysis (Figure 2-3). Looking at the integrin subtypes on B220+ GL7+ Fas+ GC B cells, the percentage of cells expressing αv, β3, and β1 was found to be higher in GC B cells when compared to naïve B cells. Meanwhile, the percentage of B cells expressing integrin α4 was similar in both cell subsets. When we evaluated the expression level of these integrin subunits, we observed a similar percentage. This outcome motivated us to investigate the role of these integrin subunits in *ex vivo* GC induction.

2.3. Approach

Hypothesizing that the B cells interact with the lymphoid microenvironment via the binding of αvβ3 integrin subunits and such contact improves the B cell generation during *ex vivo* GC reaction, we co-encapsulated primary naïve B cells and 40LB stromal cells in RGD-containing gelatin hydrogel (Figure 2-4). The rationale for such material selection is primarily driven by the presence of RGD in gelatin. RGD is the peptide sequence that can be found in several ECM proteins (e.g. gelatin) that mediates cell binding via engagement of αvβ3 or α5β1 integrin subunits. Gelatin-based 3D cell culture system has existed for decades and been well characterized in numerous studies. Gelatin is typically modified (i.e. methacrylate functionality addition) to facilitate UV- or chemical-induced crosslinking so that gelatin remains stable and not liquefying at 37 °C cell culture condition [98, 107, 108]. In this approach, we initiated ionic crosslinking of gelatin fibers with the use of silicate nanoparticles (SiNP) that were 20-30 nm in diameter and ~1 nm in thickness (Figure 2-5) [99-101, 109]. With the help of ionic interaction between the charged surface on the surface of SiNP and the opposing charges within the gelatin molecules, the resulting hydrogel was found to be physically stable at 37 °C (Figure 2-6). Primary B cells were efficiently encapsulated in the gelatin hydrogels and stained positive for Calcein after 24 hours post-encapsulation (Figure 2-7). We also ensured the absence of bacterial endotoxins in the material with the use of Limulus Amebocyte Lysate (LAL) assay that indicated 0.01 +/- 0.001 endotoxin units (EU)/ml for SiNP and 0.04 +/- 0.01 EU/ml for gelatin scaffold reinforced with SiNP. These values are far below the U.S. FDA endotoxin threshold of 0.5 EU/ml.

2.4. Organoid Design Parameters

In the development of biomaterials-based immune organoid, it is important to design one with similarity with the microarchitecture of lymphoid tissue, structural stability in culture, and capability to support both B cell proliferation and stromal network formation [110]. We investigated the design parameters by

varying gelatin and SiNP composition and then analyzing changes in hydrogel physical properties. Using scanning electron microscope (SEM) to evaluate the effect of material composition on hydrogel microarchitecture, we found that hydrogels with 2% (w/v) gelatin and 1.5% (w/v) SiNP resulted in a more uniformly porous structure in comparison to the one seen with gelatin only mixture and this could be attributed to the presence of charged SiNP surface that would prevent the ionic aggregation of gelatin fibers with each other (Figure 2-8). This concept was further supported by the decrease in pore size as gelatin concentration was raised from 2% to 4% while keeping the SiNP concentration constant at 1.5%. SiNP incorporation within the hydrogel was also confirmed using energy-dispersive X-ray spectroscopy (EDS) analysis that showed the presence of Mg and Si peaks only in gelatin hydrogels physically reinforced with SiNP but not in gelatin-only hydrogels (Figure 2-9). These outcomes indicated that SiNP was incorporated in the gelatin hydrogel and could modulate the matrix architecture.

We then hypothesized that a physiologically relevant immune organoid would require a comparable material stiffness with the one reported for spleen as a representative secondary lymphoid organ based on quantification using magnetic resonance elastography [111]. With the reported spleen stiffness of 2300 +/- 1000 Pa, we prepared hydrogels with various compositions and analyzed both storage and loss moduli at 37 °C cell culture condition (Figure 2-10). While gelatin alone remained in liquid phase with virtually zero storage and loss moduli, the addition of SiNP resulted in the formation of crosslinked gelatin network and the increased organoid stiffness. With 1% SiNP and 2% gelatin, there was a marginal increase in storage modulus to 130 +/- 40 Pa and yet the material was not physically stable as indicated by the lack of significant difference between storage and loss moduli. With 1.5% SiNP and 2% gelatin, the storage modulus increased to 1900 +/- 50 Pa and this value was seen as comparable with the previously reported spleen stiffness mentioned above. With 2% SiNP and 2% gelatin, the storage modulus further increased to 3100 +/- 410 Pa. Although the 1% SiNP and 2% gelatin composition produced a fragile mixture, keeping the ratio the same and doubling the concentration of each component (i.e. 2% SiNP and 4% gelatin composition) produced a stable hydrogel as indicated by the significant difference between

storage and loss moduli. This finding could be attributed to the excess of non-crosslinked gelatin as made evident in the case of 1.5% SiNP and 4% gelatin that had a low storage modulus and no significant difference between the storage and loss moduli. These observations suggested that SiNP could successfully crosslink gelatin and facilitate the formation of stable scaffold for biological experiments.

We next assessed the influence of material composition toward the 40LB stromal network formation. This study was carried out by staining stromal cells with CellTracker Green CMFDA Dye and encapsulating 40,000 stromal cells per hydrogel with varying compositions (Figure 2-11). By keeping the adhesive ligand density the same with gelatin concentration kept constant at 2% (w/v), 40LB stromal cells demonstrated improved spreading with 1.5% SiNP than 2% SiNP. Increasing the adhesive ligand density with 4% gelatin concentration produced a marked increase in stromal cell clusters.

We then examined the effect of 40LB stromal seeding density within the hydrogel made using 2% gelatin and 1.5% SiNP (Figure 2-12). While 20,000 cells/gel stromal seeding density resulted in small cell clusters, 40,000 cells/gel stromal seeding density produced a tightly connected cellular network and 60,000 cells/gel stromal seeding density formed a dense tubular-like network. These findings indicate that the 2% gelatin with 1.5% SiNP composition facilitates the formation of a hydrogel network that is both physically stable under cell culture conditions and capable of supporting uniform stromal cell spreading.

When we assessed the expression level of membrane-bound CD40L on the surface of stromal cells, we found that 3D encapsulation resulted in a significantly higher expression of CD40L surface marker (9500 +/- 430 MFI) compared to the one exhibited by 2D co-culture (4600 +/- 620 MFI) following 6 days of culture (Figure 2-13). With these observations, we selected the 1.5% SiNP and 2% gelatin composition to go ahead with B cell experimentations based on physical characteristics and 40LB stromal responses.

2.5. B Cell Expansion

After characterizing the immune organoid from both material and stromal perspectives, we moved into studying the proliferation of primary B cells within the immune organoid. As we expected the interaction between B cells and 40LB cells to depend on stromal density, we co-cultured both cell types with an increasing amount of stromal cells in the presence of soluble IL-4. From analyzing organoid phase contrast images collected as a function of time, we observed distinct regions of closely packed cells in hydrogels that morphologically resembled *in vivo* GC reactions and the morphological structure of these cell clusters interestingly depended stromal density (Figure 2-14).

As such appearance qualitatively indicated high B cell proliferation in the organoid, we next assessed the number of live cells based on Calcein positive cells detected using flow cytometry and observed a significant increase in the number of viable cells in our 3D organoids after 4 days of culture when compared to the number seen with 2D co-culture systems (Figure 2-15). It is encouraging to see the increased number of live cells because they can only be attributable to B cells since the 40LB stromal cells have been previously treated with mitomycin C to prevent proliferation inside the organoid.

We next quantified the number of CD19+ B cells following culture with increasing stromal density (Figure 2-16). We found that the use 3D system improved B cell generation as indicated by the higher number of B cells in 3D (3,390 +/- 295 cells) when compared to the one seen in 2D (1261 +/- 72 cells) and the maximum proliferation of CD19+ cells was facilitated with 40,000 stromal cells per hydrogel usage with the resulting cell number (5,477 +/- 477 cells) being either higher than the one seen with 20,000 stromal cells (3,390 +/- 295 cells) or comparable to the one observed with 60,000 stromal cells. These findings indicate that increased CD40L density and stromal spreading could promote the proliferation of CD19+ B cells in culture, yet we had yet to identify the important driver behind improved B cell generation in the 3D system.

We hypothesized that the higher number of CD19+ B cells was facilitated by the pro-survival signal generated by the binding of RGD motifs in gelatin by integrin subunits on B cell surface. We investigated this idea by culturing B cells in the organoid without any stromal support and we observed a greater decrease in CD19+ B cells with 2D approach when compared to 3D organoid (Figure 2-17). In order to test the importance of the RGD motifs found in gelatin, we blocked RGD-mediated signaling with Cilengitide, a cyclic RGD pentapeptide that could selectively inhibit RGD binding via αvβ3 and/or α5β1 integrin subunits (Figure 2-17) [112, 113]. Interestingly, we observed a partial but significant decrease in CD19+ B cells when blocked with Cilengitide. This finding confirmed the partial role of αvβ3 and/or α5β1 integrins in supporting B cell survival in *ex vivo* culture systems. At the same time, we hypothesized that αvβ3 signaling played a more important role in this integrin-mediated B cell survival when compared to α5β1 signaling due to the very low α5 integrin gene expression value seen earlier.

2.6. GC Phenotype Induction

In order to study GC phenotype induction inside the organoid, it is critical to figure out the relevant markers that can be used to distinguish the GC B cell population. We assessed the relevant GC surface markers by immunizing mice with SRBC and assessing GC reaction in the spleen (Figure 2-18). From the splenic tissue, we found that PNA+ GC clusters were formed within the B220+ B cell follicle compartment in the secondary lymphoid tissue. These GC clusters were also found to be positive for both B220 and GL7. Flow cytometry analysis of splenic B220+ B cells further indicated that the GC B cell population could be delineated with a double expression of GL7 and Fas surface markers.

Based on this assessment regarding characteristic GC markers, we looked into GL7 surface marker expression on the surface of *ex vivo* activated B cells (Figure 2-19). We observed the significantly higher number of CD19+ GL7+ GC-like B cells with 20,000 40LB stromal cells in 3D organoid (57 +/- 5 fold)

when compared to the one seen in 2D co-culture (10-20 fold). Making comparison within the 3D organoid cultures, the CD19+ GL7+ response was dependent on 40LB stromal density since 40,000 40LB stromal cells usage produced 96 +/- fold increase that was higher than the one seen with 20,000 40LB stromal cells and comparable (i.e. no statistically significant difference) with 60,000 40LB stromal cells. The results were further confirmed by confocal imaging studies that demonstrated the co-localization of GL7+ B cells on 40LB stromal networks (Figure 2-20). These results emphasized the importance of 3D organoid in facilitating an efficient *ex vivo* GC reaction. We next examined the expression of Fas surface marker within the CD19+ GL7+ GC-like B cell population in the organoid (Figure 2-21). The data indicated that 3D immune organoids with 40,000 and 60,000 stromal cells demonstrated a significant 55-fold increase in CD19+ GL7+ Fas+ GC-like B cell when compared to 3D with 20,000 stromal cells (16 +/- 2 fold) and 2D with 20,000 stromal cells (7 +/- 1 fold). As expected with the dependence of CD40L on inducing GC phenotype, organoids with no stromal failed to induce the generation of GC-like B cells.

2.7. Isotype Class Switch Induction

In addition to surface markers upregulation, another hallmark of GC reaction is the cytokine-dependent isotype class switch that occurs in GC B cells to facilitate the production of immunoglobulin molecules with distinct effector functions [114, 115]. B cells activated with CD40L have been known to undergo isotype class switch in the presence of specific cytokine combinations. Recognizing that the 3D immune organoid induced GC phenotype, we next assessed the functional capabilities of GC-like B cells based on their ability to undergo class switching from IgM to IgG1 and IgE in the presence of soluble IL-4 cytokine (Figure 2-22). Based on the flow cytometry readout, we observed a robust generation of class switched B cells where the number of IgG1+ B cells increased significantly from 185 +/- 14 cells on day 0 to 7,120 +/- 612 cells on day 6 in 3D organoid with 40,000 40LB cells. This number was found to be comparable with the one seen in 3D organoid with 60,000 40LB cells. We then examined the level of membrane-bound IgE expression level and we observed a marked shift in IgE expression in 3D when

compared to 2D or day 0. We also observed that the significant increase in CD19+ IgE+ B cell number with 40,000 stromal cells (5,446 +/- 535 cells) and 60,000 stromal cells (4,441 +/- 510 cells) as compared to the number seen with 20,000 stromal cells (1,687 +/- 116 cells).

2.8. Discussion

Since very few studies have been done on engineering artificial tissues to culture primary immune cells and study their interactions with the cell microenvironment, this study represented an early attempt at the development of modular B cell follicle organoid with an ability to accelerate immune reaction via tunable design parameters. Here we specifically described the development of 3D immune organoid that morphologically and functionally resembles the GC reaction that typically occurs in the secondary lymphoid tissues following infection. Inspired by the mechanical and cellular compositions of the secondary lymphoid tissues, the organoid was designed to have comparable stiffness level and stromal component. From this approach, we learn how integrins are capable of mediating B cell survival in culture and CD40 signaling is critical for inducing GC phenotype in activated B cells.

While the current study demonstrates the role of αvβ3 in maintaining B cell number in the absence of stromal support, we cannot rule out the role of other integrin types presented in either gelatin matrix or lymphoid microenvironment. Future investigations will be geared toward investigating the role of other integrin subunits including α5β1 and α4β1. We will also need to comprehensively characterize the resulting GC-like B cells to determine how they compare with *in vivo* GC B cells from immunized mice, assess the induction of other GC hallmark events, and determine the capability of *ex vivo* GC models to recapitulate mechanistic events seen in the animal models. In conclusion, this immune organoid provides a simple strategy for recapitulating the lymphoid microenvironment in *ex vivo* GC reaction protocols to ensure long-term cell survival. This approach can be distinguished from conventional B cell activation methods that require culturing B cells with other cells and soluble factors in 2D format or transplanting

cell-seeded scaffold into live animal models. We anticipate biomaterials-based *ex vivo* immune organoids representing a new approach to study cell-matrix interactions, affinity-based clonal selection, and lymphoid transformation process.

2.9. Materials and Methods

2.9.1. GC B Cell Assessment in Mice

Surface integrin expression on the surface of *in vivo* GC B cells was studied by first immunizing two C57BL/6 mice intraperitoneally at 8 weeks of age with 0.5 ml of a 2% sheep red blood cell (SRBC) suspension in PBS (Cocalico Biologicals) and then sacrificing the mice after 8 days post-immunization. Splenocyte suspension was stained with the following fluorophore-conjugated anti-mouse antibodies: B220 (PerCP-Cy5.5), Fas (PE-Cy7), GL7 (Alexa Fluor 647), integrin α4 (PE), integrin αv (PE), β1 (FITC), integrin β3 (FITC), IgG2bκ isotype control (PE), IgG1κ isotype control (PE), and IgG isotype control (FITC). Dead cells were excluded using DAPI. GC B cells were identified as B220+ Fas+ GL7+, and naïve B cells were defined as B220+ Fas- GL7-. Surface integrin expression level versus isotype control was determined for both naïve B and GC B cells. Flow cytometry data was acquired with BD FACSCanto flow cytometer (BD Biosciences) and analyzed using FlowJo software package.

GC formation in immunized mice was assessed by challenging C57BL/6 mice with 2% SRBC suspension (Cocalico Biologicals, Inc) and harvesting the spleens 10 days post-immunization for further examinations. We then used the spleens to examine B cell follicles for GC formation using immunohistochemistry (IHC), flow cytometry, and immunofluorescence (IF). For IHC assessment, paraffin-embedded spleen tissue sections were stained with B220 (BD Pharmingen) for B cells and biotinylated peanut agglutinin (PNA, Vector Laboratories) for GC B cells [116]. For flow cytometry analysis, splenocytes were isolated with mechanical and gradient separation methods (Fico/Lite-LM,

Atlanta Biologicals) and then stained for B220 for B cells and GL7 + Fas for GC B cells. For IF evaluation, spleen tissue sections were stained for B220 to visualize B cells throughout the lymphoid tissue and GL7 to define B cells exhibiting GC phenotype.

2.9.2. Naïve B Cells and 40LB Stromal Cells Preparation

Organoid fabrication was done by first harvesting spleens from C57BL/6 mice, purifying B cells from splenocytes through negative selection using EasySep Mouse B Cell Isolation Kit (Stem Cell Technologies) with yield ~ 90% CD19+ B cells. 40LB stromal cells expressing CD40L and secreting BAFF were generated as reported earlier [48] and cultured in high glucose DMEM medium (Life Technologies) containing 10% FBS and 1% P/S. 40LB cells were mitotically inhibited through incubation in medium containing 0.01 mg/ml Mitomycin C at 37 °C for 45 minutes and then rinsed twice with 10 ml of 1X PBS prior to encapsulation.

2.9.3. Immune Organoid Fabrication

Gelatin stock solution was freshly prepared by dissolving gelatin powder (Sigma Aldrich) in RPMI 1640 medium and then sterilizing the solution with a syringe filter. Cells were suspended in warmed gelatin stock solution and diluted accordingly using cell culture medium. SiNP with 25-30 nm in diameter and 1 nm in thickness were obtained from Southern Clay Products Inc., USA. The SiNP suspension was freshly prepared prior to the encapsulation procedure by mixing SiNP powder with deionized water and vortexing the resulting solution immediately before use. Organoids were fabricated in 96-well plates by first adding 5 ml of SiNP, injecting 5 ml cell-containing gelatin solution into the initial SiNP droplet, and then mixing the entire hydrogel through repeated pipetting. Each organoid was cured for approximately 10 minutes prior to the addition of RPMI 1640 medium. The entire plate was then placed in the cell culture incubator for 1 hour before exchanging the cell culture medium in each well with the one containing 10 ng/ml

murine recombinant IL-4 (Peprotech) and replacing the medium every 3 days. The IL-4 stock solution was reconstituted in deionized water at 0.1 mg/ml and kept as aliquots in 20 °C.

2.9.4. Material Characterizations

Gelatin solutions of 2% and 4% (w/v) were prepared in PBS, mixed and vortexed with aqueous suspensions of SiNP to obtain homogeneously crosslinked gels. Modulus measurements were done for strain sweep (1-10% strain) at a fixed frequency of 0.1 Hz and 37 °C temperature using a rheometer (Anton Paar) equipped with 50 mm flat-plate geometry and a gap of 50 mm. For scanning electron microscopy (SEM) imaging of various hydrogel compositions, samples were freeze-dried and sliced into transverse sections by razor slitting. The sections were then sputter coated with Pt/Pd to provide conductivity and imaged using Quanta 600 (FEI) at 20 kV equipped with energy-dispersive X-ray spectroscopy (EDS) detector (Oxford Instruments). The recorded EDS spectra were further analyzed by INCA software (Oxford Instruments) to confirm the presence of elements. For transmission electron microscopy (TEM) imaging of the SiNP, approximately 5 ml of SiNP in water was drop-casted onto a carbon-coated copper grid, air-dried, and then imaged under 200 keV voltage using JEOL JEM-2010 instrument (Japan). Bacterial endotoxin analysis was done with the LAL assay based on the US Food and Drug Administration (FDA) guidelines [117].

2.9.5. Cell Extraction from Organoids

For enzymatic degradation, cell culture medium was aspirated from each well and the organoids were washed once using 1X PBS before covered with 10 U/ml collagenase solution (Worthington Biosciences) for overnight incubation in cell culture conditions. The collagenase solution was prepared by reconstituting collagenase powder in serum-free RPMI 1640 medium. The organoids were then mechanically digested through pipetting and combined with excess FACS buffer for collagenase

inactivation. FACS buffer was prepared with 1X PBS++ containing 10% FBS. The resulting cell suspension was filtered using a 70 mm cell strainer to remove gel debris prior to flow cytometry analysis.

2.9.6. Immunofluorescence Microscopy and Flow Cytometry Analysis

For flow cytometry analysis, the filtered cell suspension was stained in FACS buffer containing various antibody combinations with 1:1000 dilution for 45 minutes in the dark at 4 °C. The antibodies consisted of: FITC-, APC-, or PE-Cy7-conjugated anti-mouse anti-CD19, anti-GL7, anti-Fas, anti-CD40L, anti-IgG1, anti-IgM, and anti-IgE (eBioscience). After staining, the cell suspension was then rinsed twice using FACS buffer. Flow cytometer data were acquired using BD Accuri C6 and analyzed with FlowJo software package.

For IF assessment, immune organoids were rinsed and then incubated in FACS buffer containing fluorophore-conjugated antibodies and/or live cell stains for 12 hours in cell culture conditions. The samples were washed three times with each wash involving the aspiration of old medium and the incubation in fresh FACS buffer for 1 hour. Each organoid was covered with 1X PBS during imaging with Zeiss LSM 710 confocal microscope.

2.9.7. Integrin Blocking

Freshly purified B cells were incubated in FACS buffer containing cyclic RGD pentapeptide Cilengitide at the specified final concentrations of 10 and 50 μM for 30 minutes at 4 °C.

2.9.8. Statistical Analysis

Statistical analysis was performed using GraphPad Prism software with statistical significance determined based on a p-value of less than 0.05. All studies were performed in triplicates unless otherwise noted.

2.10. Acknowledgement

The work described in this chapter was financially supported by the National Science Foundation CAREER Award DMR-1554275 to Prof. Ankur Singh, the National Institutes of Health 1R21CA185236-01 to Prof. Ankur Singh, the Cornell University and Weill Cornell Medical College Seed Grant Program to Prof. Ankur Singh, and the Howard Hughes Medical Institute Med-into-Grad Fellowship HHMI 56006761 to Alberto Purwada. The concept was developed by Prof. Ankur Singh and the project design was carried out by both Alberto Purwada and Prof. Ankur Singh. 40LB stromal cells were generated by Takuya Nojima, Ph.D. and Prof. Daisuke Kitamura (Tokyo University of Science). Mechanical characterization experiments were performed by Manish Jaiswal, Ph.D. and Prof. Akhilesh Gaharwar (Texas A&M University). Immunohistochemistry imaging was done by Haelee Ahn and Leandro Cerchietti (Weill Cornell Medicine). *In vivo* GC B cell analysis from immunized mice was performed by Wendy Béguelin, Ph.D. and Prof. Ari Melnick (Weill Cornell Medicine). Other procedures (experiment setup, data collection, and analysis) were carried out by Alberto Purwada. Animal tissues were provided by Prof. Christopher Hernandez, Prof. Avery August, and Prof. Robert Weiss (Cornell University). All procedures were approved by Cornell University's Institutional Animal Care and Use Committee. Imaging studies were carried out using Zeiss LSM 710 Confocal Microscope - funded by NIH 1S10RR025502 - at the Cornell University Biotechnology Resource Center (BRC).

2.11. Figures

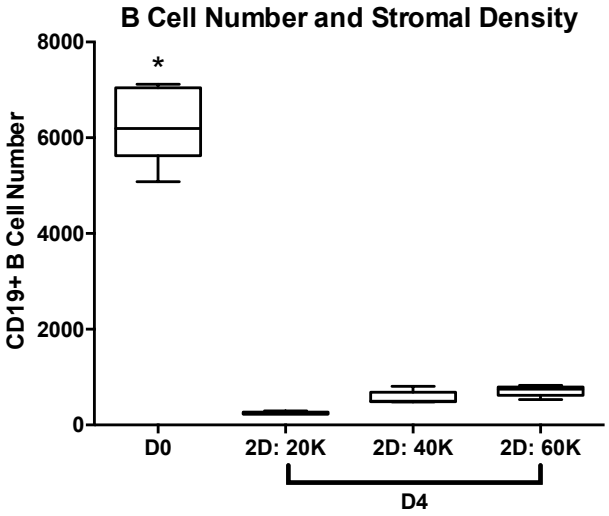

Figure 2-1: *Ex vivo* GC reaction with 2D co-culture system
(A) Number of CD19+ B cells in 2D culture. (B) Number of CD19+ IgG1+ B cells in 2D culture with varied IL-4 cytokine concentration (left) or stromal density (right). Statistical significance (*) was determined based on $P < 0.05$. Statistical test was conducted using ANOVA. Values are shown as mean ± SEM (n = 5).

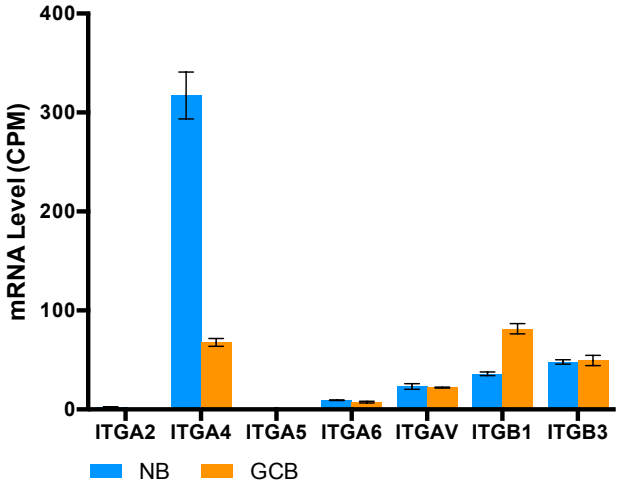

Figure 2-2: Analysis of integrin gene expression levels in murine splenic naïve and GC B cells
The values were obtained from the NIH repository linked to a published study by Dominguez et al. Statistical significance (*) was determined based on $P < 0.05$. Statistical test was conducted using ANOVA. Values are shown as mean ± SEM (n = 4).

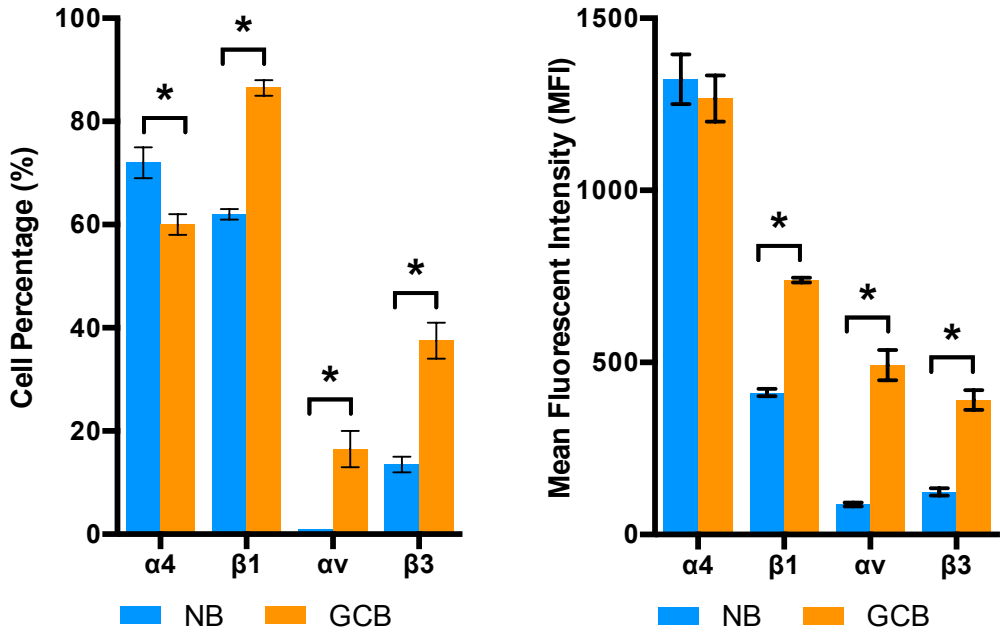

Figure 2-3: Surface integrin expression in murine splenic naïve and GC B cells
Quantitative analysis indicated the percentage of integrin-expressing cells (left) and the mean fluorescence intensity for each integrin subunit (right). Assessment was conducted on both B220+ naïve B cells and B220+ GL7+ Fas+ GC B cells from immunized mice. The cells were harvested from C57BL/6 mice after 8 days following intraperitoneal immunization with SRBC. Statistical significance (*) was determined based on $P < 0.05$. Statistical test was conducted using ANOVA. Values are shown as mean ± SEM (n = 2).

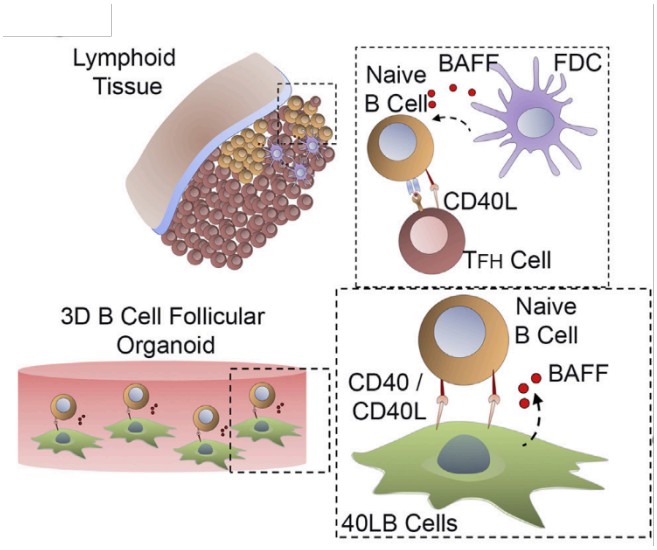

Figure 2-4: Schematic of B cell follicle immune organoid fabrication
The approach was inspired by the interaction between naïve B cells and signals provided by the neighboring cells – specifically CD40L presented by TFH cells and BAFF secreted from FDCs. In the organoid, B cells were encapsulated with 40LB stromal cells that provided both CD40L and BAFF inside RGD-presenting 3D hydrogel matrix.

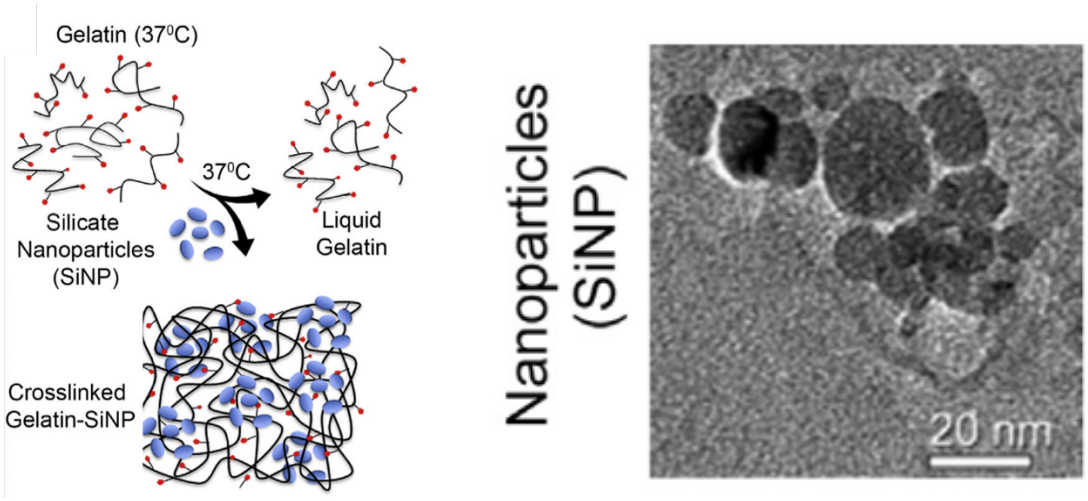

Figure 2-5: Overview of silicate nanoparticles
The schematic indicating how ionic crosslinking occurred upon the mixing of silicate nanoparticles and liquid gelatin to facilitate the formation of stable hydrogel matrix at 37 °C (left). The TEM image of silicate nanoparticles displayed with 20 nm scale bar (right).

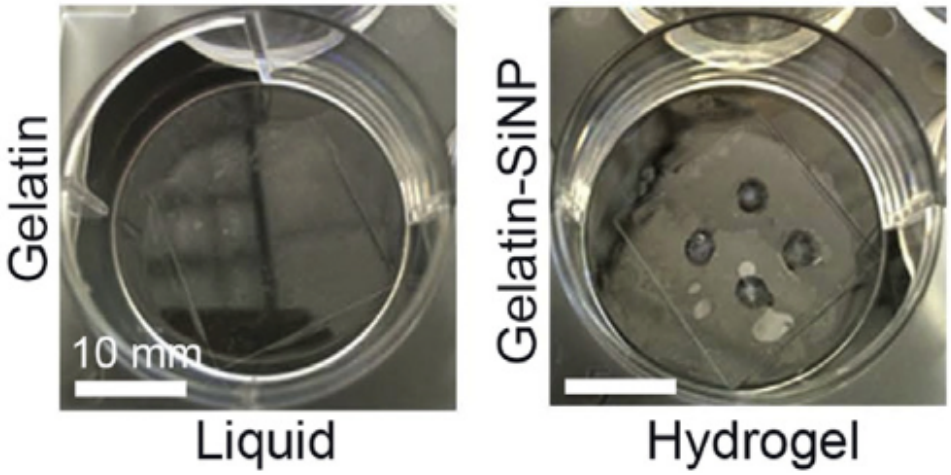

Figure 2-6: Role of SiNP addition toward gelatin matrix stability
The images indicated the visual comparison of organoid matrix stability in gelatin only (left) and ionically crosslinked gelatin (right) gels. Assessment was performed following incubation at 37 °C. The images are displayed with 10 mm scale bar.

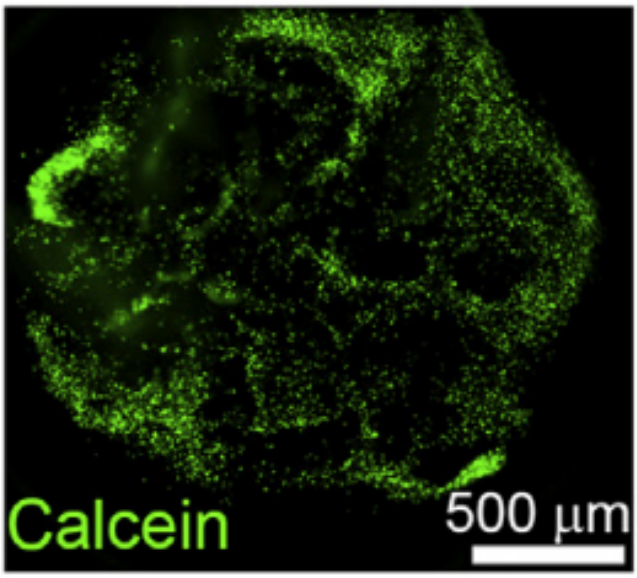

Figure 2-7: Primary B cell viability and distribution in organoid
Primary naïve CD19+ B cells were stained with Calcein prior to encapsulation and imaging was performed 24 hours after organoid fabrication with 500 µm scale bar.

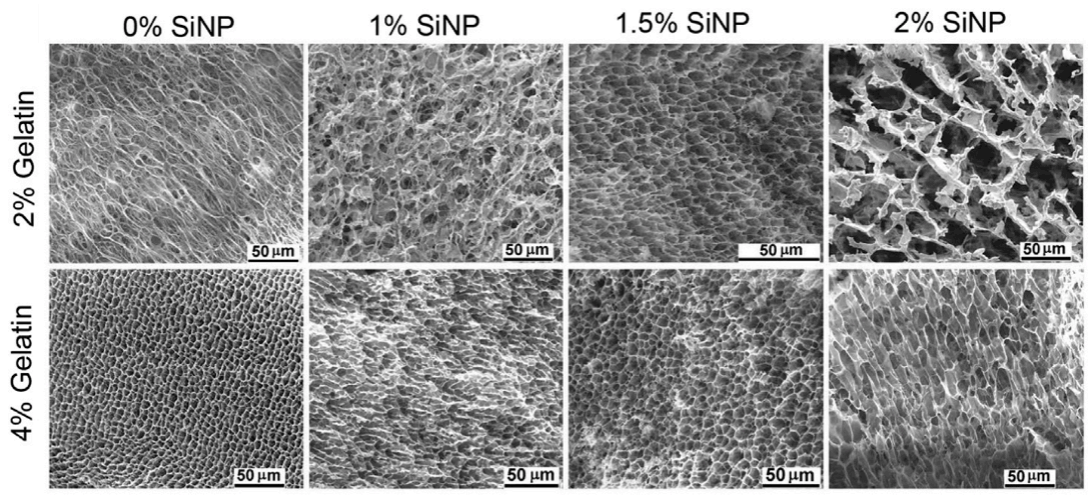

Figure 2-8: SEM analysis of gelatin matrix prepared with various compositions.
Two gelatin concentrations (2% and 4%) were prepared and each gelatin amount was mixed with several silicate nanoparticle w/v concentrations (0%, 1%, 1.5%, and 2%).

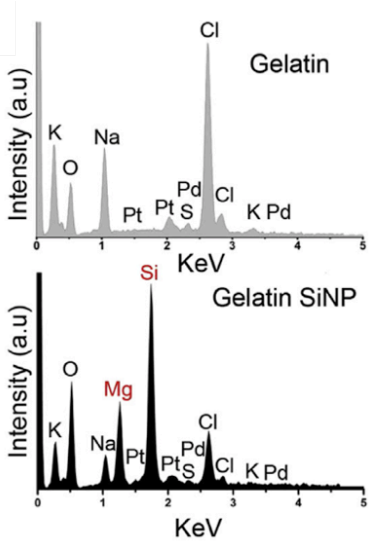

Figure 2-9: EDS analysis of gelatin matrix with and without silicate nanoparticles

Analysis was conducted to determine the presence of Si and Mg peaks in gelatin scaffold following reinforcement with silicate nanoparticles (bottom). Gelatin only group was used as control (top).

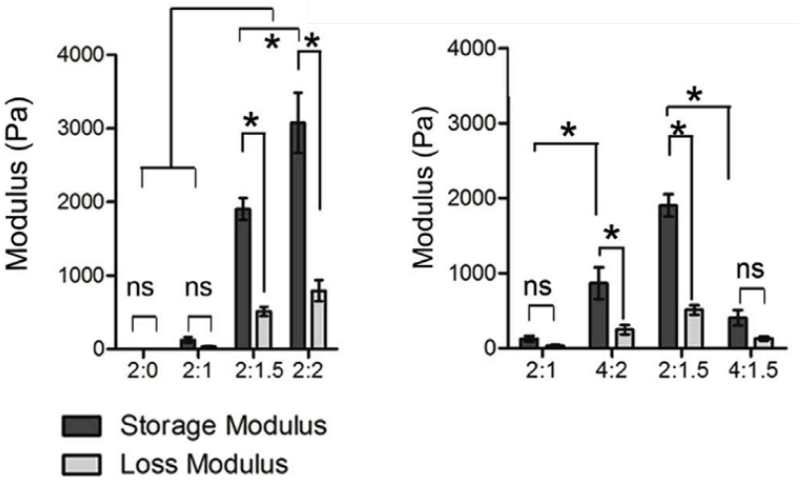

Figure 2-10: Rheological analysis of gelatin matrix with various compositions

Analysis was conducted on both storage and loss moduli. Two gelatin w/v concentrations (2% and 4%) were prepared and each gelatin amount was mixed with increasing silicate nanoparticle w/v concentrations (0%, 1%, 1.5%, and 2%). Statistical significance (*) was determined based on $P < 0.05$. Statistical test was conducted using ANOVA. Values are shown as mean ± SEM (n = 5).

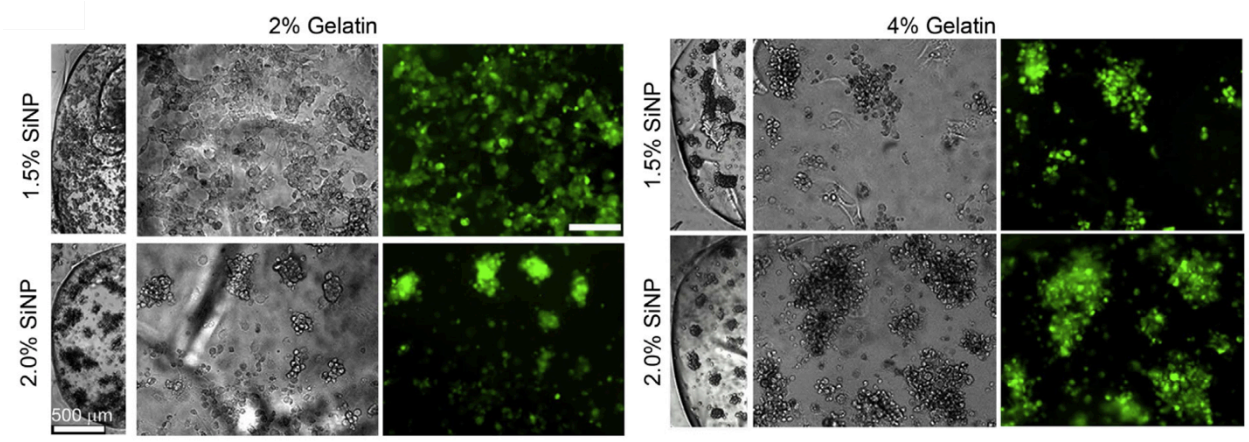

Figure 2-11: Role of organoid stiffness toward 40LB stromal cell phenotype
Fluorescence imaging was conducted on stained stromal cells encapsulated in gelatin network with varying gelatin and silicate nanoparticle concentrations. Images are displayed with 500 µm scale bar.

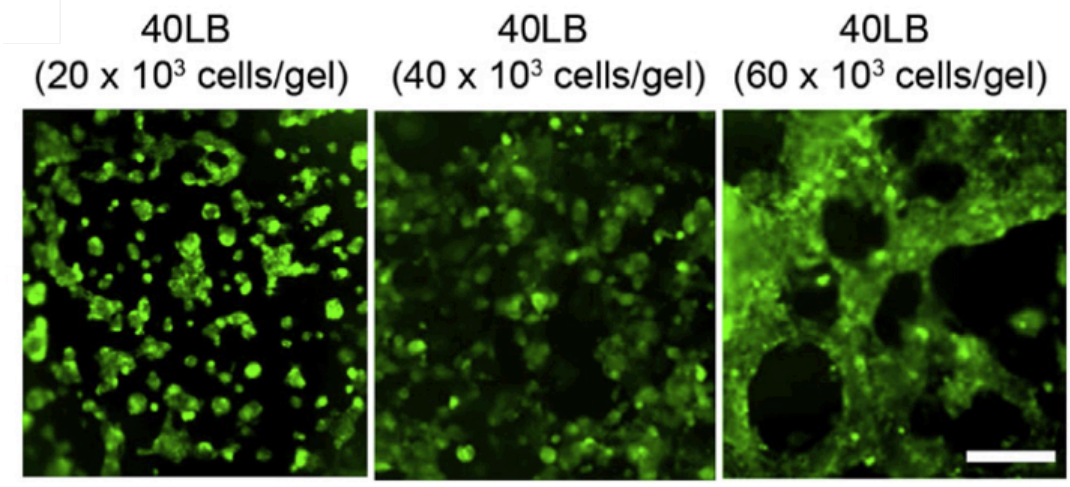

Figure 2-12: Role of stromal seeding density toward 40LB stromal cell phenotype
Fluorescence analysis was conducted on stained stromal cells in gelatin network seeded with increasing stromal cells. Images are presented with 200 µm scale bar.

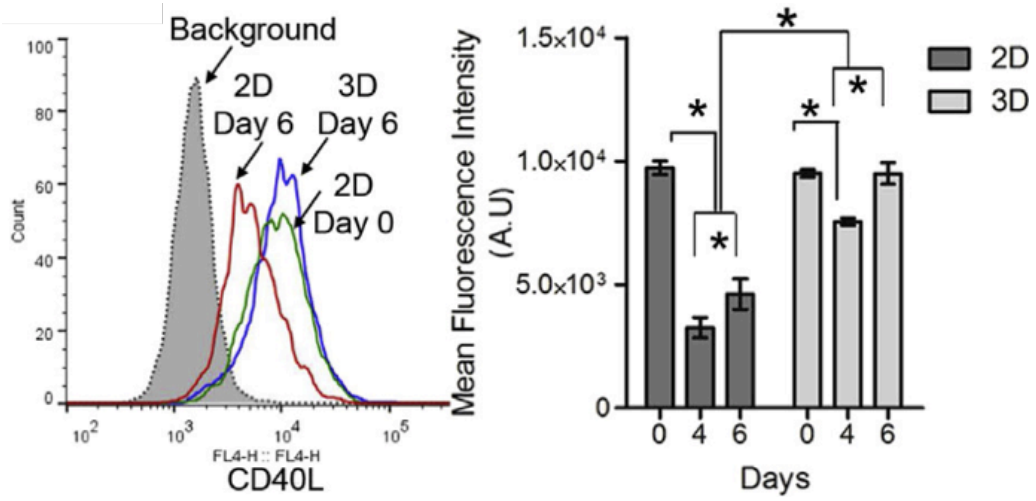

Figure 2-13: CD40L surface expression on 40LB stromal cells in 2D and 3D culture systems
Histogram on the left provided an overlay of CD40L expression in unstained, day 0, 2D (day 6), and 3D (day 6). Bar graph on the right quantified CD40L expression in mean fluorescence intensity for 40LB cells cultured with 2D or 3D culture system over 6 days. Statistical significance (*) was determined based on $P < 0.05$. Statistical test was conducted using ANOVA. Values are shown as mean ± SEM (n = 4).

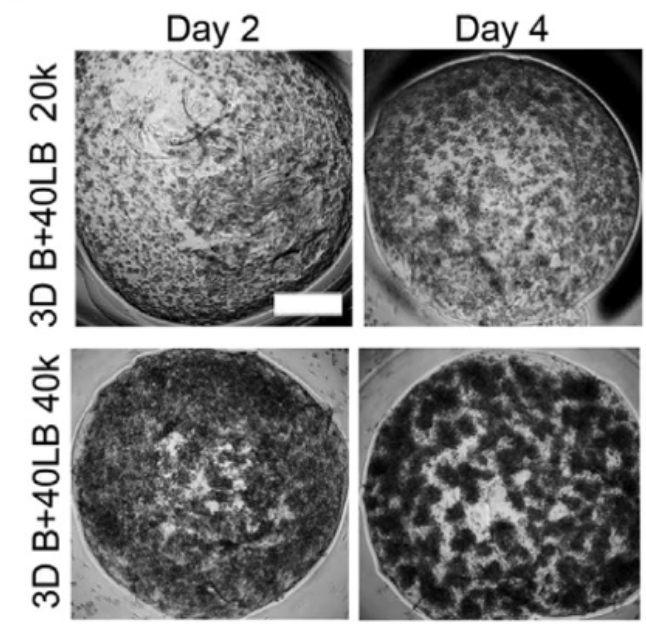

Figure 2-14: Image analysis of cell cluster formation inside immune organoid
Phase images were taken of the hydrogels containing primary B cells and 40LB stromal cells at various seeding densities. For each stromal density, two images were taken of the same hydrogel at two time points: day 2 and 4. Images are presented with 500 μm scale bar.

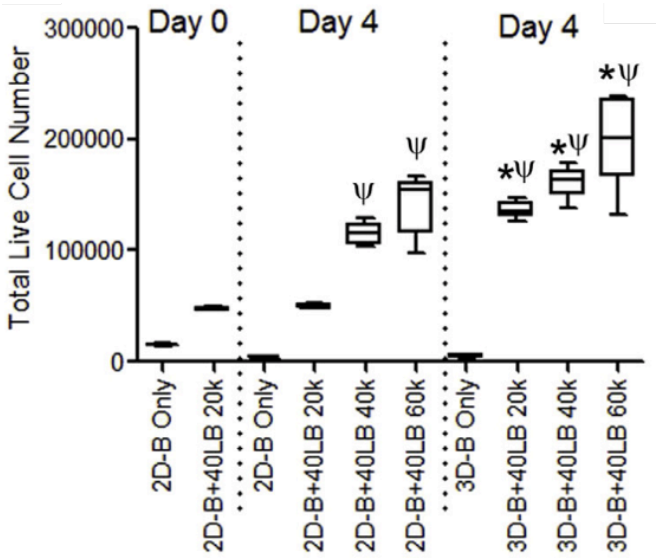

Figure 2-15: Quantification of total viable cells in *ex vivo* B cell culture systems
Analysis was done on Calcein positive cells in both 2D and 3D culture methods with increasing stromal density as a function of time. Statistical significance with regard to the 2D groups on day 4 (*) was determined based on $P < 0.05$. Statistical significance with regard to day 0 (ψ) was determined based on $P < 0.05$. Statistical test was conducted using ANOVA. Values are shown as mean ± SEM (n = 5).

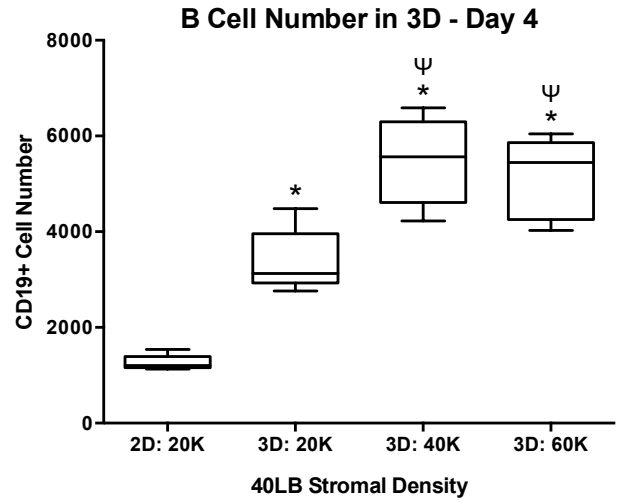

Figure 2-16: Number of CD19+ B cells in 2D culture and 3D organoid
The immune organoids were prepared with increasing 40LB stromal density. Flow cytometry analysis was conducted on day 4. Statistical significance with regard to the 2D group (*) was determined based on $P < 0.05$. Statistical significance with regard to the 3D 20K group (ψ) was determined based on $P < 0.05$. Statistical test was conducted using ANOVA. Values are shown as mean ± SEM (n = 5).

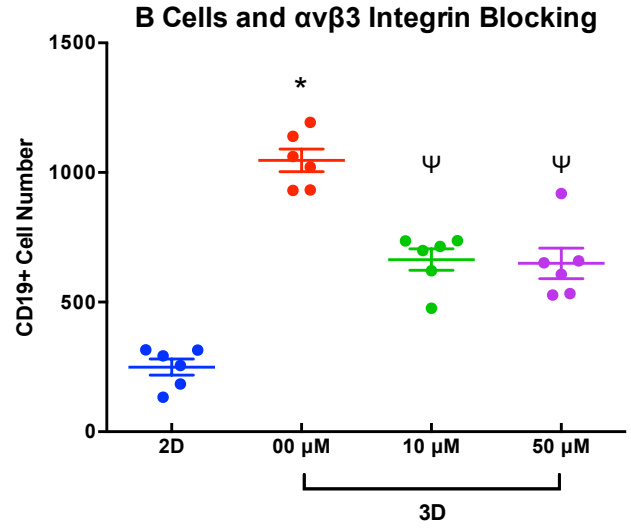

Figure 2-17: Number of CD19+ B cells in 2D culture and 3D organoid for integrin analysis
The immune organoid was cultured in the absence or presence of Cilengitide. Cilengitide was administered at doses: 10 and 50 µM. Analysis was conducted on day 2. Statistical significance with regard to the 2D group (*) was determined based on $P < 0.05$. Statistical significance with regard to the 3D 20K group (ψ) was determined based on $P < 0.05$. Statistical test was conducted using ANOVA. Values are shown as mean ± SEM (n = 5).

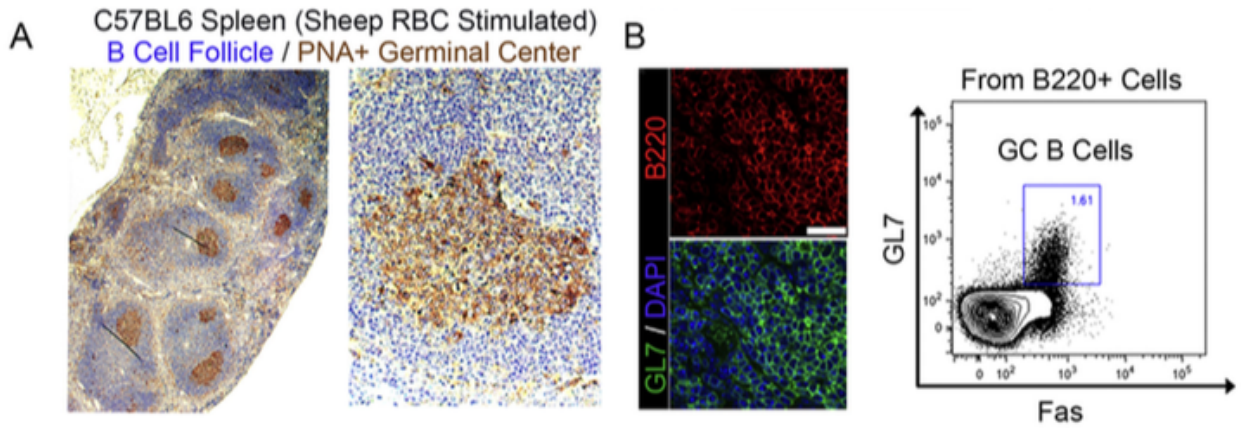

Figure 2-18: Assessment of *in vivo* GC reaction.
(A) Immunohistochemistry (IHC) analysis of B cell follicles for the presence of GC reaction based on B cell marker B220 and GC marker peanut agglutinin (PNA). IHC was obtained from paraffin-embedded murine splenic sections. (B) The left image indicated immunofluorescence (IF) analysis of B cell follicles for the presence of GC reaction using B cell marker B220, GC marker GL7, and nuclear stain DAPI. The scale bar in these images represented 50 mm. The right image showed flow cytometry analysis of B220+ primary B cell population from immunized C57BL6 mice with the gate indicating GL7+ Fas+ GC B cells.

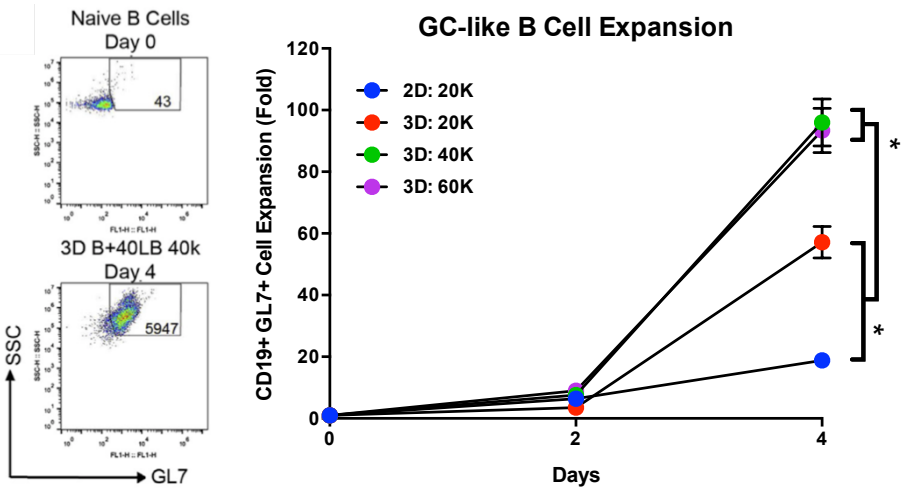

Figure 2-19: Induction of GC-like CD19+ GL7+ B cells in 2D culture and 3D organoid
The immune organoid was prepared with increasing stromal density. (Left) Gating schematic for flow cytometry analysis. (Right) Quantified GC-like B cell expansion as a function of culture period. Statistical significance (*) was determined based on $P < 0.05$. Statistical test was conducted using ANOVA. Values are shown as mean ± SEM (n = 5).

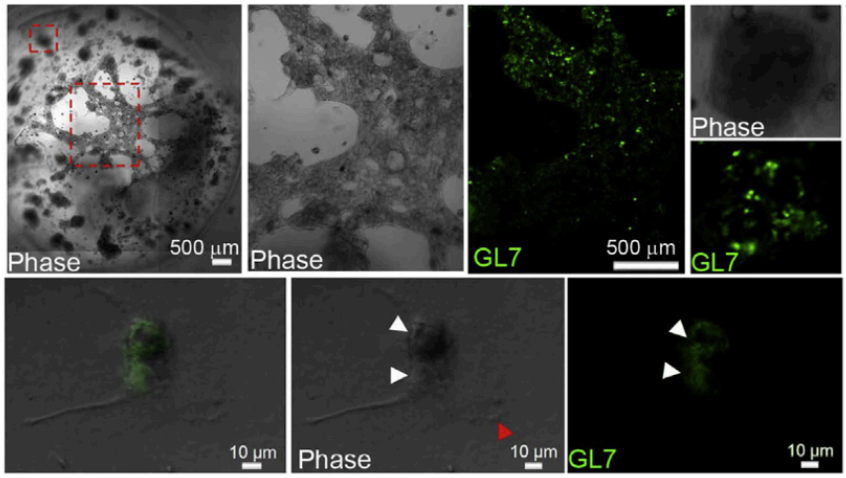

Figure 2-20: Imaging analysis of GC-like CD19+ GL7+ B cells in 3D. Imaging was conducted with phase contrast and immunofluorescence. The images were taken with either 10 or 500 µm scale bar.

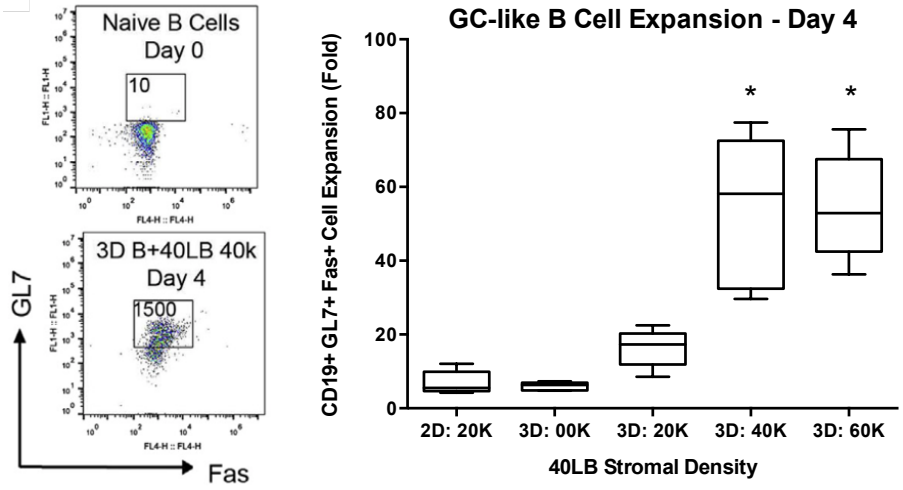

Figure 2-21: Induction of GC-like CD19+ GL7+ Fas+ B cells in 2D culture and 3D organoid
The immune organoid was prepared with increasing stromal density. (Left) Gating schematic for flow cytometry analysis. (Right) Quantified GC-like B cell fold expansion as a function of time. Statistical significance (*) was determined based on $P < 0.05$. Statistical test was conducted using ANOVA. Values are shown as mean ± SEM (n = 5).

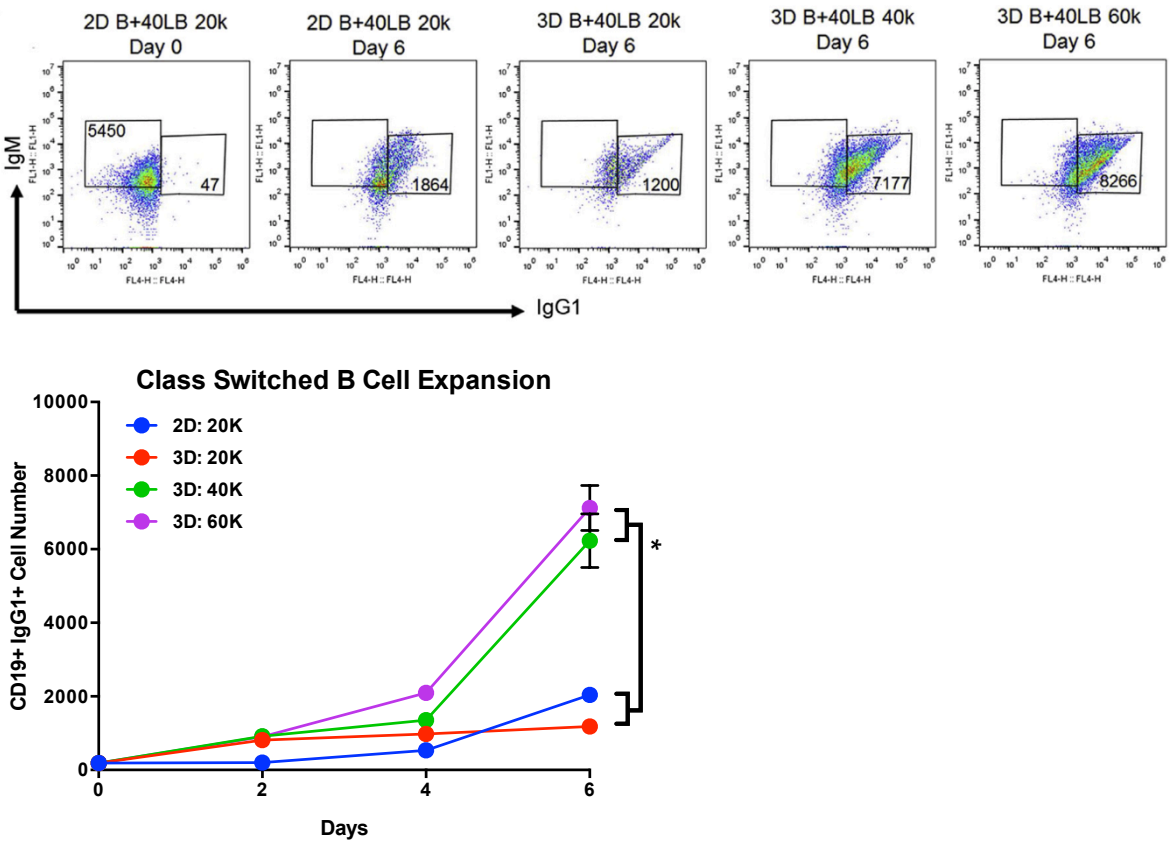

Figure 2-22: Generation of CD19+ IgG1+ B cells in 2D culture and 3D organoid
The immune organoid was prepared with increasing stromal density. (Top) Gating schematic for flow cytometry analysis. (Bottom) Quantification of class switched B cell number as a function of time. Statistical significance (*) was determined based on $P < 0.05$. Statistical test was conducted using ANOVA. Values are shown as mean ± SEM (n = 5).

CHAPTER 3

Characterizing Immune Organoids and Studying Germinal Center Maintenance Mechanisms

3.1. Abstract

Understanding the importance of characterizing the gelatin-based immune organoids, we compared *ex vivo* organoid derived GC-like B cells with *in vivo* GC B cells from immunized mice. We demonstrated that our system compares well with its native counterpart based on viability, acquisition of signature GC transcriptome, and somatic hypermutation. We also learned that the use of biomaterials impart superior viability, higher proliferation, and better acquisition of GC transcriptome when compared to the results seen using 2D co-culture method. Since tracking GC B cells in the lymphoid tissue has been difficult due to their heterogeneity and constant cycling into/from the GC reaction, we showed a potential application of this approach in studying EZH2-dependent cell cycle regulation that enables GC B cell proliferation.

3.2. Introduction

The previously described immune organoids was developed with the goal of obtaining mechanistic insights about immune response generation, modeling lymphoid transformations that trigger certain diseases, and identifying biomolecules that can interact with the immune system. Complementing the traditional animal models, the organoid platform is expected to facilitate these studies with lower cost, reduced complexity, and higher experiment throughput. As primary GC B cells have been known to quickly undergo apoptosis following isolation, it can be challenging to functionally characterize in culture and such situation has prevented us from studying GC mechanistically with *ex vivo* techniques.

This study was carried out by Wendy Béguelin, PhD, and Matt Teater from the Ari M. Melnick Lab at Weill Cornell medicine and the resulting manuscript has been submitted for publication.

Nevertheless, it is important to ensure that the B cells generated from immune organoid recapitulate the relevant cellular phenotype prior to conducting the aforementioned studies. In order to understand how the GC-like B cells from the immune organoid compare with their *in vivo* counterpart, we have to perform in-depth characterization that ranges from proliferation assay to gene expression analysis via RNA sequencing. Following these validation steps, we can then continue with performing mechanistic studies to demonstrate its utility in immunology research.

Characterization can be done primarily by using several assessment metrics to compare *ex vivo* organoid-derived GC like B cells and *in vivo* GC B cells isolated from immunized mice. From the literatures, the GC B cell population is typically identified by looking at several surface markers that include canonical B cell marker (e.g. B220 or CD19) and GC marker (e.g. GL7, Fas, and/or PNA). Further identifications are usually made by looking into the presence of GC-specific transcription factors (e.g. BCL6, PAX5, and/or EZH2). Gene expression analysis can also be done to gain a comprehensive transcriptome analysis of the cell, although such method tends to be used for understanding specific GC B cell subsets that are formed over the course of GC reaction from induction to exit and differentiation.

Upon the completion of characterization and validation steps, one mechanism that can be explored is the rapid proliferation of GC B cells over the course of humoral immune response [118, 119] . Such area of research is applicable due to the enhanced GC-like B cell formation seen in the immune organoids and the current lack of understanding regarding what exactly mediates the GC proliferative response. Our initial hypothesis is that epigenetic changes drive GC proliferation by repressing the cell cycle checkpoint genes. Based on the scientific literatures, massive cell proliferation is possibly mediated by the silencing of cell cycle checkpoint genes via epigenetic mechanisms [120, 121]. In the context of GC reaction, epigenetic silencing of several genes is partially mediated by the Polycomb protein EZH2 with a specific expression only in GC B cell population [122, 123]. EZH2 has been implicated in enabling cellular proliferation in other cell types by repressing cyclin dependent kinase inhibitors. Interestingly, only modest reduction in

cell cycle was observed in stimulated *Ezh2* KO primary B cells [124]. At the same time, depleting or inhibiting EZH2 via pharmacologic means in GC-derived lymphoma cells resulted in strong anti-proliferative effect along with reduced repression of CDKN1A relative to other checkpoint genes [123, 125]. Based on these observations, EZH2 appear to drive cellular proliferation during GC reaction.

Nevertheless, it is challenging to test the hypothesis that EZH2 promotes GC proliferation via CDKN1A suppression because the resulting data has not been that clear. This situation can be attributed to the fact that GC reactions are very heterogeneous in mice with B cells constantly entering, cycling, and leaving. Such complexity is compounded with the knowledge that EZH2 amount in mice circulation will vary following drug administration. It will not be technically or financially feasible to optimize the process because hundreds of mice over years will be required. While *ex vivo* functional studies may provide an alternative way to test the aforementioned hypothesis, there is currently no reliable technique available to obtain purified GC B cells from *Ezh2* KO mice. Based on these limitations, we will be using the organoid system to help determine if EZH2 alone can drive GC cell cycle via epigenetic repression of CDKN1A.

3.3. Approach

The biomaterials-based 3D immune organoid will be prepared as previously described by co-encapsulating both primary naïve B cells and 40LB stromal cells in RGD-presenting gelatin matrix ionically crosslinked with SiNP. Based on the frequently described characteristics of GC B cells, we plan on characterizing the organoid-derived GC-like B cells from its proliferation, viability, surface markers, gene expression, and somatic hypermutation.

The proposed application of our immune organoid platform is investigating the mechanics of GC reaction in two ways: the dependence on EZH2 and the ability of rescuing GC reaction in EZH2 null phenotype by knocking out *Cdkn1a*. The study will be carried out with the use of transgenic mice and pharmacologic

inhibition. In the first method, conditional *Ezh2*$^{fl/fl}$ knockout (KO) mice with Cγ1-Cre strain would be utilized with *Ezh2* getting knocked out following post-CSR IgG1 transcription (i.e. EZH2 would be knocked out upon GC induction). In the second method, *Ezh2* KO would be applied by GSK343 administration since this compound had been known to inactivate EZH2 by suppressing EZH2 methyltransferase activity.

3.4. Organoid Characterization

Having previously shown that immune organoids enhance GC-like B cell generation and promote the induction of GC-relevant markers, we further validated these observations with various biological assays. Similar to our previous observation, phase images showed the formation of cell clusters inside the hydrogel after 3 days of culture (Figure 3-1). In order to determine the composition of these cell clusters, IF images were obtained from hydrogels containing GFP+ B cells and the resulting data indicated that the cell clusters mainly consisted of primary B cells (Figure 3-1). While the formation of cell clusters brings to mind the morphology of a developing GC reaction, another way to define the GC phenotype is by looking into the expression of GC-specific surface markers in the B cell population. We then looked into the percentage of live B cells expressing both GL7 and Fas to measure GC induction inside the immune organoids (Figure 3-2). From the resulting data, the percentage of GL7+ Fas+ GC-like B cells increased from 20% (day 2) to 39% (day 3) and was maintained at a similar level with 38% (day 5) and 30% (day 7). Such trend indicated a sustained GC induction in the immune organoids.

Since GC phenotype is generally associated with proliferative capacity and the formation of B cells clusters is indicative of cell proliferation, we next analyzed cell expansion using eFluor670 proliferation dye with dye intensity reduction serving as a measure of cell proliferation (Figure 3-3). The resulting data showed that more than 80% of live GC-like B cells had proliferated after 7 days of culture and the biggest

increase in proliferation occurred prior to day 2 as shown by the highly reduced proliferation dye intensity. We can thus infer that massive cell proliferation occurred inside the immune organoids. Although GC B cells have been known to undergo apoptosis in culture, organoid GC-like B cells showed a similar rate of apoptosis to the one exhibited by GC B cells isolated from immunized animals (Figure 3-4). The approximate apoptosis rate of 10% was obtained based on the amount of cells that appeared positive for Annexin V. This observation suggests that organoid-derived GC-like B cells exhibit a comparable viability with their *in vivo* counterparts.

Despite the encouraging GC phenotype that includes comparable viability, the next step is to continue the benchmarking process by specifically looking into whether organoid-derived GC-like B cells have obtained the characteristic GC transcriptome. This analysis was carried out by looking into the RNA-seq profile of B220+ GL7+ Fas+ organoid-generated GC B cells. Principal component analysis (PCA) was first done to analyze the gene expression data and identify the two principal components responsible for the majority of variances. Using PCA space defined by *in vivo* GC B cells, plasma cells, and NB cells, we observed the acquisition of signature GC transcriptome based on the relative proximity of the day 4 organoid GC-like B cells cluster with the *in vivo* GC B cells cluster (Figure 3-5). Interestingly, we also noted the induction of ASC differentiation with the shift of the day 6 organoid GC-like B cells cluster toward the plasma cells cluster. Gene ontology tree analysis further supported these GC induction and differentiation trends (Figure 3-6). The resulting data implied that while day 4 organoid GC-like B cells resembled *in vivo* GC B cells, day 6 cells had undergone differentiation toward PC phenotype. Gene expression heatmap was next utilized to look into the genes that strongly influenced each principal component (Figure 3-7). Since PC2 appeared to describe the GC induction program, we saw that GC marker genes (e.g. *Aicda*) were similarly upregulated in both organoid and *in vivo* GCB cells. With PC1 seemed to define the ASC differentiation program, we noticed that ASC marker genes (e.g. Sdc1, Prdm1 and Xbp1) were similarly downregulated in both organoid and *in vivo* GCB cells. We can therefore conclude that the gene expression pattern of the organoid GC-like B cells resembled that of the *in vivo*

GC B cells instead of naïve B cells or plasma cells. Using GSEA, we also learned that the GCB gene signature (i.e. a set of genes that are strongly correlated with GCB phenotype) was enriched in the organoid gene expression profile (Figure 3-8). These results suggest that *ex vivo* organoid-derived GC-like B cells can represent *in vivo* GC B cells from the transcriptome perspective.

Further supporting the transcriptome analysis, we utilized qPCR to confirm that the characteristic GC genes (e.g. *Ezh2*, *Bcl6*, and *Aicda*) were similarly upregulated in both organoid-derived GC-like B cells and *in vivo* GC B cells (Figure 3-9). In order to verify that these genes were translated into proteins, we conducted flow cytometry analysis on intracellular EZH2 expression and showed that EZH2 was expressed at a comparable level in both populations (Figure 3-10). This observation further supports the idea that these relevant GC genes were expressed and translated in the immune organoid system.

Since *ex vivo* activation protocols have been known to result in B cell proliferation and induction of GC-like surface markers (e.g. GL7 and Fas), we wanted to determine if the 3D organoid GC-like transcriptional profile resulted simply from the proliferative phenotype. In other words, we checked whether the transcriptional similarities came purely from organoid-mediated changes in the proliferation genes or not. We tested this argument by excluding proliferation-related genes from the RNA-seq profiles of organoid GC-like B cells and then repeating the PCA analysis along with naïve B cells, GC B cells, and plasma cells (Figure 3-11). It turned out that the exclusion of proliferation-related genes did not change the previously observed trend from earlier where the cluster of day 4 organoid GC-like B cells was located close to the one for *in vivo* GC B cells.

One hallmark event that occurs during GC reaction is somatic hypermutation, specifically high rate of mutations occurring in the immunoglobulin gene variable regions. In order to determine whether somatic hypermutation transpired in the GC organoid system, immunoglobulin variable loci were amplified from naïve B cells, organoid-derived GC-like B cells, and GC B cells from primed mice (Figure 3-12).

Looking at four loci (JH4, Sμ, VHJ558, and Vλ1), the resulting data denoted a significant increase in missense mutations and indels in GC-like B cells in comparison to NB cells. Furthermore, the mutation profile of the *ex vivo* GC-like B cells appeared to be comparable to the *in vivo* GC B cells. These mutations in immunoglobulin gene variable regions further showed that the GC organoid system recapitulated the key aspects of a developing GC reaction.

We have seen that the 3D immune organoids facilitated the generation of GC-like B cells with sustained GC induction, high cell proliferation, and various similarities to *in vivo* GC B cells (e.g. viability, transcriptome, and somatic hypermutation). But we have yet to determine if these outcomes were driven by the 40LB stromal component or the biomaterials-based niche. From assessing the proliferative phenotype, a greater percentage of proliferative GC-like B cells were observed with 2-3 greater amounts at any day (Figure 3-13). This trend demonstrated that the high cell proliferation was sustained in immune organoids. Cell viability assessment with Annexin V demonstrated a greater percentage of apoptotic cells in 2D co-culture (27%) vs. 3D organoid (11%) after day 6 in culture (Figure 3-14). This behavior was consistent throughout 7 days of culture and therefore indicating high cell viability in immune organoids. Looking into the BCL6 transcription factor expression with flow cytometry, highest BCL6 expression was seen in *in vivo* GC B cells then followed by 3D organoid GC-like B cells and finally 2D GC-like B cells (Figure 3-15). Naïve B cells were used as the control group since their BCL6 expression level was close to the background level produced by isotype control.

PCA assessment on the gene expression data showed that 2D GC-like B cells were more transcriptionally distant than organoid GC-like B cells with regards to *in vivo* GC B cells (Figure 3-16). From these observations, gelatin scaffold reinforced by silicate nanoparticles appeared to generate GC-like B cells that better represent *in vivo* GC B cells based on the improved acquisition of signature GC transcriptome.

3.5. Mechanistic Investigation into EZH2 and CDKN1A

Having shown that the immune organoid platform can be used to model the GC reaction, we next assessed the EZH2 dependency of GC-like B cell generation in the immune organoid. We also verified if the *Ezh2* conditional KO system could be implemented in this platform for GC mechanistic studies. The latter was done by determining if the conditional *Ezh2*$^{fl/fl}$ Cγ1-cre *Cdkn1a*$^{-/-}$ KO phenotype observed in mice would be recreated by the immune organoids. In order to conduct this experiments, naïve B cells were isolated from four sources: *Ezh2*$^{fl/fl}$ Cγ1-cre *Cdkn1a*$^{-/-}$ (double KO), *Cdkn1a*$^{-/-}$ (*Cdkn1a* KO), E*zh2*$^{fl/fl}$ Cγ1-cre (*Ezh2* KO), and E*zh2*$^{fl/fl}$ (control). After encapsulating these cells in the organoid, reduction in the percentage of GL7+ Fas+ GC-like B cells was observed in single *Ezh2* KO system but not double KO or single *Cdkn1a* KO (Figure 3-17). Interestingly, *Ezh2* KO phenotype was rescued by *Cdkn1a* KO to prevent any disruption in the GC reaction. This data indicated that EZH2 promoted GC reaction in the organoid and conditional *Ezh2* KO system was successfully applied.

We next looked into the EZH2-dependent regulation of cell cycle in the immune organoids with the hypothesis that EZH2 suppresses CDKN1A to enable massive cell proliferation during GC reaction. Since the *Cdkn1a* gene is expected to inhibit the cell cycle transition in GC B cell from G1 to S phase, we looked into such transition based on the percentage of cells with newly synthesized DNA based on BrdU staining (Figure 3-18). The resulting data indicated that the BrdU+ cell population was reduced in *Ezh2* KO group based on flow cytometry analysis and no such effect was observed in either double KO or single *Cdkn1a* KO. While the result did not reach statistical significance possibly due to incomplete conditional *Ezh2* KO, the lack of EZH2 expression was validated in the double KO model (Figure 3-19).

Since EZH2 inactivation could also be done via pharmacologic inhibition, we exposed organoids to a single dose of EZH2 inhibitor after 1 day of culture and incubated the treated organoids for additional 4 days of culture before analysis. For the treatment, we used either GSK343 (EZH2 inhibitor) or GSK669

(control compound). The resulting data indicated a significant reduction in the percentage of GL7+ Fas+ GC-like B cells following GSK343 treatment only in the *Cdkn1a*$^{+/+}$ group (Figure 3-20). No such effect was seen in the same cell population from the *Cdkn1a*$^{-/-}$ group. Interestingly, we noted that GSK343 inhibited EZH2 methyltransferase activity as indicated by the reduced trimethylation of lysine 27 residue of histone H3 (H3K27Me3) without altering the EZH2 expression level (Figure 3-21) in both *Cdkn1a*$^{+/+}$ and *Cdkn1a*$^{-/-}$. Cell cycle analysis indicated a significant reduction of cells in S phase as indicated by the BrdU+ cell population only in the *Cdkn1a*$^{+/+}$ group following GSK343 treatment (Figure 3-22). Similar to the previous observation, no such effect was seen in the *Cdkn1a*$^{-/-}$ group after GSK343 exposure under the same protocol. These observations suggested the importance of EZH2 in mediating GC formation and proliferation with the latter by enabling cell cycle transition into S phase via CDKN1A repression. This insight also illustrates the use of immune organoids for GC mechanistic studies.

3.6. Discussion

Due to the lack of well-characterized artificial lymphoid tissues currently available for studying immune system mechanistically in culture, this study demonstrated an attempt toward characterizing our previously published B cell organoid platform and then functionally validating its application in the mechanistic investigation into GC reaction. Here we specifically analyzed the GC reaction from various dimensions: proliferation, viability, marker expression, transcriptome, and somatic hypermutation. From our understanding about GC phenotype, we demonstrated how our organoid system could model the GC reaction in animal models. Despite the strong similarities from various phenotypic studies (e.g. proliferation, viability, and marker expression), we also noticed some differences in the gene expression profile between GC-like B cells generated from the organoid and actual GC B cells harvested from immunized mice. As we have yet to understand what factors are required to increase the gene expression comparability, future investigations will be focused toward investigating the role of other variables such as antigens, specific integrins, and cytokine types.

We also showcased two potential applications of our technology: investigating the biological mechanisms behind the complex GC reaction and identifying immunomodulatory agents. While the current study was focused on understanding how EZH2 could facilitate GC B cell proliferation and demonstrating how GSK343 worked as a specific EZH2 inhibitor, we can expand this observation into studying other mechanisms that regulate the GC reaction and analyzing other relevant pharmacologic inhibitors (e.g. SYK or BTK inhibitor). We also need to utilize this approach to systematically understand the role of various microenvironment signals that may influence B cell development and activation. We anticipate that such biomaterials-based *ex vivo* immune organoids to be further utilized in mechanistic research studies and immunomodulatory drug development works.

3.7. Materials and Methods

3.7.1. Mouse Models

Conditional *Ezh2* KO mice (*loxP*-flanked *Ezh2* allele – $Ezh2^{fl/fl}$) were generously provided by Dr. Alexander Tarakhovsky at Rockefeller University [126]. By crossing $Ezh2^{fl/fl}$ with the transgenic Cγ1-cre strain we generated heterozygous $Ezh2^{fl/WT}$ mice that were then crossed to obtain $Ezh2^{fl/fl}$ mice. These mice were crossed to $Cdkn1a^{-/-}$ to obtain $Ezh2^{fl/WT}$ Cγ1-cre^{+} $Cdkn1a^{-/+}$ heterozygous that were then further crossed to yield $Ezh2^{fl/fl}$ Cγ1-cre^{+} $Cdkn1a^{-/-}$ double KO. Control groups consisted of $Ezh2^{fl/fl}$ Cγ1-cre^{-} and the single KOs $Ezh2^{fl/fl}$ Cγ1-cre^{+} and $Cdkn1a^{-/-}$ littermates. The following strains were purchased from The Jackson Laboratory: Cγ1-cre^{+} (010611), $Cdkn1a^{-/-}$ (003263), $E2F1^{-/-}$ (002785), B6129SF2/J (101045) and C57BL6 (000664).

3.7.2. GC B Cell Generation from Immunized Mice

Age- and sex-matched mice were immunized intraperitoneally at 8 to 12 weeks of age with either 0.5 ml of a 2% SRBC suspension in PBS (Cocalico Biologicals) or 100 μg of highly substituted NP(32)-KLH (Biosearch Technologies) in alum (Thermo Scientific) and sacrificed after 8-10 or 14 days, respectively. All procedures have been approved by the Research Animal Resource Center of the Weill Cornell Medicine.

3.7.3. Immune Organoid Fabrication

Spleens were harvested from C57BL6, B6129SF2/J, *Cdkn1a*$^{-/-}$ single KO, *Ezh2*$^{fl/fl}$ Cγ1-cre single KO, *Ezh2*$^{fl/fl}$ Cγ1-cre *Cdkn1a*$^{-/-}$ double KO and *Ezh2*$^{fl/fl}$ mice. Splenocytes were prepared using mechanical and gradient separation methods (Fico/Lite-LM, Atlanta Biologicals). B cells were purified from splenocytes using EasySep Mouse B Cell Isolation Kit (Stem Cell Technologies, 19854) with a yield of ~90% B220+ B cells. 40LB stromal cells expressing CD40L and secreting BAFF were generated as reported earlier by Nojima et al [48] and cultured in DMEM medium with 10% FBS and penicillin G/streptomycin. 40LB stromal cells were mitotically inhibited by incubation in medium containing 0.01 mg/ml Mitomycin C (Sigma-Aldrich, MO503) at 37 °C for 55 minutes and were rinsed twice with PBS before encapsulation.

Gelatin stock solution was freshly prepared by dissolving gelatin powder (Sigma Aldrich) in RPMI 1640 medium and sterilizing it with syringe filter. Cells were suspended in 5% gelatin stock solution and diluted accordingly using cell culture medium. Silicate nanoparticles (SiNP) with 25-30 nm in diameter and 1 nm in thickness was obtained from Southern Clay Products Inc., USA. 3% hydrogel SiNP suspension was freshly prepared prior to the encapsulation procedure by mixing SiNP powder with deionized water and vortexing the resulting solution immediately before use. Organoids were fabricated in 96-well plates by first adding 10 μL of 3% hydrogel SiNP, injecting 10 μL of cell-containing gelatin

solution into the initial SiNP droplet, and then mixing the entire hydrogel through repeated pipetting. Each organoid contained 50,000 B cells and 80,000 40LB cells. Organoids were cured for approximately 10 minutes and then covered with RPMI medium containing 10% FBS, penicillin G/streptomycin, and 50 ng/ml murine recombinant IL-4 (R&D, 404-ML). The organoids were incubated at 37 °C with 5% CO2 and the cell culture medium was replaced every 3 days.

3.7.4. Flow Cytometry Analysis

Cell suspensions from mouse spleens or immune organoids were stained using the following fluorophore-conjugated anti-mouse antibodies: PE-Cy7 conjugated anti-B220, APC conjugated anti-CD38 (eBioscience), APC conjugated anti-B220, PE and PE-Cy7 conjugated anti-Fas, FITC conjugated anti-GL7, Alexa Fluor 488 conjugated anti-EZH2, Alexa Fluor 488 conjugated IgG1κ isotype control, V450 conjugated anti-BrdU (BD Biosciences), Alexa Fluor 674 conjugated anti-H3K27Me3, Alexa Fluor 674 conjugated IgG isotype control (Cell Signaling), PerCP-Cy5.5 conjugated anti-GL7 (BioLegend). DAPI was used for the exclusion of dead cells. 7AAD was used to determine DNA content in cell cycle analysis. For internal markers, cells were fixed and permeabilized with BD Cytofix/Cytoperm Fixation/Permeabilization Solution Kit (BD Biosciences) and further permeabilized with cold Phosflow Perm Buffer III (BD Biosciences). Cell proliferation was measured by first labeling B cells with the proliferation dye eFluor670 (eBioscience) prior to encapsulation. PE-conjugated Annexin V in Annexin V binding buffer (BD Biosciences) was used to identify apoptotic cells. Flow cytometry data were acquired using BD FACSCanto (BD Biosciences) and analyzed with FlowJo software package.

3.7.5. RT-qPCR

RNA was prepared using Trizol extraction (Invitrogen). cDNA was prepared using cDNA synthesis kit (Thermo Scientific) and detected by fast SyberGreen (Applied Biosystems) on 7900HT Fast Real-Time PCR System (Applied Biosystems). Gene expression was normalized to HPRT1 and the values were

presented relative to control with the ΔΔCT method. qPCR results were provided as fold expression with the standard deviation for 2 series of triplicates.

3.7.6. qPCR Primers

Used for	Gene		Oligonucleotide (5'-3')
cDNA	*Aicda*	Fwd	CCTCCTGCTCACTGGACTTC
		Rev	CAGGAGGTGAACCAGGTGAC
	Bcl6	Fwd	GCGAACCTTGATCTCCAGTC
		Rev	TGACTCTCACTGCTGCTTCG
	Cdkn1a	Fwd	GTGGCCTTGTCGCTGTCT
		Rev	TTTTCTCTTGCAGAAGACCAATC
	Ezh2	Fwd	ATCTGAGAAGGGACCGGTTT
		Rev	GCTGCTTCCACTCTTGGTTT
	Hprt1	Fwd	TATGCCGAGGATTTGGAAAA
		Rev	AATCCAGCAGGTCAGCAAAG

3.7.7. RNA-seq library preparation and Illumina sequencing processing

RNA-seq libraries were constructed with TruSeq RNA Sample Prep Kit (Illumina). Libraries were validated using the Agilent Technologies 2100 Bioanalyzer and Quant-iT dsDNA HS Assay (Life Technologies) and 8-10 pM sequenced on HiSeq2000 sequencer mRNA-seq, 2 x 50.

3.7.8. RNA-seq analysis

RNA sequencing results were aligned to mm10 using STAR [127] and annotated to RefSeq using the R subread package [128]. Genes with differential expression between naïve B and GC B cells were identified using the EdgeR package GLM [129] with thresholds of fold-change >1.5 and $p<0.01$ adjusted

for multiple testing using Benjamini-Hochberg correction. PCA was performed on centered, log-transformed FPKM values using the prcomp() function within R framework. Principal component genes were defined as those with 2 standard deviations above or below the respective mean loading factor. Unrooted phylogenetic tree was created using neighbor-joining tree estimation within the ape R package [130]. GSEA was conducted using the previously described algorithm [131].

3.7.9. Immunoglobulin Somatic Hypermutation Analysis

Somatic hypermutation analysis was conducted using genomic DNA from (1) naïve B and GC B cells sorted from 3 immunized WT mice, (2) naïve B cells from 3 naïve WT mice used for immune organoid fabrication, and (3) GC B cells sorted from day 6 immune organoids. IgH and Igλ regions were amplified with PCR using primers that anneal to the framework region of the most abundant families of immunoglobulin rearrangements as previously described [132-135]. PCR products were cleaned up using the MinElute PCR Purification kit (QIAGEN) and then purified using the Gel Extraction Kit (QIAGEN). Sequencing libraries were constructed from the purified PCR product with TruSeq DNA Sample Preparation Kit v2 (Illumina). Each sample was tagged with a unique index and sequenced on the Illumina MiSeq platform producing 2x151 base-pair paired-end reads. Paired-end reads were mapped against the *Mus musculus* primary assembly GRCm38 using aligner Star 2.4.0 [127]. A pileup of the resulting sorted bam files was made in samtools for each targeted region and filtered using >20 quality score. A list of all single nucleotide polymorphisms was made using VarScan 2.3.4 on each base with minimum read depth of 10 reads and tabulated per targeted region into bed-files [136]. The mutation rate per kilobase was calculated by dividing the average missense or indels per base by the average coverage of sequenced read and multiplying by 1000 to obtain the rate of missense or indels per kilobase.

3.7.10. Immunoglobulin Somatic Hypermutation Primers

Locus		Oligonucleotide (5'-3')
JH4	Fwd	GTCAAGGAACCTCAGTCACCGTCT
	Rev	CAGACCTCTCTAGACAGCAACTACC
Sμ	Fwd	AATGGATACCTCAGTGGTTTTTAATGGTGGGTTTA
	Rev	GCGGCCCGGCTCATTCCAGTTCATTACAG
VHJ558	Fwd	CGAGCTCTCCARCACAGCCTWCATGCARCTCARC
	Rev	TCTCAGCCGGCTCCCTCAGGG
Vλ1 - Jλ1,3	Fwd	GCCATTTCCCCAGGCTGTTGTGACTCAGG
	Rev	ACTCACCTAGGACAGTCAGCTTGGTTCC

3.8. Acknowledgement

The work described in this chapter was financially supported by the American Society of Hematology Scholar to Wendy Béguelin, Ph.D., the National Cancer Institute R01 CA187109 to Prof. Ari Melnick, and the Leukemia and Lymphoma Society Translational Research Program 6141-14 to Prof. Ari Melnick. The biological concept and the methodology were developed by Wendy Béguelin, Ph.D. and Prof. Ari Melnick. Software, formal analysis, and data curation was carried out by Matt Teater. Resources pertaining to immune organoid application, fabrication, experiment setup, and analysis were provided by Alberto Purwada and Prof. Ankur Singh (Cornell University). Gene expression sample preparation was done by Wendy Béguelin, Ph.D., and Alberto Purwada. Visualization was performed by Wendy Béguelin, Ph.D. and Matt Teater. *Ezh2* KO mouse model was provided by Dr. Alexander Tarakhovsky (Rockefeller University). GSK compounds were provided by GlaxoSmithKline.

3.9. Figures

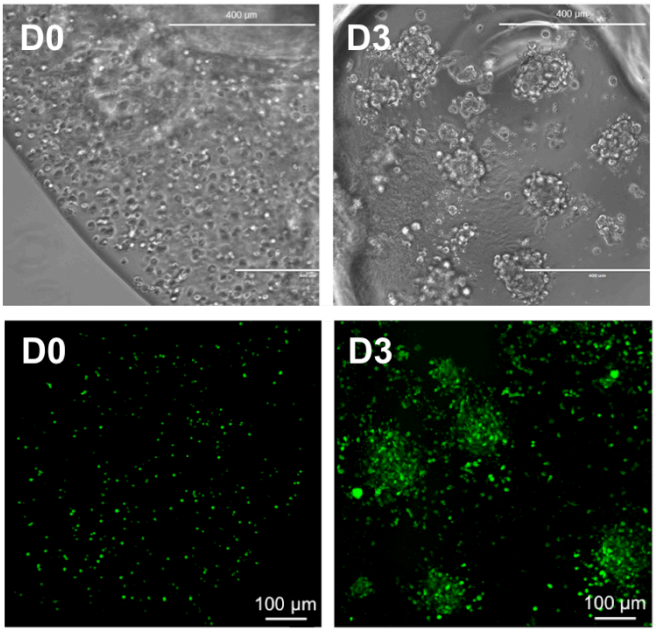

Figure 3-1: Imaging analysis of cell clustering in the organoid
(Top) Phase images were taken of the immune organoids. Images were taken with 400 µm scale bar. (Bottom) IF images were obtained from immune organoids containing GFP+ B cells. These B cells were isolated from the spleen of GFP mice prior to encapsulation. Images were taken with 100 µm scale bar.

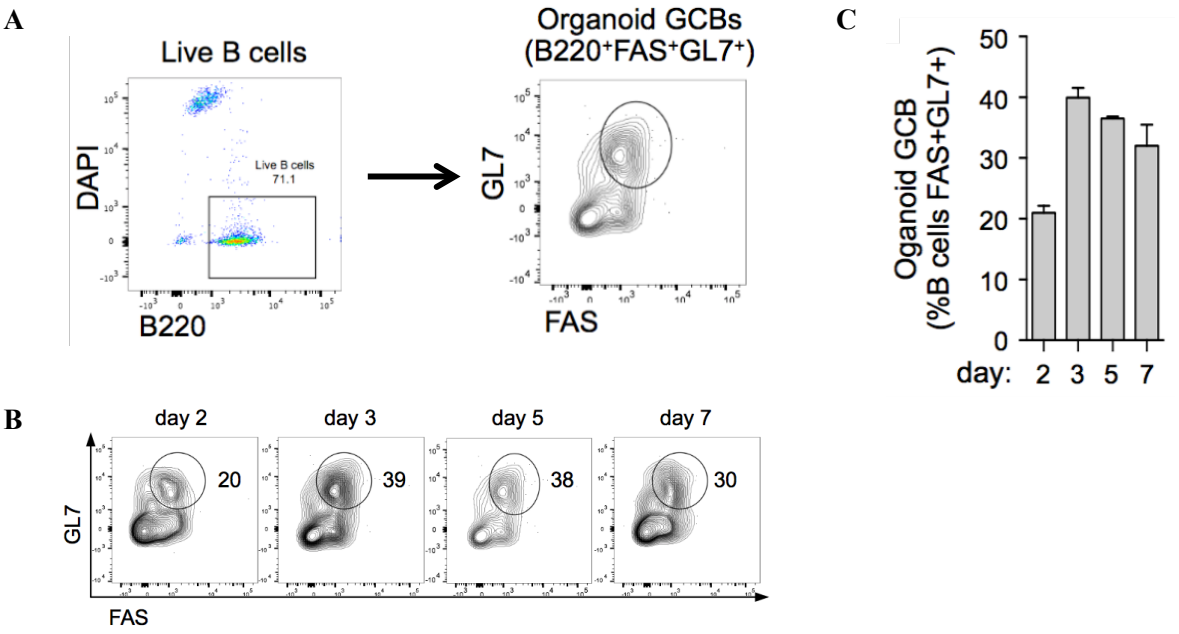

Figure 3-2: GC-like B cell generation in the immune organoid
GC induction was assessed based on GL7 and Fas double expression and measured as a function of time. (A) Gating schematic for flow cytometry analysis showing the initial selection of B220+ DAPI- live B cells and the subsequent selection of GL7+ Fas+ GC B cells within the live B cell population. (B) Representative flow cytometry plot indicating GC-like B cell percentage after 2, 3, 5, and 7 days in culture. Similar to the previously shown gating schematic, the gated area indicating organoid GC-like B cells was based on GL7+ Fas+ GC subset within B220+ DAPI- live B cell population. (C) Bar graph quantifying the average percentage of GC-like B cell subset in culture with flow cytometry analysis. Values are shown as mean ± SEM (n = 6).

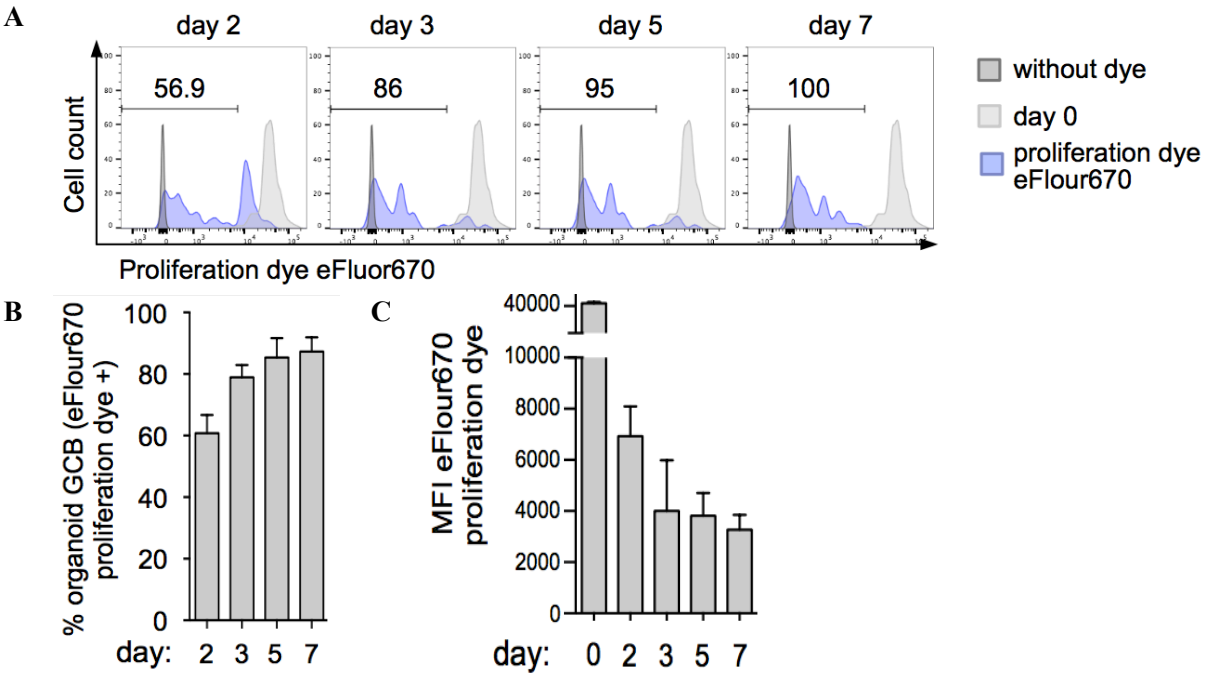

Figure 3-3: GC-like B cell proliferation in the immune organoid
Cell proliferation was measured using proliferation dye eFluor670. (A) Representative flow cytometry histogram for measuring the percentage of proliferating cells based on the fluorescence intensity of proliferation dye eFluor670 in organoid B220+ GL7+ Fas+ GC-like B cell population cultured for several days. (B) Bar graph quantifying the average percentage of proliferating GC-like B cells in culture with flow cytometry analysis. (C) Bar graph quantifying the average mean fluorescence intensity of proliferation dye eFluor670 in the organoid GC-like B cells. Values are shown as mean ± SEM (n = 6).

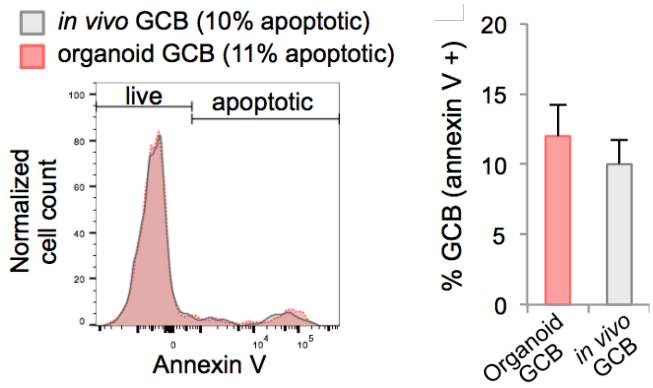

Figure 3-4: Cell viability assessment in both *in vivo* GC B cells and organoid GC-like B cells
Cell viability was measured using Annexin V. Organoid GC-like B cells that have been cultured for 5 days and GC B cells from immunized mice were used in this experiment. Positive Annexin V staining was used to identify apoptotic cells. (Left) Representative flow cytometry histogram for dividing the cell population into live and apoptotic based on Annexin V staining. (Right) Bar graph quantifying the average percentage of apoptotic GC B cells based on Annexin V intensity in both cell populations with

flow cytometry analysis. Values are shown as mean ± SEM (n = 6 for *ex vivo* GC-like B cells from immune organoids and n = 3 for *in vivo* GC B cells from immunized mice).

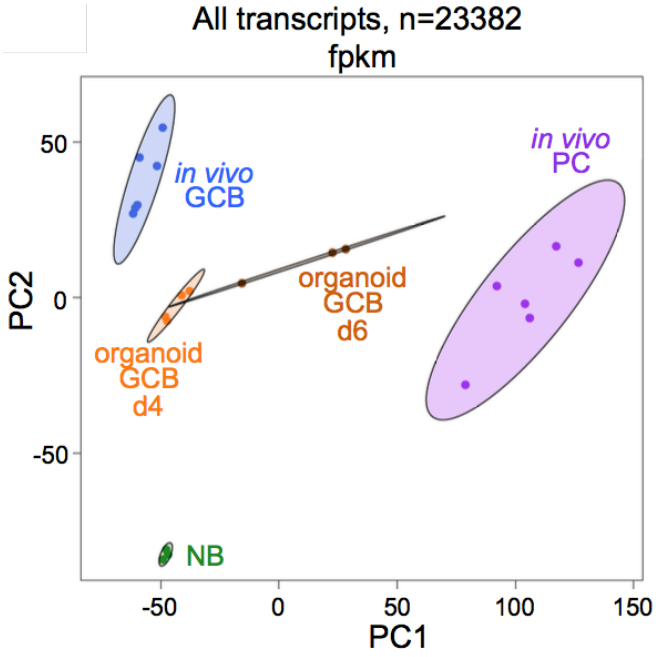

Figure 3-5: Principal component analysis on gene expression data
Gene expression was analyzed based on RNAseq profile from the following cell populations: B220+ GL7+ Fas+ *in vivo* GC B cells from immunized mice (*in vivo* GCB, n = 6), *in vivo* CD138+ PC (n = 6), B220+ GL7+ Fas+ *ex vivo* GC-like B cells from immune organoids (organoid GCB, n = 4 for day 4 and n = 3 for day 6), and B220+ IgD+ Fas- GL7- naïve B cells (NB, n = 3). The RNAseq profile from organoid GCB was projected into the principal component space defined by *in vivo* GCB, *in vivo* PC, and NB.

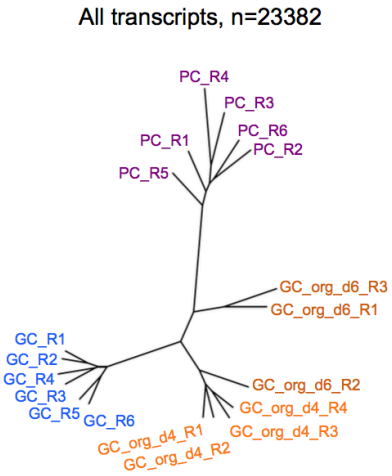

Figure 3-6: Gene ontology tree analysis
Unrooted phylogenetic tree analysis was conducted using RNAseq gene expression profile from B220+ GL7+ Fas+ *ex vivo* GC-like B cells from immune organoids cultured for 4 days (GC_org_d4, n=4) and 6 days (GC_org_d6, n=3), B220+ GL7+ Fas+ *in vivo* GC B cells from immunized mice (GC, n=6) and CD138+ *in vivo* plasma cells (PC, n=6).

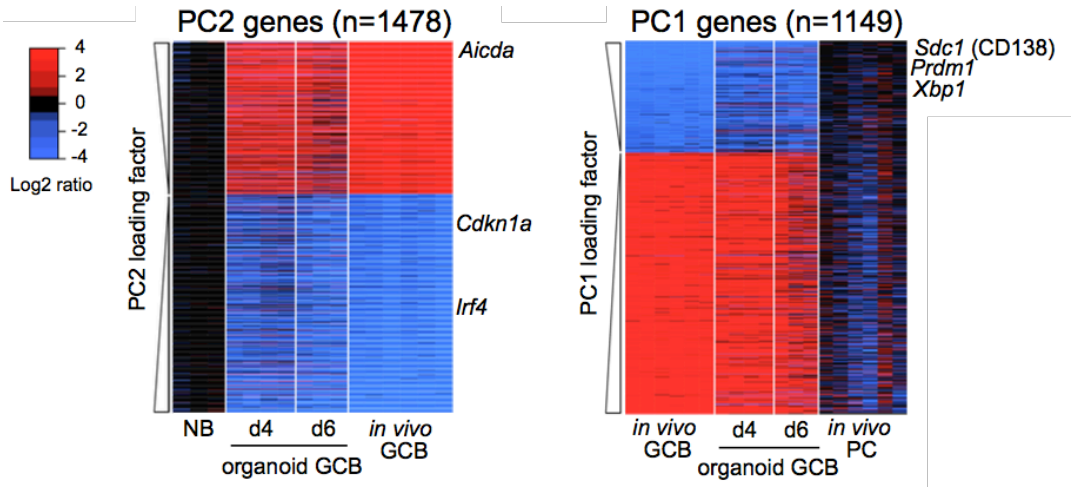

Figure 3-7: Heat map analysis on gene expression data
Gene expression level was represented as log2 ratio relative to either mean naïve B cells (left) or mean plasma cells (right). PC was defined as the principal component described in the previous PCA analysis. (Left) PC2 genes that explained the variances between *ex vivo* organoid GC-like B cells and *in vivo* GC B cells. (Right) PC1 genes that described the variances between *in vivo* GC B cells, *ex vivo* organoid GC-like B cells, and PC.

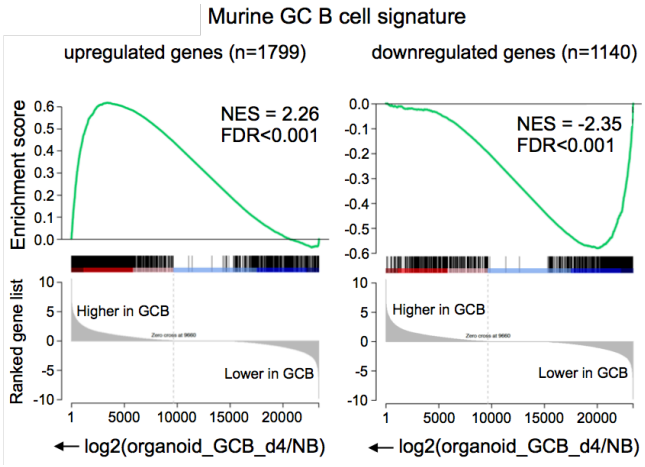

Figure 3-8: GC B cell signature enrichment analysis in organoid GC-like B cells
Analysis was conducted to measure the enrichment of murine GC B cell signature genes. Enrichment of upregulated (n=1,799) and downregulated (n = 1,140) genes in day 4 *ex vivo* organoid GC-like B cells was assessed relative to those of naïve B cells (B cells from day 0 prior to culture).

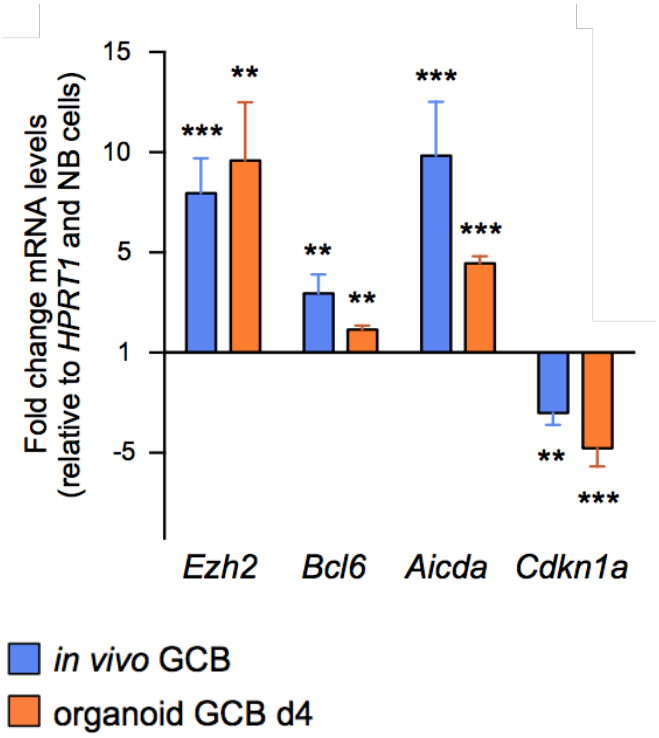

Figure 3-9: Expression of GC signature genes

RT-qPCR was conducted on several mRNAs from *ex vivo* organoid GC-like B cells (n = 3) and *in vivo GC* B cells (n = 3). Gene expression values were shown as mean fold change mRNA levels ± SEM normalized to the housekeeping gene HPRT1 and further normalized to mean mRNA levels in naïve B cells. Analysis was conducted on four genes: *Ezh2*, *Bcl6*, *Aicda*, and *Cdkn1a*. Statistical significance (*, **, and ***) was based on $p < 0.05$, $p < 0.01$, and $p < 0.001$, respectively. Statistical test was conducted using t test. Values are shown as mean ± SEM (n = 3).

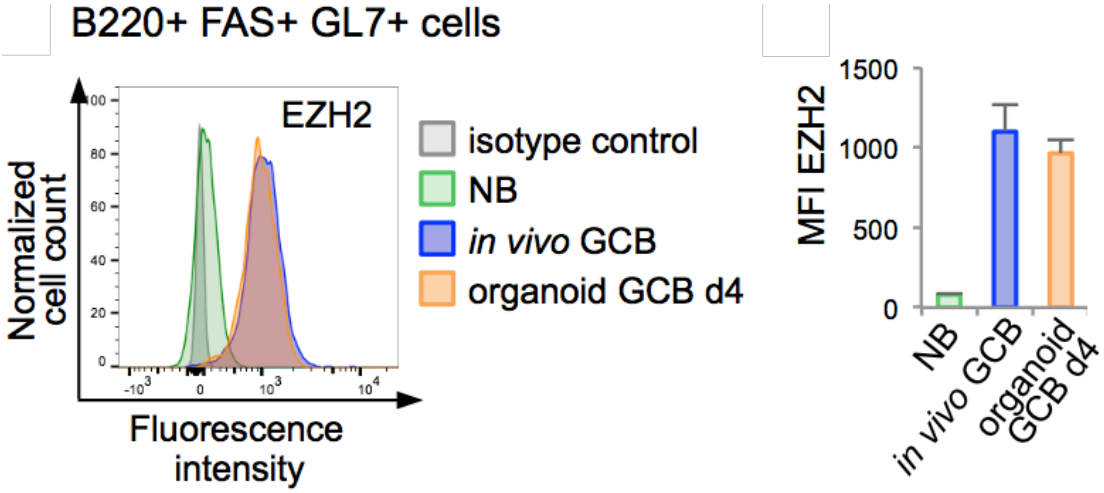

Figure 3-10: Intracellular EZH2 expression in various B cell populations

Cells from both immune organoids and immunized mice were fixed, permeabilized, and then stained for EZH2. Cells were co-stained to identify B220+ GL7+ Fas+ GC B cells and B220+ IgD+ GL7- Fas- naïve B cells. (Left) Representative flow cytometry histogram indicating the mean fluorescence intensity of EZH2 in various cell populations and isotype control. (Right) Bar graph quantifying the average mean fluorescence intensity of EZH2 intracellular expression in various B cell populations. Values are shown as mean ± SEM (n = 6 for *ex vivo* organoid GC-like B cells from immune organoids, n = 3 for *in vivo* GC B cells from immunized mice, and n = 3 for naïve B cells).

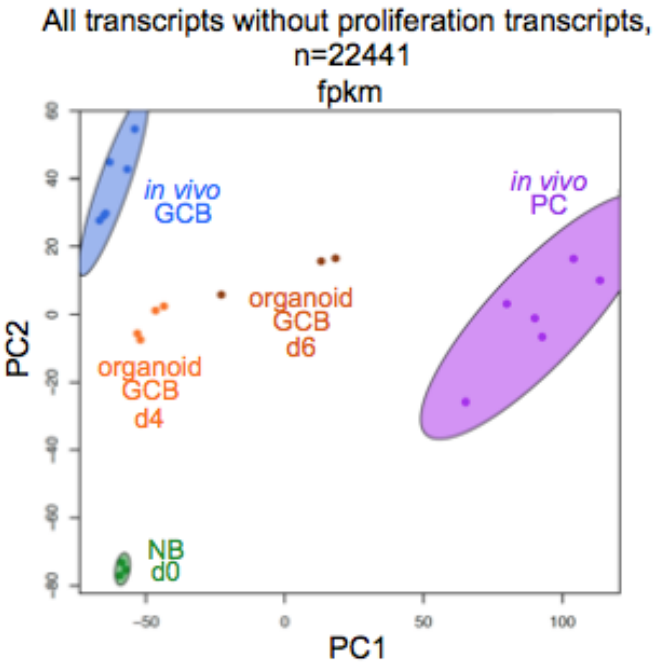

Figure 3-11: Principal component analysis on gene expression data without proliferation genes
Gene expression was analyzed based on RNAseq profile - excluding 941 proliferation-related genes - from the following cell populations: B220+ GL7+ Fas+ *in vivo* GC B cells from immunized mice (*in vivo* GCB, n = 6), *in vivo* CD138+ PC (n = 6), B220+ GL7+ Fas+ *ex vivo* GC-like B cells from immune organoids (organoid GCB, n = 4 for day 4 and n = 3 for day 6), and B220+ IgD+ Fas- GL7- naïve B cells (NB, n = 3). The RNAseq profile from organoid GCB was projected into the principal component space defined by *in vivo* GCB, *in vivo* PC, and NB.

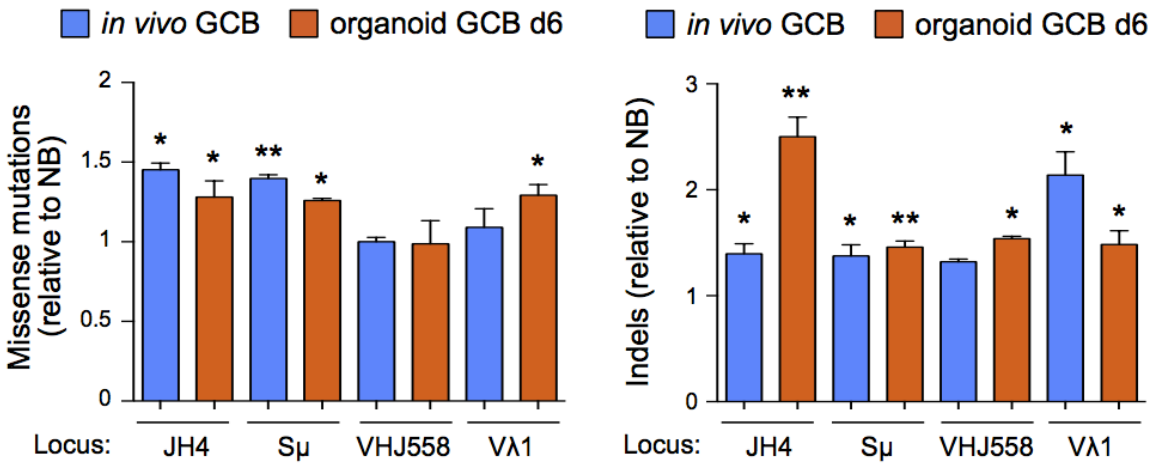

Figure 3-12: Somatic hypermutation analysis with immunoglobulin loci amplification
Measurement of missense mutations (left) and indels (right) in both *in vivo* GC B cells and day 6 organoid GC-like B cells was normalized to that of naïve B cells. Analysis was conducted on the following four loci: JH4, Sμ, VHJ558, and Vλ1. PCR was utilized to amplify the specified immunoglobulin variable loci from genomic DNA extracted from purified naïve B cells (day 0 before culture), *ex vivo* organoid GC-like B cells (day 6 in culture), *in vivo* GC B cells from immunized mice, and naïve B cells from the same mice. Sequencing libraries were constructed from the purified PCR products and sequenced on the Illumina MiSeq platform. The mutation rate per kilobase for each gene was calculated by dividing the average missense (N) or indels (O) per base by the average coverage of sequenced read. The average mutation rate per kilobase in GC B cells was normalized to the average in naïve B cells from the same cell source: immunized mice or immune organoids. Statistical significance (* and **) was based on $p < 0.05$ and $p < 0.01$, respectively. Statistical test was conducted using t test. Values are shown as mean ± SEM (n = 3).

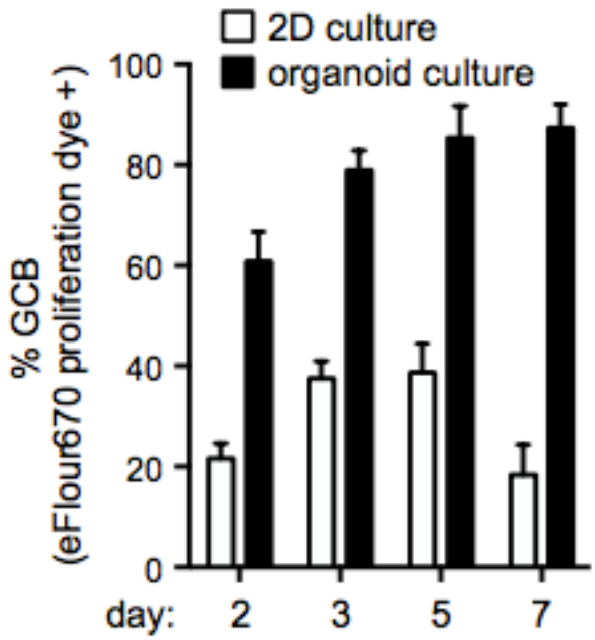

Figure 3-13: GC-like B cells proliferation in 3D immune organoids and 2D co-culture systems

Cell proliferation was measured using proliferation dye eFluor670. The percentage of proliferating cells was assessed based on the fluorescence intensity of proliferation dye eFluor670 in B220+ GL7+ Fas+ GC-like B cell population after being cultured for 2, 3, 5, and 7 days. Bar graph quantifying the average percentage of proliferating GC-like B cells in both culture methods for the specified days with flow cytometry analysis. Values are shown as mean ± SEM (n = 3).

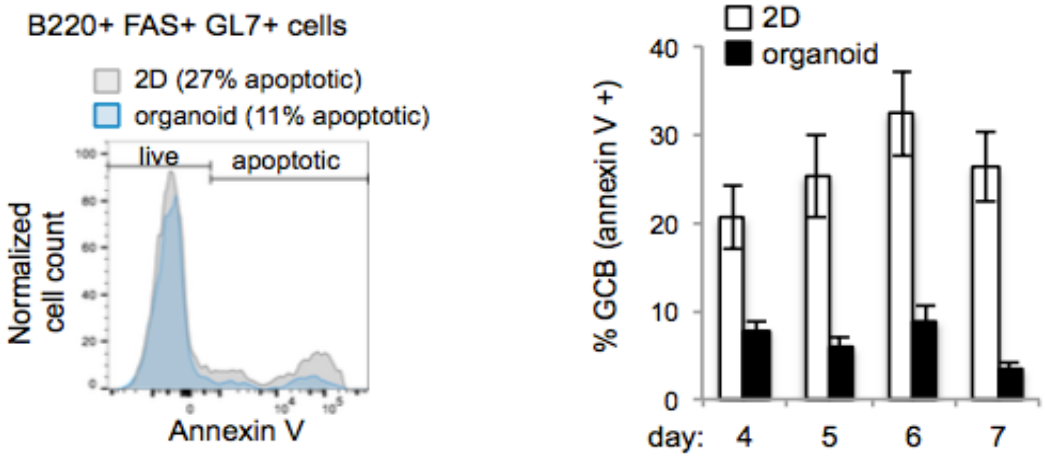

Figure 3-14: GC-like B cell viability in 3D immune organoids and 2D co-culture systems

Cell viability was measured using Annexin V. GC-like B cells that have been cultured for 5 days using both immune organoids and 2D co-culture systems were used in this experiment. Positive Annexin V staining was used to identify apoptotic cells. (Left) Representative flow cytometry histogram for dividing the cell population into live and apoptotic based on Annexin V staining. (Right) Bar graph quantifying the average percentage of apoptotic GC B cells based on Annexin V intensity in both cell populations with flow cytometry analysis. Values are shown as mean ± SEM.

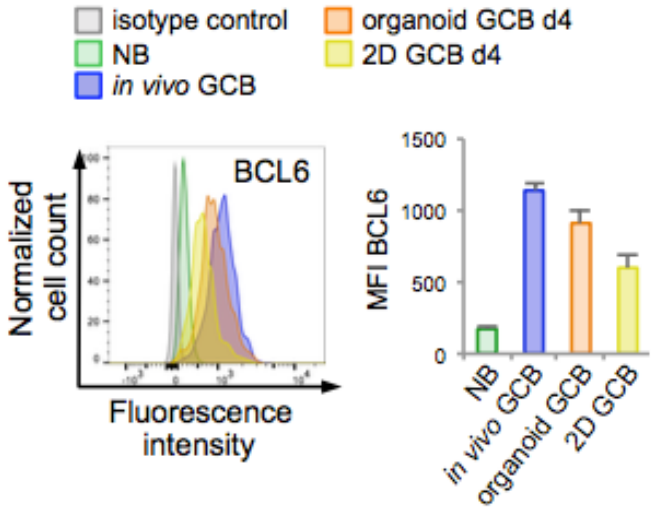

Figure 3-15: Intracellular BCL6 expression in various B cell populations
Cells from first isolated from immune organoids, co-culture systems, and immunized mice. The cells were then fixed, permeabilized, and stained for BCL6. (Left) Representative flow cytometry histogram indicating the mean fluorescence intensity of BCL6 in various cell populations and isotype control. (Right) Bar graph quantifying the average mean fluorescence intensity of BCL6 intracellular expression in various B cell populations. Values are shown as mean ± SEM (n = 3).

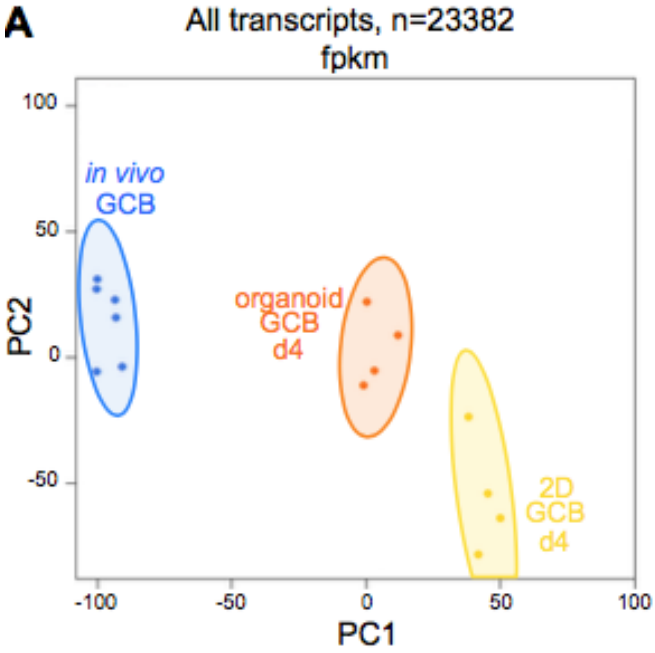

Figure 3-16: Principal component analysis of gene expression data
Gene expression was analyzed based on RNAseq profile from the following cell populations: B220+ GL7+ Fas+ *in vivo* GC B cells from immunized mice (*in vivo* GCB, n = 6) and B220+ GL7+ Fas+ *ex vivo* GC-like B cells from both immune organoids (organoid GCB, n = 4) and 2D co-culture systems (2D GCB, n = 4).

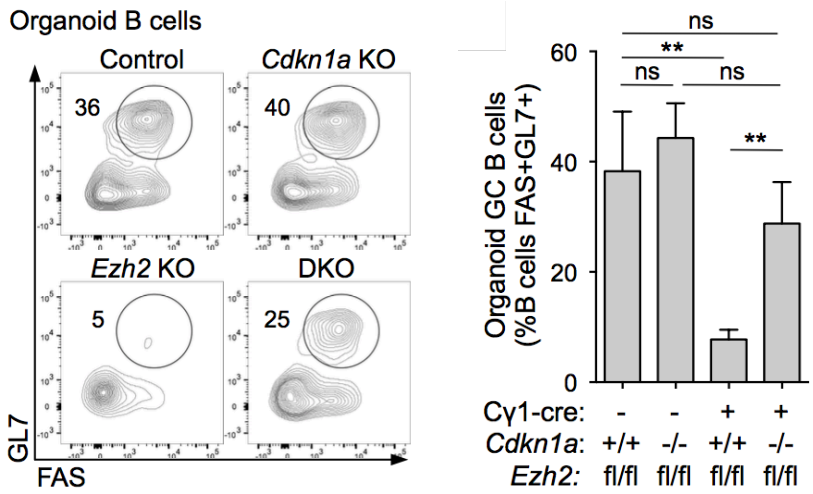

Figure 3-17: GC phenotype induction with *Ezh2* and *Cdkn1a* KO models
The assessment was conducted based on GL7 and Fas double expression. B cells were isolated from four animal models: *Ezh2*$^{fl/fl}$ Cγ1-cre, *Cdkn1a*$^{-/-}$, *Ezh2*$^{fl/fl}$ Cγ1-cre *Cdkn1a*$^{-/-}$, and *Ezh2*$^{fl/fl}$ control mice (n=3 mice per group). Immune organoids were harvested for flow cytometry analysis after 4 days in culture. (Left) Representative flow cytometry plots indicating GC-like B cell percentage from each genotype. The gated area indicating organoid GC-like B cells was based on GL7+ Fas+ GC subset within B220+ DAPI- live B cell population. (Right) Bar graph quantifying the average percentage of GC-like B cells from each genotype using flow cytometry analysis. Statistical significance (** and ***) was determined based on $p < 0.01$ and $p < 0.001$, respectively. Statistical test was conducted using t test. Values are shown as mean ± SEM (n = 9).

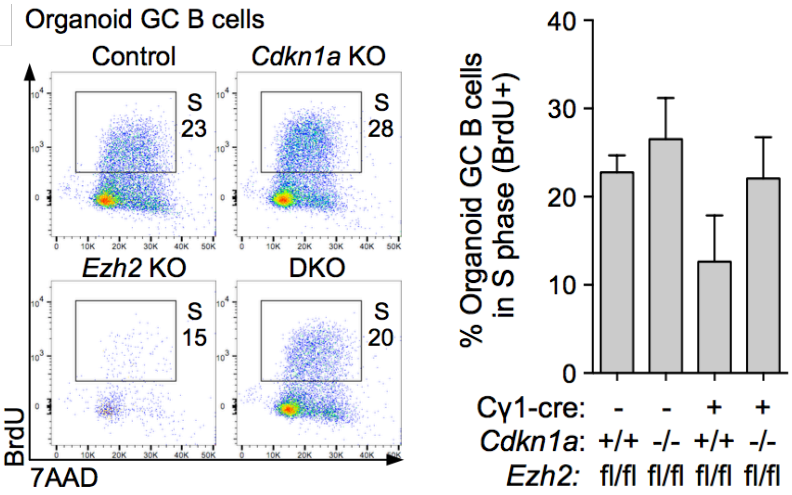

Figure 3-18: Cell cycle analysis with *Ezh2* and *Cdkn1a* KO models
The assessment was conducted using BrdU and 7AAD. BrdU was used to assess cell cycle, while 7AAD was utilized to determine DNA content. Organoids were pulsed with BrdU 2 hours before harvesting. B cells were isolated from four animal models: *Ezh2*$^{fl/fl}$ Cγ1-cre, *Cdkn1a*$^{-/-}$, *Ezh2*$^{fl/fl}$ Cγ1-cre *Cdkn1a*$^{-/-}$, and *Ezh2*$^{fl/fl}$ control mice (n=3 mice per group). Immune organoids were harvested for flow cytometry

analysis after 4 days in culture. (Left) Representative flow cytometry plots indicating the percentage of GC-like B cell in S phase from each genotype. The gated area indicated the B220+ DAPI- GL7+ Fas+ live organoid GC-like B cells that were in S phase as indicated by positive BrdU staining. (Right) Bar graph quantifying the average percentage of S phase GC-like B cell from each genotype using flow cytometry analysis. The gated area indicating organoid GC-like B cells was based on GL7+ Fas+ GC subset within B220+ DAPI- live B cell population. Statistical significance (** and ***) was determined based on $p < 0.01$ and $p < 0.001$, respectively. Statistical test was conducted using t test. Values are shown as mean ± SEM (n = 9).

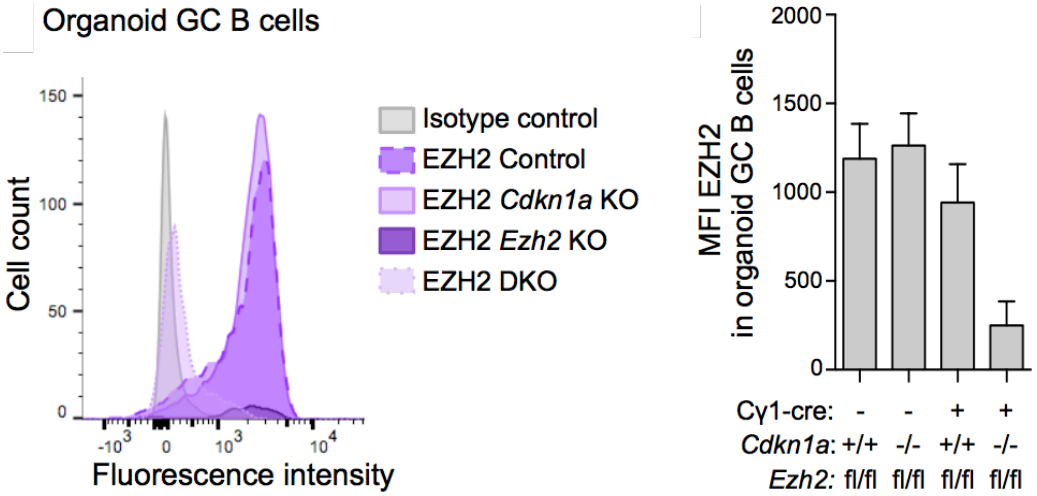

Figure 3-19: Conditional *Ezh2* KO analysis in organoid GC-like B cell population
Cells from immune organoids were fixed, permeabilized, and then stained for EZH2. Cells were co-stained to identify B220+ GL7+ Fas+ GC-like B cells. B cells were isolated from four animal models: *Ezh2*$^{fl/fl}$ Cγ1-cre, *Cdkn1a*$^{-/-}$, *Ezh2*$^{fl/fl}$ Cγ1-cre *Cdkn1a*$^{-/-}$, and *Ezh2*$^{fl/fl}$ control mice (n=3 mice per group). Immune organoids were harvested for flow cytometry analysis after 4 days in culture. (Left) Representative flow cytometry histogram indicating the mean fluorescence intensity of EZH2 in various genotype groups and isotype control. (Right) Bar graph quantifying the average mean fluorescence intensity of EZH2 intracellular expression from each genotype group using flow cytometry analysis. Statistical significance (** and ***) was determined based on $p < 0.01$ and $p < 0.001$, respectively. Statistical test was conducted using t test. Values are shown as mean ± SEM (n = 9).

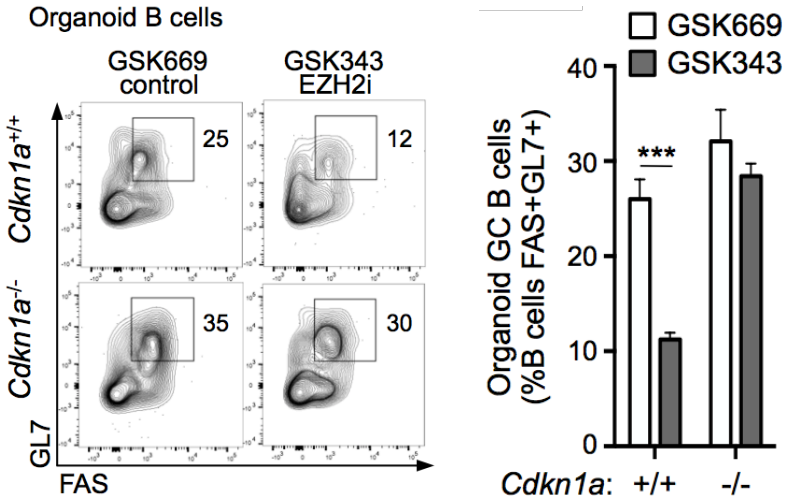

Figure 3-20: GC phenotype induction with *Cdkn1a* KO model and EZH2 inhibitor
The assessment was conducted based on GL7 and Fas double expression. B cells were isolated from two animal models: *Cdkn1a*$^{+/+}$ and *Cdkn1a*$^{-/-}$ (n=3 mice per group). The organoids were then treated with either GSK669 or GSK343. Immune organoids were harvested for flow cytometry analysis after 4 days in culture. (Left) Representative flow cytometry plots indicating GC-like B cell percentage from each genotype and treatment group. The gated area indicating organoid GC-like B cells was based on GL7+ Fas+ GC subset within B220+ DAPI- live B cell population. (Right) Bar graph quantifying the average percentage of GC-like B cells from each genotype and treatment group using flow cytometry analysis. Statistical significance (** and ***) was determined based on $p < 0.01$ and $p < 0.001$, respectively. Statistical test was conducted using t test. Values are shown as mean ± SEM (n = 9).

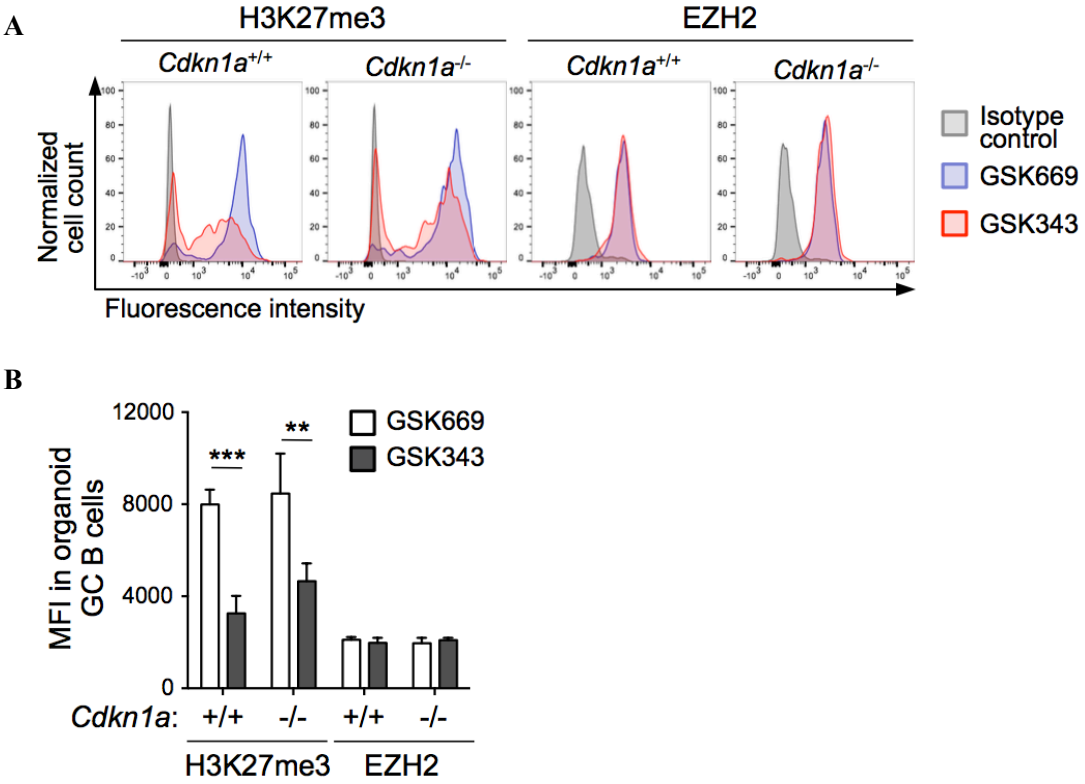

Figure 3-21: Histone methylation analysis with *Cdkn1a* KO model and EZH2 inhibitor
The assessment was carried out based on the expression of H3K27Me3 that measured the trimethylation of lysine 27 in histone 3. Cells from immune organoids were fixed, permeabilized, and then stained for H3K27Me3 and EZH2. Cells were co-stained to identify B220+ GL7+ Fas+ GC-like B cells. B cells were isolated from two animal models: *Cdkn1a*$^{+/+}$ and *Cdkn1a*$^{-/-}$ (n=3 mice per group). The organoids were then treated with either GSK669 or GSK343. Immune organoids were harvested for flow cytometry analysis after 4 days in culture. (Top) Representative flow cytometry histogram analysis indicating the fluorescence intensity of both H3K27Me3 and EZH2 from each genotype and treatment group. (Bottom) Bar graph quantifying the average mean fluorescence intensity of both H3K27Me3 and EZH2 from each genotype and treatment group using flow cytometry analysis. The gated area indicating organoid GC-like B cells was based on GL7+ Fas+ GC subset within B220+ DAPI- live B cell population. Statistical significance (** and ***) was determined based on $p < 0.01$ and $p < 0.001$, respectively. Statistical test was conducted using t test. Values are shown as mean ± SEM (n = 9).

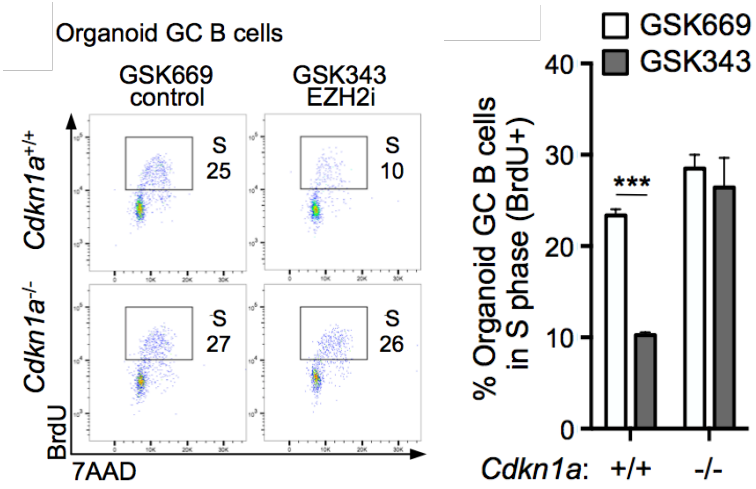

Figure 3-22: Cell cycle analysis with *Cdkn1a* KO and EZH2 inhibitor
The assessment was conducted using BrdU and 7AAD. BrdU was used to assess cell cycle, while 7AAD was utilized to determine DNA content. Organoids were pulsed with BrdU 2 hours before harvesting. B cells were isolated from two animal models: *Cdkn1a*$^{+/+}$ and *Cdkn1a*$^{-/-}$ (n=3 mice per group). The organoids were then treated with either GSK669 or GSK343. Immune organoids were harvested for flow cytometry analysis after 4 days in culture. (Left) Representative flow cytometry plots indicating the percentage of GC-like B cell in S phase from each genotype and treatment group. The gated area indicated the B220+ GL7+ Fas+ DAPI- live organoid GC-like B cells that were in S phase as indicated by positive BrdU staining. (Right) Bar graph quantifying the average percentage of S phase GC-like B cell from each genotype and treatment group using flow cytometry analysis. The gated area indicating organoid GC-like B cells was based on GL7+ Fas+ GC subset within B220+ DAPI- live B cell population. Statistical significance (** and ***) was determined based on $p < 0.01$ and $p < 0.001$, respectively. Statistical test was conducted using t test. Values are shown as mean ± SEM (n = 9).

CHAPTER 4

Integrin Ligand Specificity Differentially Regulates *Ex vivo* B Cell Activation

4.1. Abstract

Having demonstrated the importance of capturing the key aspects of lymphoid tissue microenvironment, we realize the importance of understanding the role of specific matrix signals in modulating GC reaction. As we previously noted the role of RGD - αvβ3 integrin ligand - in maintaining B cell number, we specifically looked into integrin ligand specificity using a modular immune organoid. Our studies showed that while 40LB stromal cell number controls the extent of *ex vivo* GC reaction, integrin ligand type influenced GC marker induction, integrin subunits expression, and IgM BCR characteristics (e.g. clustering, co-localization with β3 integrin subunit, and expression level). We also noted the importance of early αvβ3 integrin signaling in maintaining GC-like B cell number and regulating IgM BCR level. These results demonstrated that integrin ligand type could influence GC-like B cell phenotype inside immune organoids.

4.2. Introduction

In the previous chapters, we have demonstrated the role of 3D immune organoid approach in mediating an efficient GC-like B cell expansion in culture and facilitating *ex vivo* mechanistic investigation into GC reaction. Although the artificial matrix utilized in these cases is enriched with bioadhesive ligands, we

---

The content of this chapter has been published as Purwada, Alberto, Shivem B. Shah, Wendy Beguelin, Ari M. Melnick, and Ankur Singh. "Modular Immune Organoids with Integrin Ligand Specificity Differentially Regulate Ex Vivo B Cell Activation." *ACS Biomaterials Science & Engineering* 3, no. 2 (2017): 214-225.

have yet to understand how these signals can directly modulate the extent of *ex vivo* GC reaction. In order to answer the question above, we first assess published studies on the role of integrin in modulating specific GC B cell characteristics and the overall GC reaction.

Integrin ligands are typically found in the form of cell adhesion molecule or extracellular matrix. Within the lymphoid tissue, specific integrin ligands such as α4β1-binding vascular cell adhesion molecule 1 (VCAM-1) are upregulated on the surface of FDCs [97]. The role of α4β1 integrin has been demonstrated in several publications. Although B cells co-cultured with FDCs can remain viable in culture, such survival-boosting effect is reduced after said integrin is blocked with neutralizing antibody [39]. It has been proposed that interaction between BCR, CD19, and outside-in integrin signaling promotes short-term GC B cell survival, prevents the accumulation of pro-apoptotic and anti-proliferative proteins, and induces the expression of anti-apoptotic proteins[137]. In the lymphoid microenvironment, αvβ3-binding RGD motif is observed in ECM proteins such as vitronectin within the GC light zone [97] or laminin α5 within the marginal zone of B cell follicles [96]. While the role of αvβ3 integrin has yet to be fully explored, αvβ3 integrin subunits are expressed more in activated B cells [138] and therefore GC B cells bind vitronectin stronger than follicular B cells [97]. From the functional perspective, β3 deficiency is associated with slight overrepresentation in the splenic GC compartment [97] and increased sensitivity to TLR stimulation [138]. These studies indicate that distinct integrin-ligand interactions can have different influences on the GC reaction. At the same time, multiple integrin binding types can occur simultaneously and further increase the complexity of dissecting individual integrin contribution toward GC induction.

Despite these findings, it can be challenging to understand the role of distinct integrin-ligand interaction in conventional methods. Animal models are inherent complex and do not provide an easy control over integrin ligand density and selective presentation. Furthermore, integrin KO model can be difficult to generate because of altered development or embryonically lethal [138]. While *ex vivo* B cell stimulation can be achieved with stromal cells and/or soluble factors, 2D co-culture methods exclude 3D presentation

of bioadhesive ligands. While the main issues of imprecise control and 3D presentation could be addressed with biomaterials-based matrix, such innovation has been rarely implemented in B cell and GC studies. With these challenges illustrating the difficulty of investigating integrin function in B cell development, we were motivated to use biomaterials-based artificial matrix for achieving this goal.

4.3. Approach

Having learned the differential integrin gene and surface protein expression during B cell activation, we engineered a modular immune organoid using 4-arm maleimide-functionalized PEG (PEG-MAL) hydrogel (Figure 4-1). Such system has been demonstrated to study the role of lymphoid niche in in malignant B cell culture [139]. In this modular approach, one arm of the PEG-MAL molecule will be functionalized with thiolated adhesive peptide and the remaining arms will be crosslinked to facilitate hydrogel formation by adding non-degradable crosslinker dithiothreitol (DTT) and/or a degradable peptide crosslinker to enable stromal cell spreading. Both functionalization and crosslinking will occur via Michael Addition reaction. We designed our studies to functionalize one arm of the four-arm PEG macromers with thiolated adhesive peptides at 3.0 mM concentration to maximize adhesion sites while ensuring the availability of arms to mediate crosslinking reaction. We selected adhesive peptide concentration based on previous studies reporting that 0.025 to 3.5 mM RGD peptide support cell adhesion and spreading in PEG hydrogels [102]. We also ensured that only one arm was occupied per PEG-MAL molecule because a higher conjugation rate may prevent crosslinking or produce or a non-crosslinking cyclization as discussed earlier by Metters and Hubbell [140]. Although we did not quantify the incorporation of adhesive peptides via Michael Addition reaction, Phelps et al [102] has previously shown 100% incorporation of thiolated RGD peptides at 1:1 or higher MAL-to-RGD molar ratios.

While the biomaterials are designed to mimic ECM signals from the lymphoid microenvironment, 40LB stromal cells providing CD40L and BAFF are utilized to recapitulate the lymphoid cellular components.

Similar to our previous experiments, 40LB stromal cells were made from BALB/c 3T3 fibroblasts genetically engineered to present CD40L and secrete BAFF were used to reconstitute the same signals presented by follicular helper T cells (Tfh) cells and FDCs, respectively [48]. Since CD40L normally originates from Tfh cells, CD40L-presenting 40LB stromal cells recapitulate the role of Tfh in mediating GC reaction [141, 142]. Both 40LB stromal cells and primary naïve B cells will then be co-encapsulated in the functionalized hydrogel to help us study the role of integrin in GC B cell generation.

We then assessed the optimal hydrogel composition by looking at 40LB stromal cell spreading since we have previously demonstrated the importance of stromal cell spreading in mediating an efficient *ex vivo* GC reaction [143, 144]. We first looked into matrix degradability because previous studies have shown that cell spreading is supported in hydrogels containing protease degradable crosslinkers [102, 145-149] and the cells used here - 3T3 fibroblasts [150] and B cells [151] - are known to secrete matrix metalloprotease 9 (MMP-9). We observed that aggregated cells were produced in hydrogels with non-degradable crosslinker DTT resulted and such outcome suggested that DTT did not support the spreading of 40LB stromal cells (Figure 4-1). In contrast, superior cell spreading was observed when PEG-MAL was crosslinked using MMP-9 degradable VPM peptides mixed with DTT at 1:1 molar ratio. This combination was selected because hydrogels crosslinked with 100% VPM was quickly degraded in culture due to matrix remodeling by 40LB cells (data not shown). We hence continued with the 1:1 VPM-to-DTT molar ratio in the subsequent experiments.

We next studied the effect of adhesive ligand density toward 40LB stromal cell spreading by functionalizing the PEG macromers with RGD peptide at concentrations ranging from 0.003 to 3 mM (Figure 4-1). The resulting data indicated the appearance of 40LB spread network at 3 mM ligand density but no such phenotype was observed at 0.003 – 0.3 mM ligand concentration range. We also studied the role of integrin ligand specificity toward stromal phenotype (Figure 4-1). 40LB cells appeared to spread uniformly with well-formed actin fibers in both REDV and RGD groups. A similar CD40L expression

level was observed in 40LB stromal cells grown with both integrin ligand types with a slightly higher level seen in RGD organoids. We thus used the following adhesive ligand type and concentrations: RGD (1.5 and 3.0 mM), REDV (1.5 and 3.0 mM), and RGD + REDV (1.5 mM for each peptide type).

4.4. Integrin Ligand Composition and B Cell Activation

We hypothesized that integrin ligand specificity will modulate GC-like B cell phenotype induction. To test this hypothesis, primary CD19+ naïve B cells were isolated from mice spleen and then co-cultured with 40LB cells within the 3D organoid in the presence of IL-4. Previous studies have shown the role of IL-4 during early interaction between B and Tfh cells to facilitate GC formation [152]. We did not observe any significant difference in CD19+ B cell number across integrin ligand types and densities after 4 days of culture (Figure 4-2). Since GC B cells express the GL7 surface marker [153-156], we also examined GL7 surface expression to assess GC-like phenotype induction (Figure 4-2). Our data indicated a significantly higher percentage of GL7+ GC-like B cells in REDV organoids versus the one seen in RGD organoids. Within each integrin ligand type, changing ligand density by 2 fold from 1.5 to 3 mM did not change the GL7+ percentage. This observation indicates that integrin ligand type can modulate the induction of GL7 surface marker in GC-like B cells.

Because Fas is a highly characterized member of the pro-apoptotic receptor family and Fas expression is upregulated on GC B cells relative to naïve B cells [157], we next evaluated Fas surface expression to further analyze GC-like phenotype induction (Figure 4-2). From the functional perspective, Fas-mediated GC B cell selection has been shown to be essential in the steady state maintenance of both T and B cells [158]. We did not observe any difference in the percentage of GL7+ Fas+ GC-like B cells between integrin ligand types at 1.5 mM concentration. But we observed a significant increase in the percentage of GL7+ Fas+ GC-like B cells with REDV at 3 mM ligand density (Figure 4-2). We did not see such effect with RGD at the same dose. Since multiple integrin ligands can be present in the lymphoid

microenvironment, we next determined the effect of combined RGD and REDV ligand presentation using RGD + REDV organoids with 1.5 mM ligand density for each peptide. We observed the same percentage of GL7+ Fas+ GC-like B cells as observed with 1.5 mM RGD and REDV organoids. These outcomes further suggest the ability of integrin ligand type in controlling GC marker induction.

Based on these results and our previous work on immune organoids with RGD-presenting scaffold [143], we proposed that αvβ3 stimulation with RGD drives GC induction better than 2D co-culture and yet α4β1 further improves the activation process. Since combined RGD and REDV ligand presentation did not enhance GC formation more than RGD only, we hypothesized that αvβ3 integrin has a dominating effect over other integrin types. This conclusion is supported by a previous study observing an increased contribution by integrin β3-deficient B cells in GC reactions and thus suggesting the regulatory function of integrin β3 in GC B cells [97].

In order to ensure that GC-like phenotype induction was driven primarily by CD40L presentation instead of biomaterial immunogenicity, we encapsulated B cells in the presence or absence of CD40L-presenting 40LB stromal cells (Figure 4-2). While we observed a very low number of B cells and essentially zero GC-like B cell number with no 40LB cells, we noticed a significantly higher number of both B cells and GL7+ Fas+ GC-like B cells with 40LB cell availability. This outcome indicated the importance of CD40L in maintaining B cell number and facilitating GC-like phenotype induction. We also noted the importance of stromal density because the number of both B cells and GC-like B cells was higher with 40,000 40LB stromal cells (vs. 20,000 40LB stromal cells). These results indicated that B cell number and GC-like B cell expansion primarily depended on the amount of CD40L in the organoids.

4.5. Integrin Ligand Composition and B Cell Integrin Expression

With integrin ligand specificity affecting GC phenotype, we hypothesized that the presence of a specific

integrin ligand could alter the expression of relevant integrin subunits. We then quantified the expression level of several integrin subunits (α4, β1, αv, and β3) on B cell surface (Figure 4-3). From measuring the integrin subunit expression level with median fluorescence intensity (MFI), we found integrin α4 level to be significantly higher in REDV-functionalized organoids than RGD-functionalized organoids at both 1.5 and 3 mM ligand density (Figure 4-3). A two-fold increase in ligand density from 1.5 mM to 3 mM did not change integrin α4 expression level. We then presented a combination of RGD and REDV integrin ligands with 1.5 mM ligand density for each peptide. The resulting data indicated that the integrin α4 expression level in RGD+REDV organoids was similar to the one exhibited by 1.5 mM RGD organoids and significantly lower than that in 1.5 mM REDV organoids. While higher integrin α4 expression was detected in REDV organoids (vs. RGD organoids), a dominating effect of RGD could be seen during simultaneous RGD and REDV ligand presentation. This situation could reflect the situation where both ligands are available in the light zone compartments in GC [97, 159].

Unlike integrin α4, integrin β1 appeared to have two peaks representing low and high surface expression levels (Figure 4-3). Integrin $\beta1^{lo}$ expression pattern in GL7+ GC-like B cells was similar to integrin α4 expression pattern by being significantly higher in REDV organoids (vs. RGD organoids). Furthermore, integrin $\beta1^{lo}$ expression in RGD+REDV organoids was comparable to the one in RGD organoids and this outcome further suggested the dominant role of RGD-mediated αvβ3 signaling in GC-like B cells. While such trend was also apparent in GL7- NB-like B cells, the expression level in each peptide type was lower than the one exhibited by GL7+ GC-like B cells. Our analysis suggested that only 10% of the cells exhibited integrin $\beta1^{hi}$ expression and an opposite trend than $\beta1^{lo}$ was observed in both B cell subsets with a significantly higher expression level in RGD organoids (vs. REDV organoids). There was also no difference in expression level across both B cell populations. Focusing on integrin $\beta1^{lo}$ due to its presence in the majority of B cells in our immune organoids, we could infer its dependence on integrin ligand specificity and B cell activation state.

We next determined the expression levels of integrin αv and β3 subunits (Figure 4-3). Our data demonstrated a higher expression level for both integrins in REDV organoids (vs. RGD organoids). The expression levels of both integrin αv and β3 subunits were significantly lower in GL7- NB-like B cells when compared to those produced by GL7+ GC-like B cells. Similar to $\beta1^{lo}$, both αv and β3 appeared to be dependent on integrin ligand type and B cell activation state. Such result was indicative of our earlier surface integrin expression in Chapter 1, where the expression level for these three subunits (αv, β3, and β1) were more upregulated in GC B cells (vs. naïve B cells).

While integrin ligand has been presented continuously throughout 4 days of culture, we wanted to determine the temporal importance of integrin signaling. We then assessed the dependency of GL7 surface marker emergence on the timing of αvβ3 integrin stimulation with Cilengitide addition at various time points following encapsulation. While we noticed a significant reduction in the number of GL7+ GC-like B cells (vs. untreated control) when the αvβ3 integrin-ligand interaction was blocked at t = 0, no such effect as seen with Cilengitide addition at later time points (1, 4, 12 h). These observations indicated that early αvβ3 integrin activation was critical for GC-like induction. Although a similar inhibitory effect was observed in GL7- NB-like B cells, this cell population proliferated significantly more than GC-like B cells in RGD organoids when Cilengitide was added at >1 hour post encapsulation.

The decreased GC-like B cell generation could also be explained by the possible role of Cilengitide in inhibiting 40LB stromal cells adhesion to bioadhesive ligands. Since the spreading of 40LB stromal cells is important for *ex vivo* GC reaction [143], we studied the effect of Cilengitide addition in REDV organoids (Figure 4-4). While no reduction of GC-like B cell generation was observed, we observed an increase in GL7+ GC-like B cell number in REDV organoids when αvβ3 was blocked at 1 hour post-fabrication. This outcome suggests the availability of αvβ3 stimulation under non-RGD growth conditions and further raises the possibility of αvβ3 regulatory role in GC-like B cells.

In order to test our assertion regarding integrin β3 expression in both RGD and non-RGD conditions, we performed confocal imaging and observed integrin β3 clustering in both groups (Figure 4-5). This observation suggested the importance of integrin β3 in GC-like B cell formation. The lack of clustering in 2D condition further suggested the relevance of 3D matrix to study the role of integrin in GC reaction.

4.6. Integrin Ligand Composition and Surface IgM BCR Characteristics

We then explored IgM BCR signaling in GC-like B cells since BCR stimulation facilitated B cells activation prior to entry into GC and affinity-based selection in the light zone compartment [160]. While BCR signaling has been shown to promote the selective survival or expansion of GC-like B cells during the selection process, we have yet to fully understand the mechanism behind BCR-mediated signaling in enabling selection. It is possible that BCR on GC-like B cells produced a stronger or more sustained downstream signaling than the one seen in NB-like B cells. We were also interested in studying the interaction between integrin and BCR during GC reaction. We hypothesized that selective integrin ligand presentation will differentially alter BCR pattern and expression.

We first looked into the temporal dependence of integrin signaling toward BCR expression by inhibiting RGD-mediated αvβ3 integrin stimulation via Cilengitide addition at various time points following encapsulation (Figure 4-6). The resulting data indicated a significant increase in the surface expression level of IgM BCR in GL7+ GC-like B cells (vs. untreated control) after immediate blocking with Cilengitide post encapsulation. But such effect was not seen with Cilengitide addition at later time points (1, 4, or 12 hours) did not. Cilengitide addition had no effect on GL7+ GC-like B cells in REDV-presenting organoids. We next assessed the effect of blocking αvβ3 on IgM BCR when only REDV was present in the hydrogels (Figure 4-6). While such inhibition produced no effect on IgM BCR surface expression in GL7+ GC-like B cells, increased IgM BCR level was detected in GL7- NB-like B cells with

later Cilengitide addition. Since the timing of integrin stimulation controlled surface IgM BCR expression, we further hypothesized that integrin ligand type could control other BCR characteristics.

In order to determine if integrin ligand specificity could modulate IgM BCR clustering and localization, confocal imaging was conducted to assess IgM BCR and integrin β3 subunit on the surface of CD19+ B cells (Figure 4-7). The resulting data demonstrated the formation of BCR clusters that co-localized with integrin β3 spots in REDV-functionalized hydrogels. On contrary, uniformly diffused IgM BCR with clustered integrin β3 was detected in RGD-functionalized hydrogels. When we looked into both RDG scrambled peptide and 2D co-culture control groups, IgM BCR also appeared to be uniformly diffused and yet no β3 integrin signal was found on the surface of B cells.

We next determined whether integrin ligand type could alter surface IgM BCR expression level. Because we were also interested in understanding the role of cytokines in the presence of specific integrin ligands, we cultured immune organoids with an increasing IL-4 dose from 10 to 1000 ng/ml (Figure 4-8). While B cell number was not dependent on integrin ligand type or IL-4 cytokine amount, the percentage of IgM+ B cells was significantly higher in REDV organoids than the one in RGD organoids. Surface IgM BCR expression level was also significantly higher in REDV-functionalized organoids than in RGD-functionalized organoids and this trend was consistent at any IL-4 dose. These data suggest that integrin ligand specificity could modulate surface IgM BCR expression level in the immune organoids.

Since IL-4 cytokine addition during CD40 stimulation has been implicated in class switching from IgM to IgG1, we next assessed whether IL-4 concentration and integrin ligand specificity could modulate the generation of class-switched IgG1+ B cells (Figure 4-9). Unlike IgM BCR, the percentage of B cells expressing surface IgG1 appeared to be dependent on IL-4 concentration and the highest percentage was reached with 1000 ng/ml concentration of IL-4 in REDV organoids. No significant difference across peptide groups at lower IL-4 doses. In order to verify whether the observed differences were specific to

integrin ligands, we prepared hydrogel functionalized with 3mM RDG scrambled peptide. No difference was seen in the percentage of CD19+ IgG1+ B cells with RDG versus RGD at 1,000 ng/ml IL-4 cytokine concentration. Since the percentage of IgG1+ B cells in RDG group was lower than the one in REDV group, the high IgG1+ B cell percentage seen earlier appeared to be specific to REDV-functionalized immune organoids. It is important to note that CD40L was available through the 40LB cells in all conditions such that we observed the similar response between RGD and RDG groups. We also did not see any change in IgG1 expression level across peptide types. These data suggested that a higher dose of IL-4 cytokine led to an improved generation of IgG1+ B cells in the presence of REDV peptide. Future studies will be done to determine whether IgG1+ B cells originate from B cells with downregulated surface IgM and if the generation of IgG1+ B cell is indicative of class switching.

In order to verify whether class switching into IgG1 isotype occurred in the immune organoids, we utilized *Ezh2*$^{fl/fl}$ Cγ1-cre transgenic mouse model (Figure 4-10). In this approach, *Ezh2* excision will occur following the expression of Cre recombinase. Since Cre will be expressed following the transcription of Cγ1 and class switching with IL-4 is characterized by the replacement of Cμ with Cγ1, *Ezh2* knockdown can serve as an indirect measure of class switching. We observed a significant decrease in the percentage of EZH2+ B cells in the KO group (vs. WT group). We also noted a significantly lower EZH2 expression in EZH2+ B cell population from the KO group (vs. WT group). These EZH2 reduction data suggested the occurrence of class switching into IgG1 isotype in our system.

4.7. Discussion

Although we have yet to fully understand the role of integrin ligands with regards to GC formation and BCR activation, more studies are being done to understand the role of integrin signaling during GC reaction. Several *ex vivo* studies have been focusing on the integrin-dependent adhesion between GC B cells and FDCs [34, 37]. A previously published study utilized *in vivo* models to show that distinct

integrin ligand presentations differentially modulate the GC reaction [97]. While some *in vivo* studies showed that the removal of a single pair of integrin subunits (e.g. α4β1) or integrin ligands did not greatly influence B cell entry into GC reaction, α4 integrin subunit deficiency has been shown to compromise B cell participation in GC response [97]. Considering the oversimplified 2D systems and the complexity of *in vivo* models, we utilized biomaterials-based modular immune organoids to study the role of specific integrin ligand presentation during GC formation. Based on previously published data on integrin ligands present in the GC compartment of lymphoid tissue, we chose to focus on both α4β1 and αvβ3 integrin subunits. In order to study the effect of stimulating a specific pair of integrin subunits, we functionalized the immune organoids with adhesive ligands specific for α4β1 and/or αvβ3 integrin subunits by functionalizing with REDV and/or RGD peptides, respectively.

While we have yet to look into other GC-associated hallmark events (e.g. somatic hypermutation and selection), this current study demonstrated the role of integrin ligand specificity in engineering GC-like phenotype and BCR characteristics. We discovered that an improved GL7+ GC-like phenotype induction in REDV organoids when compared to the effect seen in RGD organoids. GC phenotype induction in RGD+REDV organoids was similar to the one seen in RGD organoids, suggesting the dominant and/or regulatory role of αvβ3 integrin in the lymphoid tissue. Unlike the RDG scrambled peptide and 2D co-culture control groups, both RGD and REDV organoids clustered β3 integrin on the surface of B cells.

This work also showed that surface IgM BCR could cluster and co-localize with β3 integrin subunit depending on the available adhesive ligand. Further investigations are required to determine the regulatory roles of αvβ3 integrins. We believe that the ability to control *ex vivo* GC reaction from several design parameters will provide us with a better understanding of B cell differentiation, enable the generation of high-affinity antigen-specific cells in culture and accelerate therapeutics development.

4.8. Materials and Methods

4.8.1. Polymers, peptides, and compounds

Four-arm PEG-MAL with 20 kDa molecular weight was purchased from Laysan Bio, Inc. (Arab, AL) with >90% purity. Integrin αvβ3-binding RGD peptide [145, 161, 162] (GRGDSPC, 96% purity), integrin α4β1-binding REDV peptide [163] (GREDVGC, 96% purity), and MMP-9 degradable VPM peptide (GCRDVPMSMRGGDRCG) were purchased from AAPPTec, LLC (Louisville, KY) with above 90% purity. Integrin αvβ3 inhibitor Cilengitide (a cyclic RGD) was purchased from Selleck Chemicals. Mitomycin C was purchased from Santa Cruz Biotechnology. Murine recombinant IL-4 was purchased from Peprotech (Rocky Hill, NJ).

4.8.2. Cells

Spleens were harvested from female C57BL/6 mice that were aged 10-16 weeks and purchased from the Jackson Laboratory (Bar Harbor, ME). Naïve B cells were isolated from digested spleen via negative selection through the EasySep Mouse B Cell Isolation Kit, purchased from Stem Cell Technologies (Vancouver, Canada). 40LB stromal cells were generated from NIH/3T3 fibroblasts genetically engineered to express membrane-bound CD40L and secrete B cell activating factor (BAFF) as previously described by us [143] and Nojima et al. [48]. 40LB stromal cells were cultured with high glucose DMEM medium containing 10% fetal bovine serum (FBS) and 1% penicillin-streptomycin (P/S) with all components bought from Thermo Fisher Scientific (Waltham, MA). All procedures were approved by Cornell University's Institutional Animal Care and Use Committee.

4.8.3. Antibodies

Fluorophore-conjugated anti-mouse antibodies used for flow cytometry consist of anti-CD19 (eBioscience, PE-Cy7, eBio1D3), anti-IgM (eBioscience, FITC, eB121-15F9), anti-IgG1 (eBioscience, APC, M1-14D12), anti-integrin αv (eBioscience, PE, RMV-7), anti-integrin β3 (eBioscience, FITC, 2C9.G3), anti-integrin α4 (eBioscience, PE, R1-2), anti-integrin β1 (eBioscience, FITC, eBioHMb1-1), anti-GL7 (eBioscience, FITC and APC, GL-7), and anti-Fas (BD, APC, Jo2). Antibodies used for confocal microscopy included anti-mouse anti-integrin β3 (eBioscience, purified, armenian hamster, 2C9.G3), anti-mouse anti-CD19 (eBioscience, purified, Rat, eBio1D3), anti-IgM (Abcam, purified, Rabbit, II/41), anti-armenian secondary antibody (Abcam, Alexa Fluor 488, Goat), anti-rat secondary antibody (Abcam, Alexa Fluor 594, goat), and anti-rabbit secondary antibody (Thermo Fisher Scientific, Alexa Fluor 633, goat).

4.8.4. Immune organoid fabrication

Synthetic hydrogel organoids with 7.5% (w/v) macromer concentration were fabricated using PEG-MAL and thiolated crosslinkers. PEG-MAL macromers were initially functionalized with thiolated bioadhesive peptides RGD or REDV with 4:1 macromer-to-peptide molar ratio. MMP-9 degradable VPM peptide and non-degradable DTT thiolated crosslinkers were combined at a 50:50 molar ratio and 4:1.5 macromer-to-crosslinker molar ratio. All components were diluted using PBS++ solution with pH 7.4 and 1% HEPES. Naïve B cells with 40LB stromal cells were prepared and suspended in the crosslinker solution prior to cell encapsulation. After 5 μL of PEG-MAL macromer was placed in the middle of a well of a non-treated 96 well plate, 5 μL of cell-containing crosslinker solution was injected into the initial droplet and mixed by pipetting up and down 5 times. Hydrogel droplets were prepared and cured for 15 min at 37° C inside cell culture incubator for complete crosslinking. Fresh RPMI 1640 medium supplemented with 10% FBS, 1% P/S, and 10 ng/ml IL-4 was then added to the organoid culture.

4.8.5. Confocal microscopy imaging

For imaging studies, synthetic hydrogel organoids were prepared as described above using uncoated glass-bottom (no. 1.5 coverslip and 20 mm glass diameter) 35mm dish from MatTek Corporation. On day 4 post-encapsulation, the organoids were fixed with 4% paraformaldehyde, rinsed with PBS++, incubated with blocking buffer, stained with primary antibodies overnight, stained with secondary antibodies for 4 hours, and then immediately imaged using Zeiss LSM 710 confocal microscope. Blocking buffer was prepared using PBS++ containing 20% goat serum. Staining was performed with flow buffer containing antibodies (1:500 dilution). Washing was done using PBS solution.

4.8.6. Flow cytometry analysis

After 4 days of culture, cells were harvested from the hydrogel organoids by enzymatic degradation for 1 hour using a 125 U/ml collagenase-1 from Worthington Biochemical (Lakewood, NJ), dissolved in serum-free RPMI medium. Cells were then collected by passing the cell suspension through a 70 μm cell strainer (BD Falcon). Cells were re-suspended in flow buffer containing antibodies (1:500 dilution) and washed two times with the flow buffer solution. Flow buffer solution was prepared using PBS++ containing 2% (v/v) FBS and 5 mM EDTA. Flow cytometry data was acquired with Accuri C6 (BD Biosciences) and analyzed with FlowJo software package.

4.8.7. Statistical analysis

Statistical analysis was performed using GraphPad Prism software with significance based on a p-value of less than 0.05. All studies were performed with five technical triplicates unless otherwise noted.

4.9. Acknowledgement

The work described in this chapter was financially supported by the National Science Foundation CAREER award (DMR-1554275). The concept was developed by Prof. Ankur Singh. Alberto Purwada and Shivem Shah contributed equally to the work (data collection and project design). Data analysis was carried out by Alberto Purwada and Prof. Ankur Singh. Academic scholarship support toward Shivem Shah was provided by Cornell University's Presidential Life Sciences Fellowship. Imaging studies were carried out using Zeiss LSM 710 Confocal Microscope - funded by NIH 1S10RR025502 - at the Cornell University Biotechnology Resource Center (BRC).

4.10. Figures

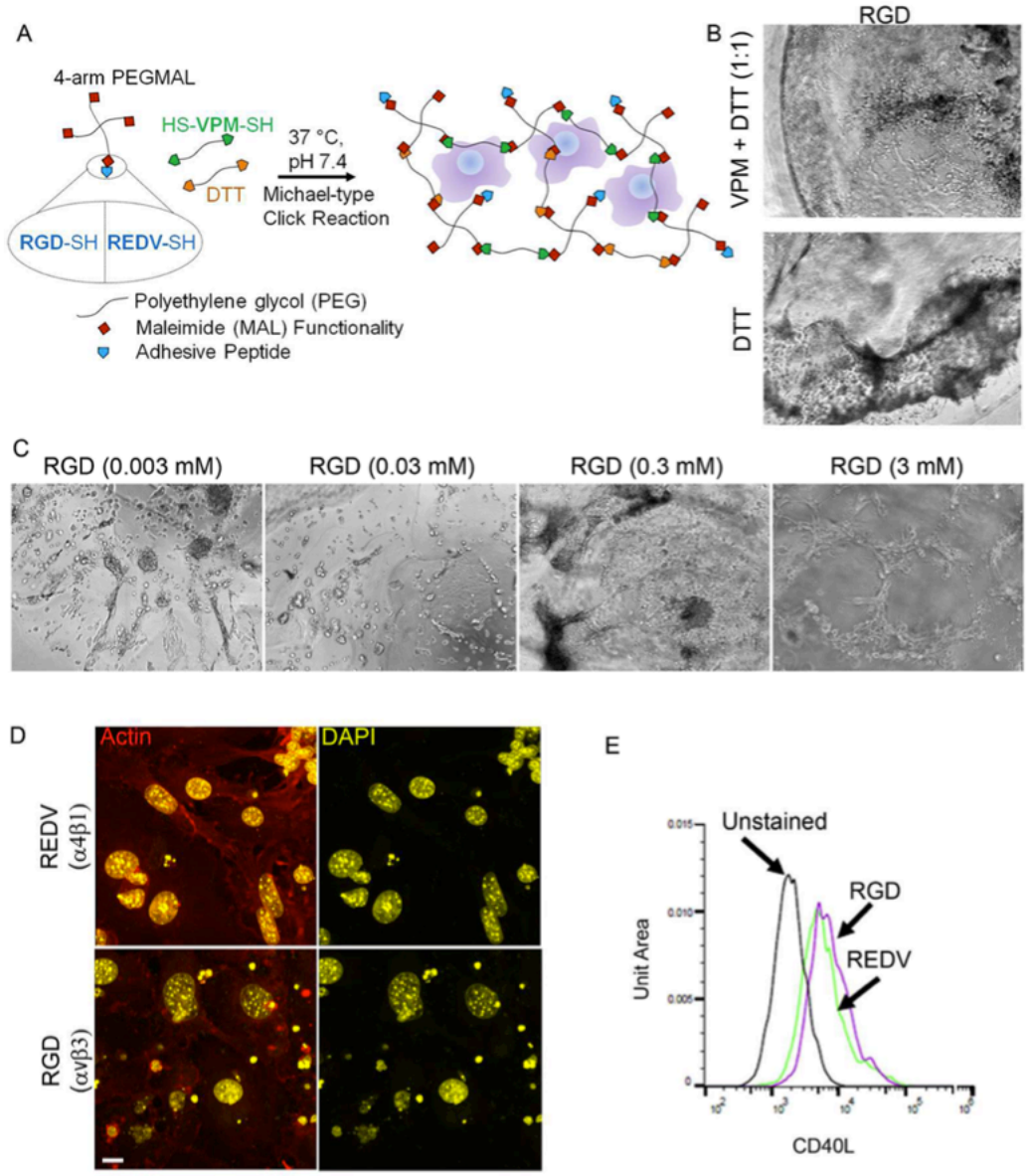

Figure 4-1: Modular immune organoids with degradable crosslinker and bioadhesive ligand
(A) Schematic representing PEG-MAL organoids modified with integrin-specific adhesive ligands and cross-linked with a mixture of MMP-9 degradable and non-degradable cross-linkers. (B,C) Phase image assessment of 40LB stromal cells in hydrogels with differing matrix degradability (B) and varying RGD peptide density (C). Matrix degradability study was performed at 3 mM RGD ligand density and ligand density study was conducted at 1:1 VPM +DTT cross-linking ratio. All images show 20× magnifications using a Nikon TE2000 microscope. (D) Stromal cells cultured in 3D immune organoids functionalized with integrin α4β1-binding REDV peptide and integrin αvβ3-binding RGD peptide. Cells were stained with phalloidin (actin) and DAPI (nucleus, false colored here for improved representation). Scale 20 μm. (E) Surface expression levels of CD40L in 40LB cells cultured for 4 days in RGD- or REDV-functionalized immune organoids.

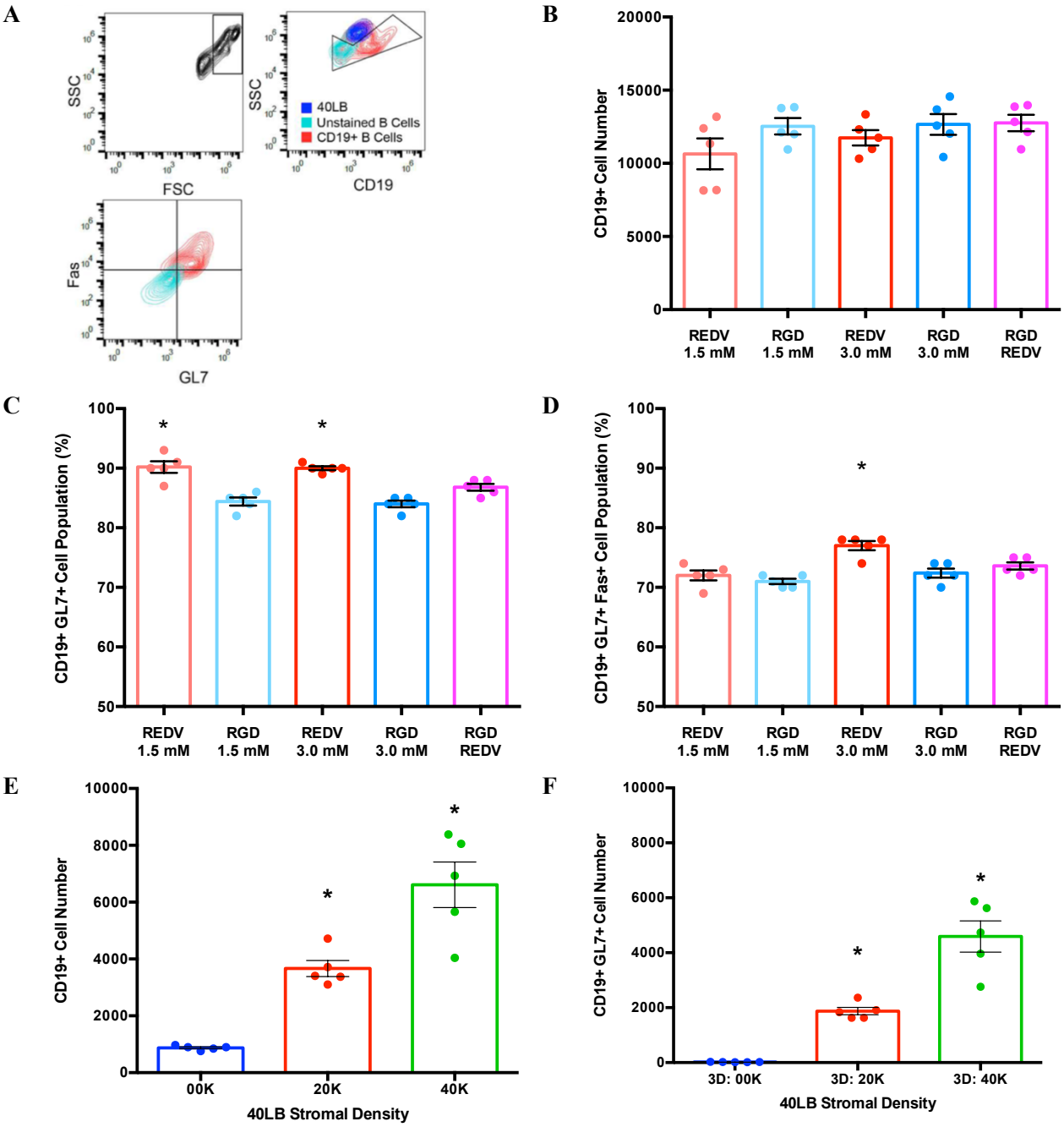

Figure 4-2: Integrin ligand specificity and stromal density on B cell activation

(A) Gating schematic for the analysis of CD19+ GL7+ Fas+ GC-like B cells. (B-D) The number of CD19+ (B), CD19+ GL7+ (C), and CD19+ GL7+ Fas+ (D) cells in RGD and/or REDV-functionalized immune organoids. (E-F) The number of CD19+ (E) and CD19+ GL7+ cells as a function of 40LB seeding density in 3 mM RGD-functionalized immune organoids. Three stromal densities were used: 0, 20,000, and 40,000 cells per organoid. Statistical significance (*) with regard to RGD organoid group (n = 5) was determined based on $p < 0.05$. Statistical test was conducted using ANOVA. Values are shown as mean ± SEM (n = 5).

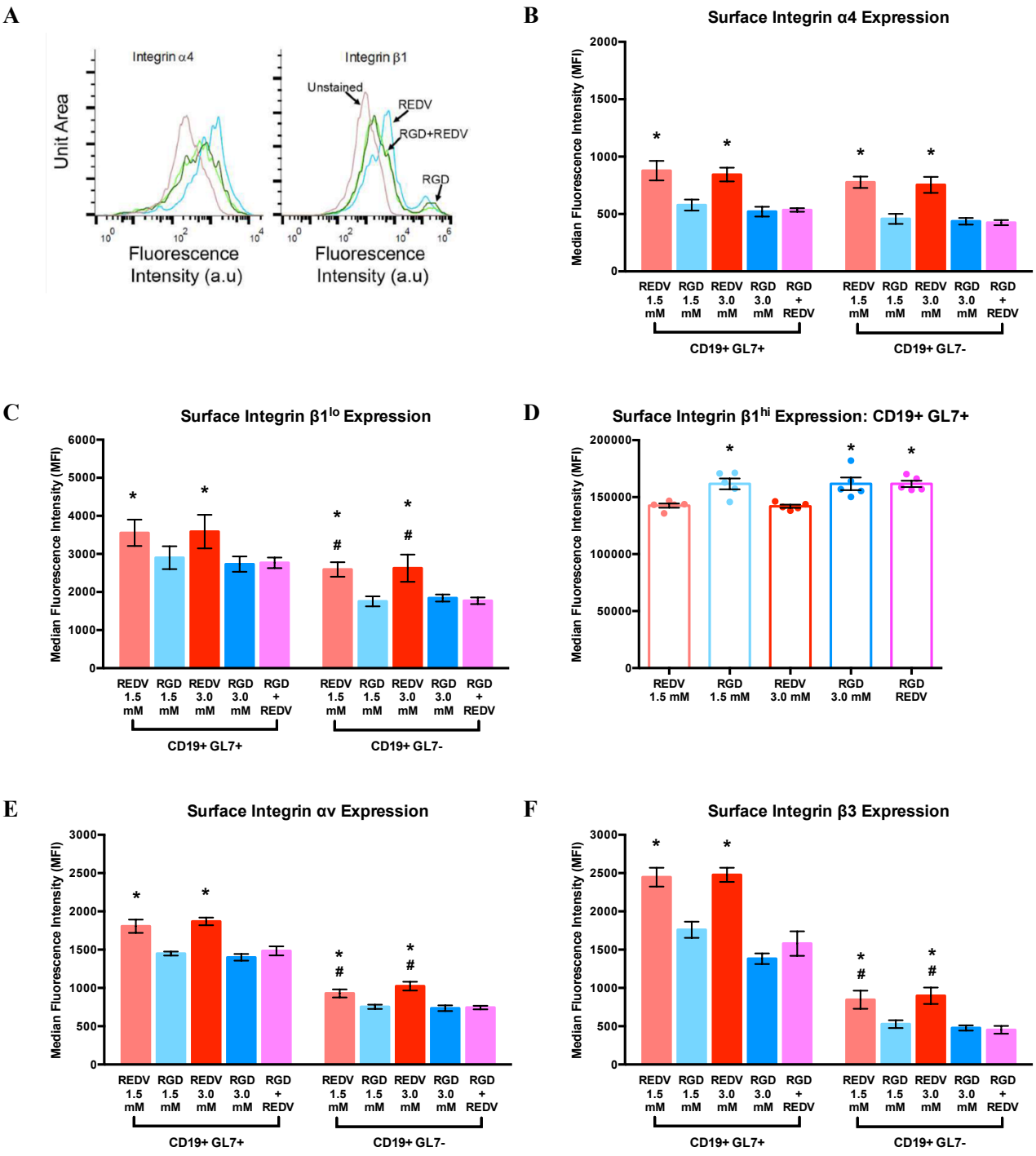

Figure 4-3: Integrin subunit expression profile in activated B cells

(A) Histogram representing the expression profile of α4 and β1 integrin subunits. (B) The MFI of α4 integrin when cultured with specific integrin ligand type and density. (C,D) The MFI of β1 integrin in the subset of B cells expressing $\beta1^{lo}$ (C) and $\beta1^{hi}$ (D). (E,F) The MFI of αv integrin (E) and β3 integrin (F) on B cells when cultured in 3D organoids with specific integrin ligand type and density. Analysis was performed after 4 days of differentiation. Statistical significance (*) was determined based on $p < 0.05$. Statistical test was conducted using ANOVA. Values are shown as mean ± SEM (n = 5).

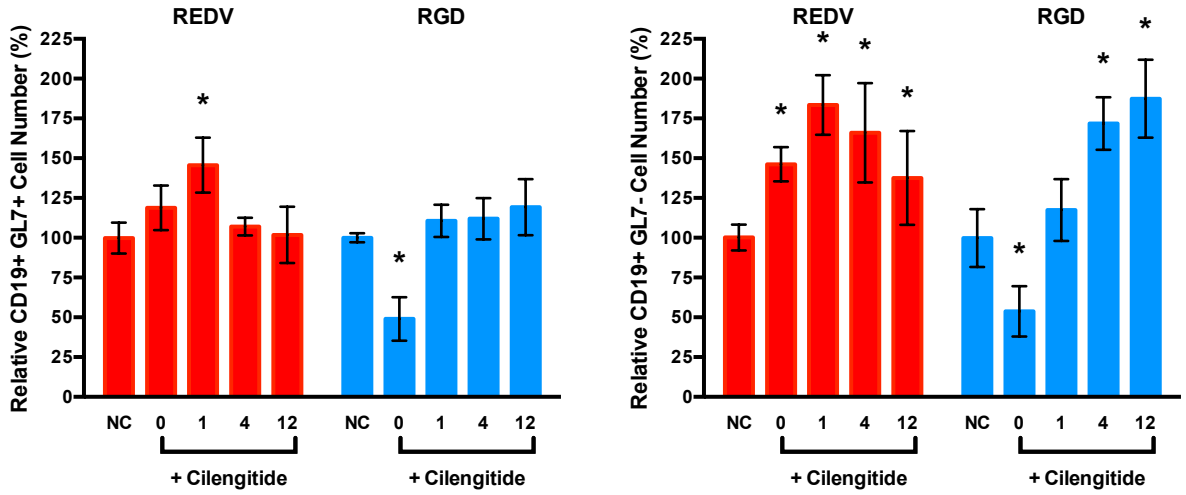

Figure 4-4: Temporal control of integrin ligand presentation on B cell activation
Relative percentage of CD19+ GL7+ GC-like (left) and CD19+ GL7- non-GC-like B cells (right) following the addition of integrin αvβ3-inhibiting Cilengitide at indicated time points. Statistical significance (*) with regard to negative control group was determined based on $p < 0.05$. Statistical test was conducted using ANOVA. Values are shown as mean ± SEM (n = 5).

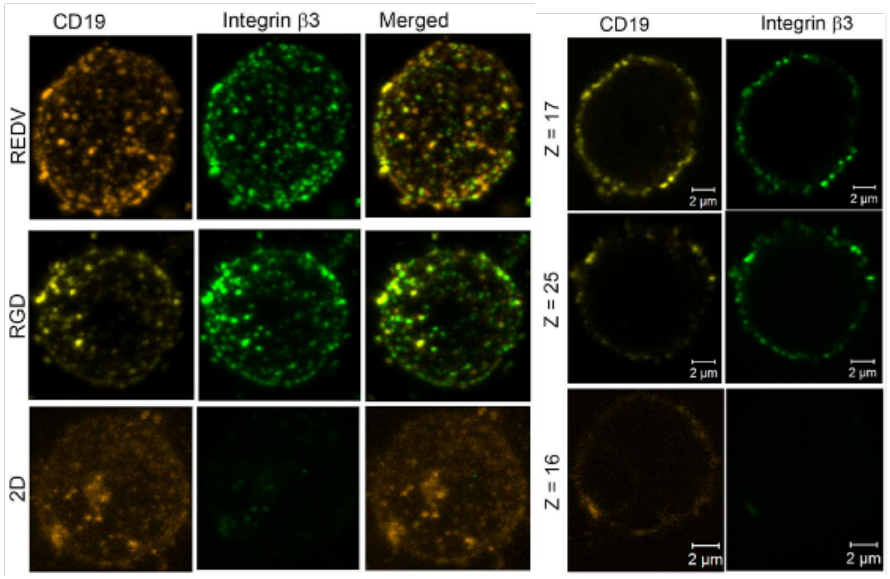

Figure 4-5: Integrin β3 expression and clustering
(Left) 3D reconstructed confocal images of REDV-functionalized organoid (left) and RGD-functionalized organoid (middle), and 2D co-culture system (bottom). (Right) A representative z-section from each culture condition is displayed to indicate localization of CD19 and integrin β3. Scale bar = 2 µm.

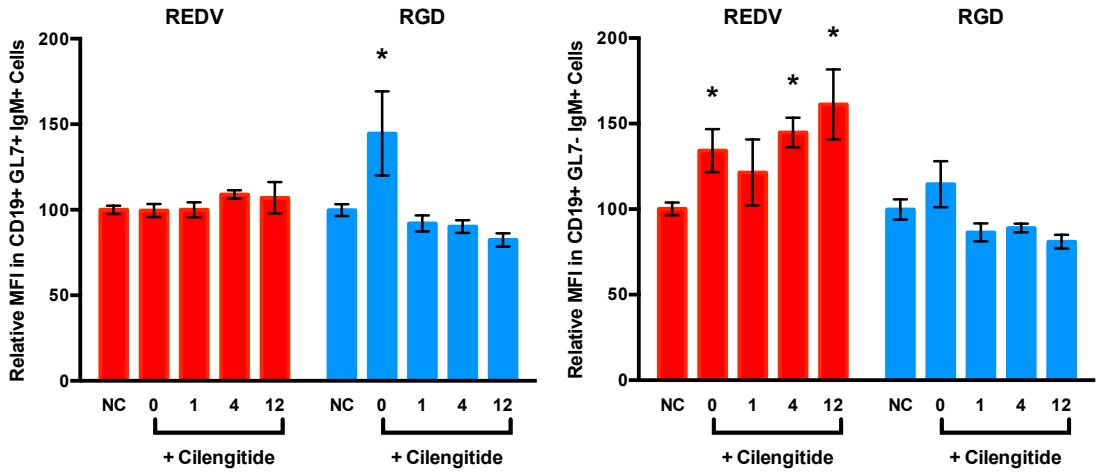

Figure 4-6: Temporal dependency of integrin−ligand interaction on IgM BCR expression
IgM BCR expression was quantified for both CD19+ GL7+ GC-like (left) and CD19+ GL7− non-GC-like (right) B cells following culture in hydrogel functionalized with either REDV (red) or RGD (blue) in the presence of Cilengitide added at various time points in culture. IgM BCR expression was normalized to the one on B cells cultured in immune organoids functionalized with the corresponding integrin ligand and no Cilengitide treatment (negative control, NC, group). Statistical significance (*) with regard to negative control group was determined based on $p < 0.05$. Statistical test was conducted using ANOVA. Values are shown as mean ± SEM (n = 5).

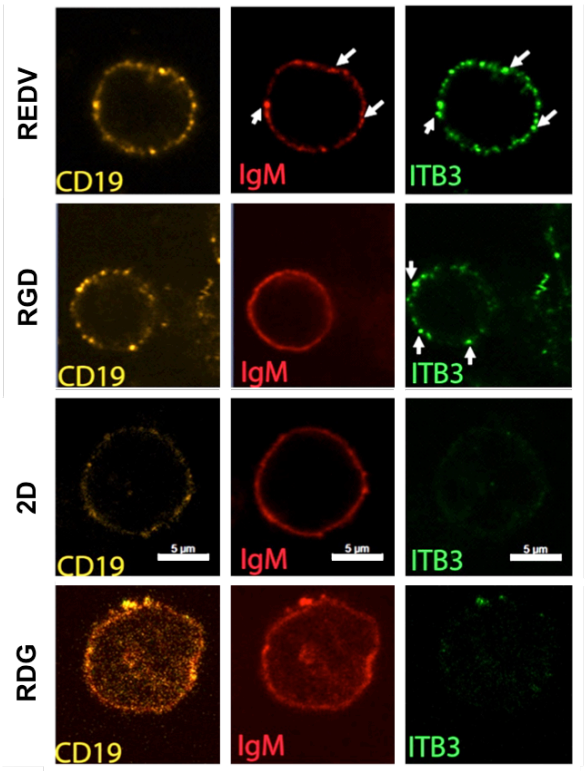

Figure 4-7: IgM BCR clustering and co-localization with integrin β3 subunit
Confocal z-sections of day 4 B cells cultured in 3D immune organoids functionalized with a specific peptide (REDV, RGD, or RDG scrambled peptide) or 2D co-culture control. Staining was done to indicate the localization of IgM BCR and integrin β3 subunit on the surface of CD19+ B cells with scale bar of 2 μm.

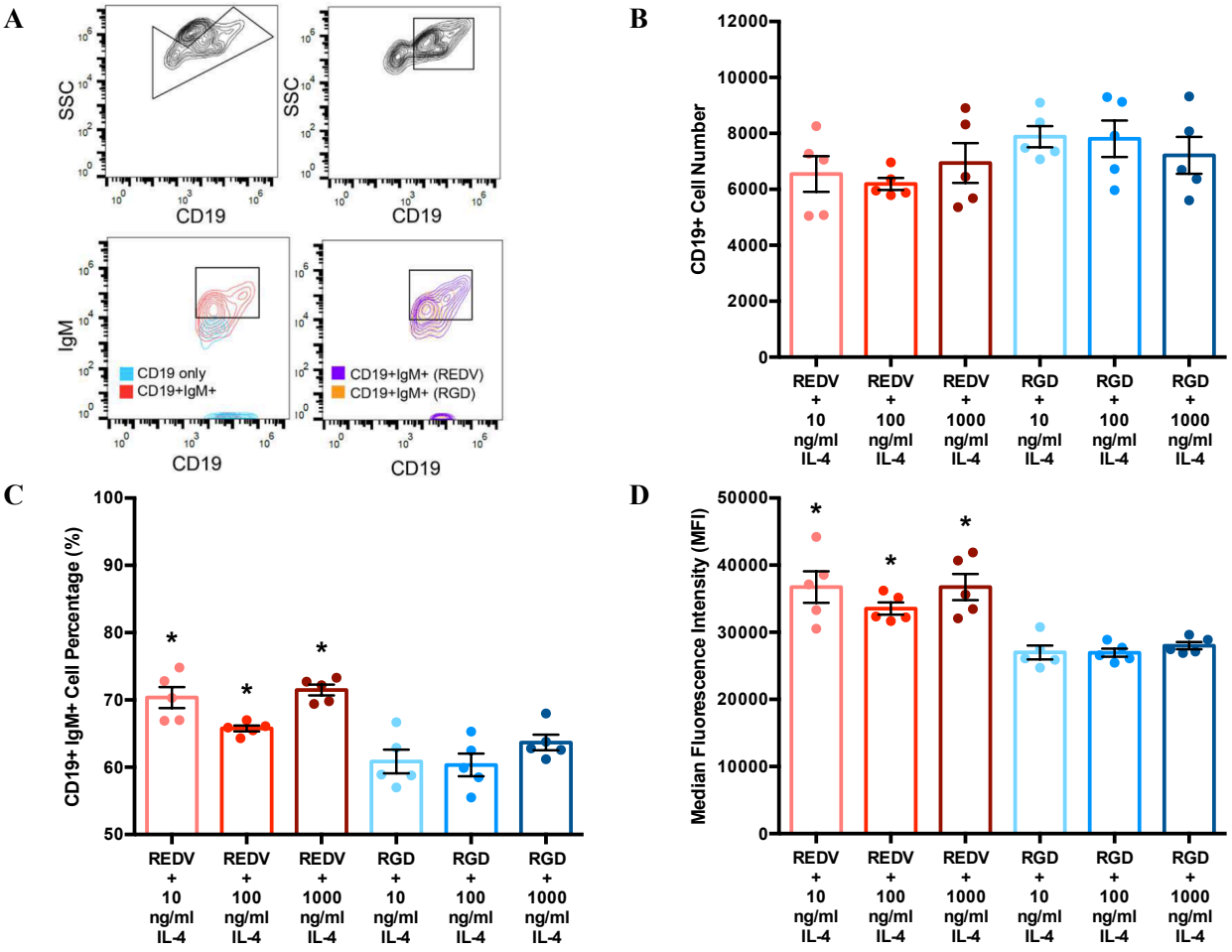

Figure 4-8: IgM BCR surface expression in 3D immune organoids and IL-4 concentration
(A) Gating schematic for the analysis of IgM+ cells inside the organoid. (B-D) Quantitative analysis of CD19+ cell number (B), CD19+ IgM+ cell percentage (C), and IgM BCR MFI expression in CD19+ cells (D) following culture with increasing amounts of soluble recombinant IL-4 from 10 to 1000 ng/ml added into the organoid culture media. Statistical significance (*) with regard to RGD organoid group was determined based on $p < 0.05$. Statistical test was conducted using ANOVA. Values are shown as mean ± SEM (n = 5).

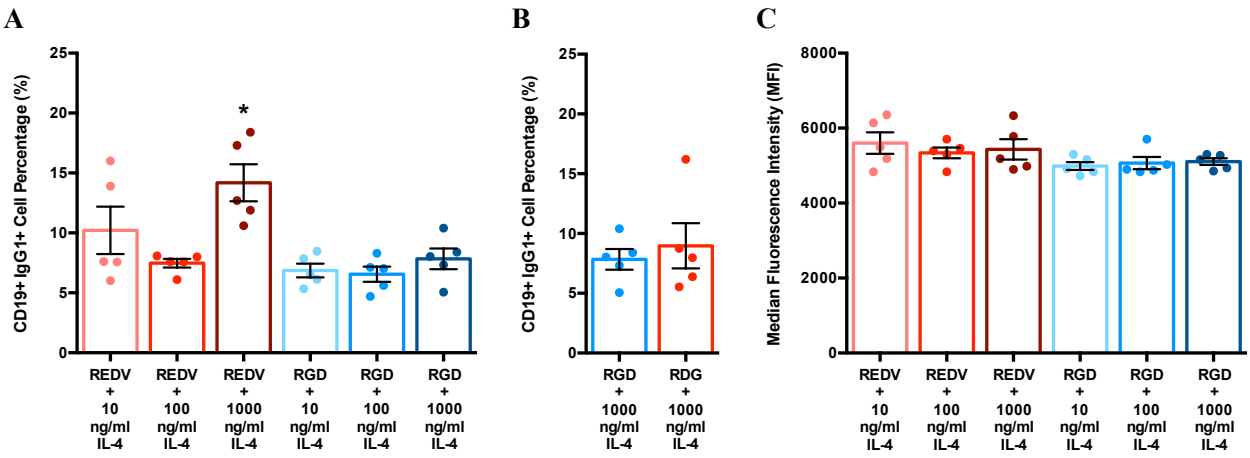

Figure 4-9: IgG1 BCR surface expression and IL-4 concentration
(A) Analysis of IgG1+ CD19+ B cell percentage in REDV- or RGD-functionalized immune organoids with increasing IL-4 cytokine concentration. (B) Assessment of IgG1+ CD19+ B cell percentage in immune organoids functionalized with either RGD or scrambled RDG peptide. (C) Quantification of IgG1 BCR MFI expression in CD19+ B cells (right). Statistical significance (*) with regard to RGD organoid group was determined based on $p < 0.05$. Statistical test was conducted using ANOVA. Values are shown as mean ± SEM (n = 5).

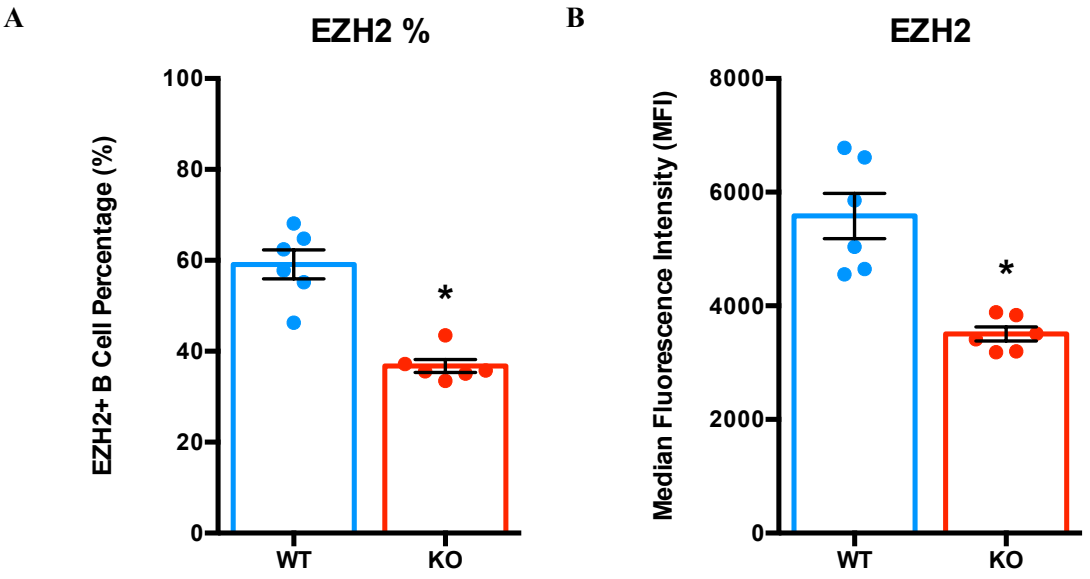

Figure 4-10: Class switch assessment with *Ezh2* KO mouse model
The assessment of class switching based on Cre-mediated *Ezh2* knockdown following Cγ1 transcription based on (A) the percentage of B cells with intracellular EZH2 expression and (B) the EZH2 intracellular expression level in EZH2+ B cell population. Statistical significance (*) with regard to WT group was determined based on $p < 0.05$. Statistical test was conducted using t test. Values are shown as mean ± SEM (n = 6).

CHAPTER 5

Integrin Ligand and BCR Crosslinking Modulate *Ex Vivo* GC-like B Cell Phenotype

5.1. Abstract

Upon learning that integrin ligand specificity could modulate surface IgM BCR clustering and expression level, we studied if such effect would result in altered response toward BCR crosslinking. We learned that integrin ligand type determined responsiveness toward BCR stimulation in terms of GC reaction maintenance, ASC differentiation program, and phosphorylation of BCR target molecules. We also showed that BCR activation could produce resistance toward Fas-mediated apoptosis and this concept could be extended to enrich antigen-specific B cells from a mixed B cell population. Enrichment was assessed from the absolute number and relative percentage of antigen-specific GC-like B cells subset. Interestingly, integrin ligand specificity appeared to determine the percentage increase in antigen-specific GC-like B cells and the number of cells with fully bound BCR post-enrichment. These results suggested the importance of both integrin and BCR to control GC-like B cell phenotype inside immune organoids.

5.2. Introduction

In the previous chapter, we have demonstrated the ability of 3D immune organoid to induce the formation of GC-like B cells and the role of integrin ligand specificity in controlling the B cell activation process [164]. While we observed that integrin ligand type could modulate surface IgM BCR expression level and clustering, it is still unclear whether such change translates to any altered signaling pathway following BCR crosslinking. We also have yet to know if it is possible to control the phenotype of *ex vivo* GC-like B cells after the activation process. In order to answer these questions, we have to first functionalize 3D

immune organoid with a specific integrin ligand and then induce BCR crosslinking in culture prior to analyzing the resulting GC-like B cell phenotype.

BCR crosslinking is defined as the binding of antigen by its corresponding BCR and this process typically occurs at two time points: early before GC induction and later during the selection process within GC LZ compartment. In the first phase, soluble antigen binding activates naïve B cells within the follicle and the activated B cells will migrate toward the interfollicular region for interaction with the corresponding antigen-specific Tfh cells [3]. Primarily driven by CD40-signaling, this cell-cell binding will initiate GC formation in the secondary lymphoid tissue. Over the course of GC reaction, two cellular compartments will develop and they can be distinguished based on their appearances under the microscope into DZ and LZ. While DZ tends to be associated with proliferating GC B cells, LZ generally consists of activated GC B cells that are undergoing key GC events (e.g. CSR, selection, and differentiation). LZ is also the site where the second phase of BCR crosslinking occurs with the ligand being FDC-bound antigen binding and this process will mediate the selection of high-affinity antigen-specific B cells. While researchers are still trying to understand the selection process, several mechanisms may occur in parallel. It has been proposed that a higher BCR affinity results in increased antigen uptake and greater density of peptide-MHC complex on the surface of GC B cells, which in turn helps the high-affinity GC B cell clone to compete for survival signal from Tfh cells [1]. It has also been proposed that activated B cells without BCR signaling will be sensitive to Fas-induced apoptosis following FasL presentation by activated helper T cells [165]. These results suggest that BCR primarily functions by binding antigen and facilitating the selection process during the GC reaction.

Nevertheless, there are still numerous open questions regarding the role of BCR in GC reaction. This can be illustrated by the recent finding that BCR signaling is suppressed in proliferating GC B cells and such inhibition appears to be necessary for GC maintenance [160]. Without the *ex vivo* capability of modulating BCR signaling and reconstituting the GC B cell selection process, it can be difficult to

understand how BCR functions during GC reaction and what role it plays in modulating GC B cell phenotype. Such situation is compounded by the fact that GC B cell population is both rare and heterogeneous. With these challenges illustrating the need for a functional GC model, we improved our immune organoids with BCR crosslinking to initiate *ex vivo* ASC differentiation and selection.

5.3. Approach

Similar to our previously published modular immune organoid platform [164], we utilized 4-arm PEG-MAL hydrogel in this study. The PEG-MAL macromer was first functionalized with thiolated integrin ligand peptide and then crosslinked to facilitate hydrogel formation using both non-degradable crosslinker DTT and dithiol protease-cleavable peptide crosslinker. The adhesive peptide molar concentration was adjusted to be 3.0 mM such that one arm of the PEG-MAL macromer would be functionalized with the integrin ligand peptide. From the cellular perspective, the organoid contained both primary murine naïve B cells and 40LB stromal cells. 40LB cells were derived from fibroblasts genetically engineered to present CD40L and secrete BAFF for facilitating B cell activation and inducing *ex vivo* GC-like B cell generation [48, 49, 143]. This stromal-driven approach allows the reconstitution of relevant signals. B cells were freshly isolated prior to each experiment while 40LB is maintained in culture. The immune organoids were prepared by encapsulating cells in the crosslinker mixture, placing each functionalized macromer droplet in several individual wells of a 96-well plate, mixing them with cell-containing crosslinker mixture to induce hydrogel polymerization, and finally curing the droplets at 37 °C for 15 minutes before adding cell culture medium.

For inducing BCR crosslinking in the organoid, we added soluble anti-IgM antibody into the cell culture medium immediately after encapsulation. Several studies have shown the use of anti-IgM antibody as antigen mimic to stimulate BCR signaling in B cells [20, 21, 166]. This approach was selected as we started with primary naïve B cells with heterogonous BCR that were isolated from WT mice and the use

of anti-IgM antibody will facilitate a consistent BCR stimulation across the entire B cell population. While the use of soluble anti-IgM antibody represents a simple but proven way to stimulate BCR on GC-like B cells, it is important to reproduce the binding between a specific antigen and its corresponding BCR will be important to better model the selection process.

In order to test the hypothesis that GC B cells with BCR stimulation are resistant toward Fas-induced apoptosis, Fas stimulation was conducted in a similar manner by adding soluble anti-Fas antibody into the cell culture medium. This approach was picked for several reasons. Some works have demonstrated that soluble anti-Fas antibody can induce Fas-induced cytotoxicity in certain cells [167, 168]. The technique was relatively simple because anti-Fas antibody can be added in soluble form. While FasL can produce a more consistent response across a broader range of cell types, FasL requires immobilization or oligomerization for its pro-apoptotic function [169, 170]. It is thus more challenging to use FasL since FasL has to be immobilized via matrix conjugation or membrane-bound presentation.

For studying antigen-specific GC-like B cell enrichment, we utilized primary B cells isolated from B1-8^{hi} mice. This mouse model was generated with gene targeting to introduce B1-8 variable region (V_H) containing point mutations that conferred higher 4-hydroxy-3-nitrophenyl (NP) affinity into the immunoglobulin heavy chain (IgH) locus [171]. Such system can facilitate the specific binding of NP hapten because B1-8 heavy chain paired with λ1 light chain can bind NP with an affinity of 5×10^5 M^{-1} and the additional point mutations will further increase the affinity to 5×10^6 M^{-1}. It has also been shown that the heavy chain has a dominant role in determining affinity and light chain mutations have little influence toward affinity [160]. Soluble NP hapten was therefore used as the model antigen to target NP-specific B cells throughout the selection experiments.

5.4. GC Marker Downregulation with BCR Crosslinking

We first hypothesized that BCR crosslinking will reduce GC phenotype with a greater effect seen in REDV-functionalized hydrogel due to the previous data indicating increased clustering and greater expression level of surface IgM BCR. In order to test this hypothesis, modular immune organoids incorporating REDV or RGD peptide were prepared and then cultured with increasing concentration of soluble anti-IgM antibody. Assessment of GC phenotype was conducted by analyzing the expression level of two intracellular GC markers - BCL6 and EZH2 - in CD19+ GL7+ GC-like B cells.

BCL6 transcription factor regulates GC B cell development primarily by suppressing the transcription of ASC differentiation genes and this marker is only expressed in GC B cells [4]. BCL6 has also been shown to facilitate GC B cell proliferation in various ways including the suppression of apoptotic and cell cycle arrest responses. The importance of BCL6 toward GC reaction is further supported by the lack of GC formation in BCL6-deficient mice. Our hypothesis on BCL6 downregulation with anti-IgM antibody originated from the report that BCR stimulation targets BCL6 for rapid degradation [172]. We first looked into BCL6 expression level and observed that the 0 - 2.5 μg/ml soluble anti-IgM antibody concentration range resulted in a significantly higher BCL6 expression level in REDV organoids when compared to the one seen in RGD organoids (Figure 5-1). While a significant reduction in BCL6 level could already be seen at 0.5 and 2.5 μg/ml doses in REDV organoids, a similar effect was only seen at 2.5 μg/ml dose in RGD organoids. At 5 μg/ml dose, BCL6 expression was lowered to the same level in both organoid types. Looking into the change in expression level after normalization based on BCL6 level in 0 μg/ml dose group, a greater reduction in every dose could be seen with REDV organoids. These observations indicated that the use of REDV-functionalized organoid resulted in greater BCL6 induction during *ex vivo* GC reaction and increased responsiveness toward BCR stimulation.

In addition to BCL6, EZH2 is another relevant GC marker. EZH2 is specifically expressed in GC B cells and primarily works by epigenetically silencing differentiation genes [125]. EZH2 is critical for the GC reaction because GC hyperplasia could be observed with mutant *Ezh2* and GC reaction failed to form in *Ezh2* KO mice. We then studied the change in EZH2 expression after BCR stimulation and noticed a significant reduction in the percentage of EZH2+ GC-like B cells with 5.0 μg/ml anti-IgM antibody dose in both organoid types (Figure 5-2). Without BCR stimulation, a greater EZH2+ population was seen in REDV group than RGD group. While the percentage of EZH2+ cells was similar at 5 μg/ml dose across integrin types, a greater drop occurred in REDV group when compared to that in RGD group.

Since EZH2 works by catalyzing the methylation of lysine 27 residue of histone 3 (H3K27), we further validated this EZH2+ percentage reduction by looking into the percentage of B cells with trimethylated histone H3 lysine 27 (H3K27Me3) and observed a slight but significant decline in H3K27Me3+ B cells. Looking into EZH2 expression level in EZH2+ GC-like B cells, we observed a similar trend with greater expression level in REDV group and decline to the same level following the addition of 5 μg/ml soluble IgM antibody (Figure 5-3). Assessing the change in expression level after normalization based on the EZH2 level in EZH2+ cells with 0 μg/ml anti-IgM antibody, a greater reduction could be seen in REDV-functionalized organoid. Similar to the BCL6 data, these observations demonstrated both improved EZH2 induction during *ex vivo* GC reaction and greater sensitivity toward BCR stimulation in REDV group.

5.5. ASC Marker Upregulation with BCR Crosslinking

Upon observing the reduced expression of intracellular GC markers (BCL6 and EZH2) upon BCR stimulation and realizing that these markers function by suppressing GC B cell differentiation, we next hypothesized that BCR crosslinking could improve the expression of relevant differentiation genes. In order to test this hypothesis, modular immune organoids functionalized with REDV or RGD peptide were

prepared and then exposed to the soluble anti-IgM antibody at varying doses. Assessment of ASC differentiation was done based on the expression level of intracellular IRF4 in organoid-derived B cells.

IRF4 is a transcription factor that regulates GC B cell terminal differentiation toward the ASC fate, occurs later during the GC process, and suppresses BCL6 for terminating the GC reaction [4]. We developed our hypothesis regarding IRF4 upregulation with BCR stimulation after learning the role of BCR signaling in inducing IRF4 expression in B cells [173]. Our data demonstrated the increase in IRF4 expression following the addition of soluble anti-IgM antibody into the immune organoids (Figure 5-4). While a statistically significant increase in IRF4 level was observed at 0.5 – 5 μg/ml doses in REDV group, such significance was only noticed at 2.5 – 5 μg/ml in RGD group. A greater IRF4 expression was seen at each dose in REDV groups when compared to the one in RGD group. Looking at the change in expression level after normalization based on the level in 0 μg/ml dose group, a greater increase in IRF4 could be seen with REDV group when contrasted to the one seen in RGD group. These observations suggested that while BCR crosslinking facilitates IRF4 induction in both REDV and RGD immune organoids, a greater responsiveness toward BCR stimulation was seen in REDV group.

Since IRF4 has been proposed to act either upstream or parallel with BLIMP1 and BLIMP1 is known to facilitate GC B cell differentiation toward the ASC pathway, we followed up our IRF4 observation by looking into the expression level of intracellular BLIMP1 in organoid-derived B cells (Figure 5-5). Our data indicated that 5 μg/ml anti-IgM antibody addition produced a significant increase in BLIMP1 expression. As CD138 is a well-known ASC marker that gets upregulated throughout the terminal differentiation following GC exit, we also assessed CD138 surface expression level (Figure 5-5). We saw that CD138 was significantly increased following 5 μg/ml anti-IgM antibody addition. These trends suggested that BCR stimulation indeed facilitates the ASC differentiation program in B cells.

While the aforementioned differentiation markers are highly upregulated in ASCs, they are also expressed by a subset of LZ GC B cells [4]. Under the assumption that these ASC markers are generated upon BCR stimulation, LZ GC B cells may demonstrate a more differentiated phenotype because of the interaction between BCR and FDC-bound antigen in the LZ compartment. Since LZ B cells can be characterized with CD83 [174], we hypothesized that organoid-derived B cells may share a similar set of surface markers following BCR stimulation and looked into the CD83 expression on B cell surface. Our data demonstrated a small but significant increase in the percentage of CD83+ B cells following anti-IgM antibody addition and the majority of B cells were CD83+ in the immune organoids (Figure 5-6). Analysis on the CD83 expression level on the surface of CD83+ B cells also indicated a significant increase following BCR crosslinking. This data interestingly suggested that CD83+ phenotype, which was indicative of LZ phenotype, could be induced upon the addition of soluble anti-IgM antibody.

Although CD83 function is still unclear, CD83 has been proposed to help stabilize MHC Class II (MHCII) expression during its constant turnover throughout the GC reaction and therefore *Cd83* KO mice have been shown to have a reduced GC B cell population with $MHCII^{hi}$ [175]. Another study also showed that knocking out *Cd83* resulted in a defective MHCII upregulation after B cell stimulation [176]. We hypothesized that BCR-induced CD83 upregulation would increase MHCII surface level and we then assessed MHCII expression on the surface of organoid-derived B cells after BCR stimulation in culture. Analyzing the expression of MHCII subclass I-A and I-E in B cells isolated from C57BL/6J mice, our data showed a significant increase in MHCII expression with 5 μg/ml anti-IgM antibody dose (Figure 5-7). Looking into the relative expression level after normalization to the expression in 0 μg/ml dose, we saw a 40% increase in MHCII surface expression and such trend further supported the functional aspect of CD83 upregulation seen earlier upon BCR stimulation.

5.6. Phosphorylation of BCR Target Proteins

While we have observed changes in GC-like B cell phenotype following BCR stimulation and differential responses across integrin ligand groups, we have yet to determine if BCR crosslinking effects are mediated by the phosphorylation of BCR target proteins and whether such process is dependent on integrin ligand specificity. BCR stimulation can be assessed by analyzing a set of proteins that are known to undergo phosphorylation. These target proteins are located downstream of BCR signal transduction component and their phosphorylation can be measured upon BCR crosslinking. While there are many target proteins, we looked into three representative members: pSYK, pBTK, and pERK. Upon antigen binding, SRC family kinases are activated quickly prior to the phosphorylation of both SYK and BTK [177]. ERK phosphorylation occurs downstream of SYK activation [160] and therefore can be induced following BCR stimulation [178].

Our data showed a significant increase in the amount of pBTK in REDV group with 5 μg/ml anti-IgM antibody addition (Figure 5-8). Analysis on the normalized expression level indicated that pBTK amount almost doubled after BCR stimulation in REDV group. In contrast, no significant increase in pBTK could be seen in RGD group. Analysis of the phosphorylation of pSYK (Figure 5-9) and pERK1/2 (Figure 5-10) also demonstrated a significant increase in both phosphorylated proteins after BCR crosslinking in REDV group. Similar to the previous data, no significant increase in both phosphorylated proteins could be detected in RGD group. These observations suggested a more sustained BCR signaling throughout 4 days of culture in REDV organoids when contrasted to the one seen in the RGD group. This data further suggested the increased BCR responsiveness in REDV-functionalized organoid.

5.7. Enrichment of Antigen-specific GC-like B Cells

Having demonstrated the role of BCR in inducing ASC differentiation program, the next step is to determine its importance during the selection process. Fas-dependent elimination of specific B cell clones has been proposed based on the observed elimination of B cells that have desensitized BCR when co-cultured with helper T cells and such process can be prevented with Fas deficiency on B cell surface [165]. This process may be explained by the observation that CD40L-stimulated B cells become extremely sensitive to Fas-mediated apoptosis and BCR crosslinking will induce resistance to Fas [166]. Since our modular immune organoid platform contained CD40L-presenting 40LB stromal cells and demonstrated Fas upregulation during *ex vivo* GC reaction, we hypothesized that Fas-mediated selection could be modeled with Fas-mediated apoptosis occurring only in GC-like B cells without BCR stimulation. Our data indicated a significant reduction in the number of CD19+ GL7+ GC-like B cells with 5 μg/ml anti-Fas antibody addition and yet no such effect was seen in the presence of 5 μg/ml anti-IgM antibody (Figure 5-11). This observation demonstrated the sensitivity of GC-like B cells toward Fas-dependent cytotoxicity and BCR crosslinking conferred resistance against Fas stimulation.

We further hypothesized that such approach could be applied to selectively enrich a particular GC B cell clone with antigen-bound GC B cells being resistant toward Fas-induced apoptosis. In order to test this concept, we used the B1-8^{hi} mouse model to obtain primary B cells containing a high number of NP-specific B cells. In the B1-8^{hi} mouse model, gene targeting was used to introduce pre-recombined V_HDJ_H genes into the mouse immunoglobulin heavy chain locus [171] and the resulting B1-8 heavy chain can bind NP hapten upon pairing with the Igλ light chain [179]. An additional mutation of Trp to Leu was introduced at codon 33 of the B1-8 heavy chain to increase the NP binding affinity by a factor of 10 [171]. We then developed a gating schematic to separate non-specific and NP-specific GC-like B cells for the enrichment study with antigen specificity identified based on positive staining by fluorophore-conjugated NP and/or anti-NP antibody (Figure 5-12). Such approach enabled us to identify NP-specific

B cells with free BCR and/or NP-bound BCR. We first examined the NP antigen dose required to obtain a high number of NP-bound GC-like B cells and this experiment was carried out by increasing the amount of soluble NP antigen in the cell culture medium. Our data showed that 3332 nM NP dose produced a significantly higher NP-bound GC-like B cells and lower doses produced no detectable NP-bound population at all (Figure 5-13). The data also showed that while NP-bound population increased significantly, the percentage of NP-specific GC-like B cells was not altered by high dose NP addition.

Having shown the ability to generate NP-bound GC B cell population in the organoid, we next tried to selectively enrich NP-specific population with Fas stimulation using 5 μg/ml anti-Fas antibody. Fas stimulation appeared to significantly decrease the number of non-specific CD19+ GL7+ GC-like B cells and increase the number of NP-specific CD19+ GL7+ B cells (Figure 5-14). From analyzing the GC-like B cell composition, Fas stimulation appeared to significantly decrease the percentage of non-specific CD19+ GL7+ GC-like B cells and increase the percentage of NP-specific CD19+ GL7+ GC-like B cells. Such outcome suggested the enrichment of antigen-specific GC-like B cells in the immune organoids.

We next studied if integrin ligand specificity could modulate this enrichment process because we observed an improved BCR responsiveness with REDV-functionalized hydrogels. The final NP-specific GC-like B cell percentage appeared to be similar in both peptide groups following soluble NP antigen presentation and Fas stimulation (Figure 5-15). But further analysis of the GC-like B cells post-enrichment suggested a greater increase in NP-specific GC-like B cell population in REDV group during selection and a different composition of NP-specific GC-like B cells (Figure 5-16). We specifically observed a significantly higher percentage of fully bound GC-like B cells in REDV-functionalized immune organoids when compared to the one in RGD group (Figure 5-17). This trend was followed by a significantly greater percentage of partially bound GC-like B cells in RGD organoids than the one in REDV organoids. This observation implied the integrin ligand dependency of this *ex vivo* selection.

5.8. Discussion

This chapter describes how BCR crosslinking can modulate the phenotype of GC-like B cells in our modular immune organoids by reducing GC markers and inducing ASC differentiation markers. While similar trends could be observed in both immune organoid types, greater GC phenotype induction and improved responsiveness toward BCR stimulation were seen in REDV-functionalized organoids. Because BCR activation produced GC-like B cell phenotype resembling the one seen in the GC compartment associated with both differentiation and selection, we attempted to reconstitute the selection process with Fas-based negative pressure. Our enrichment method increased antigen-specific GC-like B cell percentage with soluble antigen addition and Fas stimulation. This approach also showed a higher increase in both NP-specific GC-like B cells and the percentage of fully bound GC-like B cell in REDV-functionalized immune organoids. These observations suggested that 3D modular immune organoids could control over GC phenotype and enrich a particular antigen-specific GC B cell clone.

In this study, we have provided important design parameters for controlling the phenotype of *ex vivo* GC-like B cells and reconstituting two hallmark GC events. Further investigations are required to understand whether introducing a particular stimulation at a specific time point can differentially alter GC-like B cell phenotype. We also need to understand how the extracellular cues can be presented to induce antibody secretion and generate long-lived ASCs. The introduction of additional cell types will be important to increase the complexity of our immune organoids and understand cell-cell interactions that occur within secondary lymphoid tissues. We anticipate that the ability to fully control immune reactions *ex vivo* will provide us with the ability to reconstitute the important elements of humoral immune response generation for rapid antibody development and improved understanding of B cell generation.

5.9. Materials and Methods

5.9.1. Compounds

Four-arm PEG-MAL with 20 kDa molecular weight was purchased from Laysan Bio (Arab, AL) with >90% purity. Integrin αvβ3-binding RGD peptide [145, 161, 162] (GRGDSPC, >90% purity), integrin α4β1-binding REDV peptide [163] (GREDVGC, >90% purity), and MMP-9 degradable VPM peptide (GCRDVPMSMRGGDRCG, >90% purity) were purchased from AAPPTec (Louisville, KY).

5.9.2. Cells

For experiments involving WT B cells, spleens were harvested from female C57BL/6 mice (Stock #: 000664) aged 10-18 weeks from the Jackson Laboratory (Bar Harbor, ME). For experiments utilizing antigen-specific B cells, spleens were obtained from male B1-8^{hi} mice (Stock #: 007594) aged 10-12 weeks from the Jackson Laboratory (Bar Harbor, ME). Splenocyte suspension was obtained by mechanical digestion. Naïve B cells were isolated from splenocyte with EasySep Mouse B Cell Isolation Kit from Stem Cell Technologies (Vancouver, Canada). 40LB cells were generated from NIH/3T3 fibroblasts genetically engineered to express CD40L and secrete BAFF as previously described [48, 143]. 40LB cells were cultured with high glucose DMEM medium containing 10% FBS and 1% P/S with all components bought from Thermo Fisher Scientific (Waltham, MA). 40LB cells were mitotically inhibited prior to encapsulation with Mitomycin C from Santa Cruz Biotechnology (Dallas, TX). All procedures were approved by Cornell University's Institutional Animal Care and Use Committee.

5.9.3. Antibodies

Anti-mouse antibodies used for flow cytometry included anti-CD19 (eBioscience, PE-Cy7, eBio1D3), anti-GL7 (eBioscience, Alexa Fluor 488, GL-7), anti-BCL6 (eBioscience, PE, BCL-DWN), EZH2 (eBioscience, eFluor 660, AC22), anti-H3K27Me3 (Cell Signaling Technology, Alexa Fluor 488, C36B11), anti-IRF4 (eBioscience, PE, 3E4), anti-BLIMP1 (BD Pharmingen, Alexa Fluor 647, 5E7), anti-CD138 (Thermo Fisher, APC, 300506), anti-CD83 (eBioscience, eFluor 660, Michel-17), anti-MHC Class II (BD Pharmingen, I-A/I-E, PE, 2G9), anti-p-Btk (eBioscience, Tyr551, PE, M4G3LN), anti-p-Syk (eBioscience, Tyr348, APC, moch1ct), and anti-p-Erk1/2 (eBioscience, Thr202/Tyr204, PerCP-eFluor 710, MILAN8R). NP-specific GC-like B cells assessment was carried out with fluorophore-conjugated NP (PE, Biosearch Technologies) to target free NP-specific BCR and anti-mouse anti-NP antibody (Alexa Fluor 647, Novus Biologicals, B1-8) to target BCR-bound NP.

5.9.4. Soluble Factors

Murine recombinant IL-4 was purchased from Peprotech (Rocky Hill, NJ). BCR activation was performed with the anti-mouse anti-IgM antibody (eBioscience, II/41). Fas stimulation was achieved with the anti-mouse anti-Fas antibody (BD Pharmingen, Jo2). NP antigen was introduced with soluble NP(17)-OVA (Biosearch Technologies, 17 NP-to-OVA conjugation/molar ratio). These soluble factors were mixed with cell culture medium and added into the organoid immediately following encapsulation.

5.9.5. Immune organoid fabrication

Synthetic immune organoids containing 7.5% PEG-MAL were fabricated using PEG-MAL macromer, adhesive peptides, and crosslinkers. PEG-MAL macromers were initially functionalized with thiolated adhesive peptides RGD or REDV with 4:1 MAL-to-peptide molar ratio for 30 minutes at 37 °C. MMP-9

degradable VPM peptide and non-degradable DTT crosslinkers were combined at a 50:50 VPM-to-DTT molar ratio and 4:1.5 MAL-to-crosslinker molar ratio. All components were diluted using PBS++ solution with pH 7.4 and 1% HEPES. Naïve B cells and 40LB stromal cells were suspended in the crosslinker solution prior to cell encapsulation. After 5 µL of PEG-MAL macromer solution was placed in the middle of a well of a non-treated 96 well plate, 5 µL of cell-containing crosslinker solution was injected into the droplet and mixed by pipetting 5 times. Hydrogel droplets were prepared and cured for 15 min at 37° C for complete crosslinking. Fresh RPMI 1640 medium supplemented with 10% FBS, 1% P/S, and 10 ng/ml IL-4 was then added to each organoid.

5.9.6. Flow cytometry analysis

Cells were harvested from the organoids after 4 days of culture with enzymatic degradation for 1 hour using a 125 U/ml Collagenase Type 1 (Worthington Biochemical) dissolved in serum-free RPMI medium. Cells suspension was then filtered to remove gel debris using MultiScreen Mesh Filter Plates with 96 Well Receiver Plate (EMD Millipore). Cells were re-suspended in FACS buffer containing antibodies (1:500 dilution), incubated on ice in the dark for 45 minutes, and then re-suspended in FACS buffer. Intracellular marker staining was performed with one-step protocol for intracellular (nuclear) proteins using eBioscience Foxp3 / Transcription Factor Staining Buffer Set. Phosphorylation signaling protein staining was conducted with two-step protocol for fixation/methanol using eBioscience Intracellular Fixation and Permeabilization Buffer Set. FACS buffer was prepared using PBS++ containing 2% (v/v) FBS and 5 mM EDTA. Flow cytometry data were acquired using Accuri C6 Flow Cytometer (BD Biosciences) and analyzed with FlowJo software package.

5.9.7. Statistical analysis

Statistical analysis was performed using GraphPad Prism software with significance based on a p-value of less than 0.05. All studies were performed with five technical triplicates unless otherwise noted.

5.10. Acknowledgement

The work described in this chapter was financially supported by the National Science Foundation CAREER award (DMR-1554275). The concept was developed by Prof. Ankur Singh. Project design and data analysis were carried out by Alberto Purwada and Prof. Ankur Singh. Other procedures (experiment setup and data collection) were performed by Alberto Purwada. All procedures were approved by Cornell University's Institutional Animal Care and Use Committee.

5.11. Figures

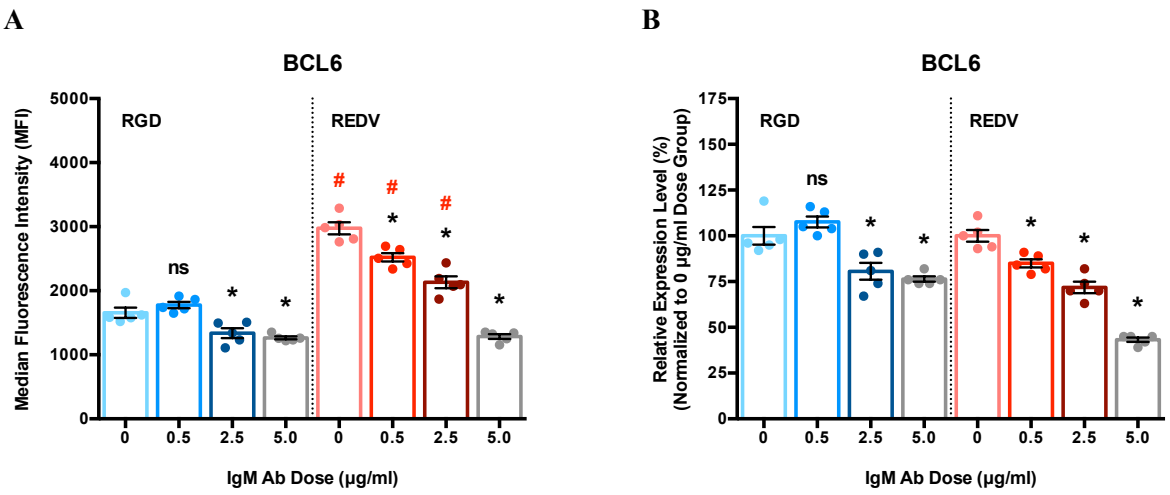

Figure 5-1: BCL6 intracellular expression in 3D immune organoids and BCR crosslinking
BCL6 (A) intracellular MFI expression level and (B) percent change in expression level normalized to 0 µg/ml dose group in CD19+ GL7+ GC-like B cells was assessed for both RGD- and REDV-functionalized immune organoids with varying amount of soluble anti-IgM antibody added to induce BCR crosslinking. Statistical significance (*) with regard to 0 µg/ml dose group was based on $p < 0.05$. Red statistical significance sign indicates comparison with the corresponding dose group from another peptide (RGD). Values are shown as mean ± SEM (n = 6).

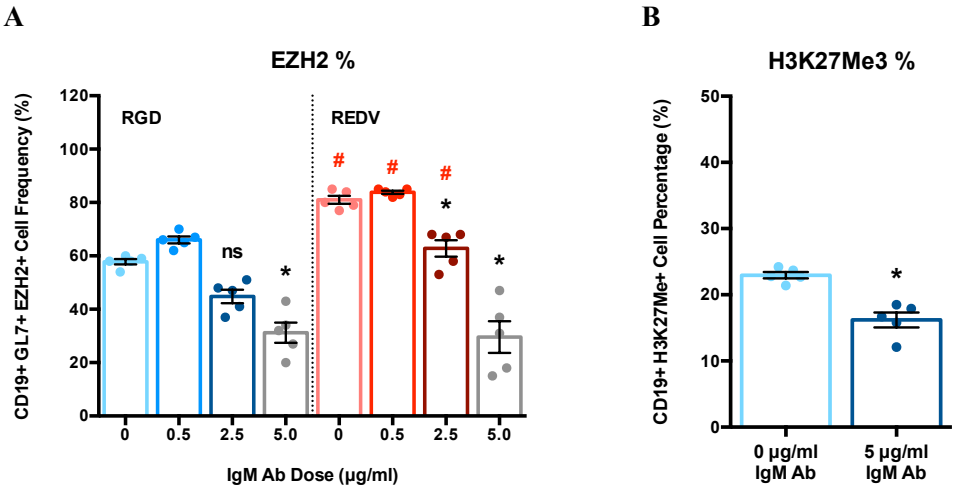

Figure 5-2: EZH2 assessment in 3D immune organoids and BCR crosslinking
(A) Percentage of EZH2+ GC-like B cells in both RGD- and REDV-functionalized immune organoids with varying amount of soluble IgM antibody added to induce BCR crosslinking. (B) Percentage of H3K27Me3+ B cells with 0 or 5 µg/ml anti-IgM antibody. Statistical significance (*) with regard to 0 µg/ml dose group was based on $p < 0.05$. Red statistical significance sign indicates comparison with the corresponding dose group from another peptide (RGD). Values are shown as mean ± SEM (n = 6).

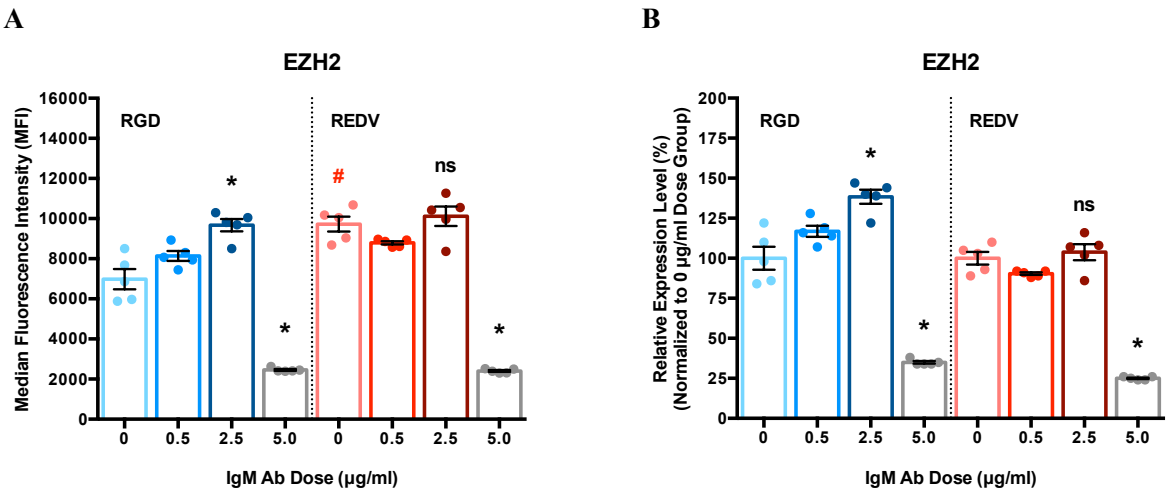

Figure 5-3: EZH2 intracellular expression in 3D immune organoids and BCR crosslinking
EZH2 (A) intracellular MFI expression level and (B) percent change in expression level normalized to 0 µg/ml dose group in CD19+ GL7+ EZH2+ GC-like B cells was assessed for both RGD- and REDV-functionalized immune organoids with varying amount of soluble anti-IgM antibody added to induce BCR crosslinking. Statistical significance (*) with regard to 0 µg/ml dose group was based on $p < 0.05$. Red statistical significance sign indicates comparison with the corresponding dose group from another peptide (RGD). Values are shown as mean ± SEM (n = 6).

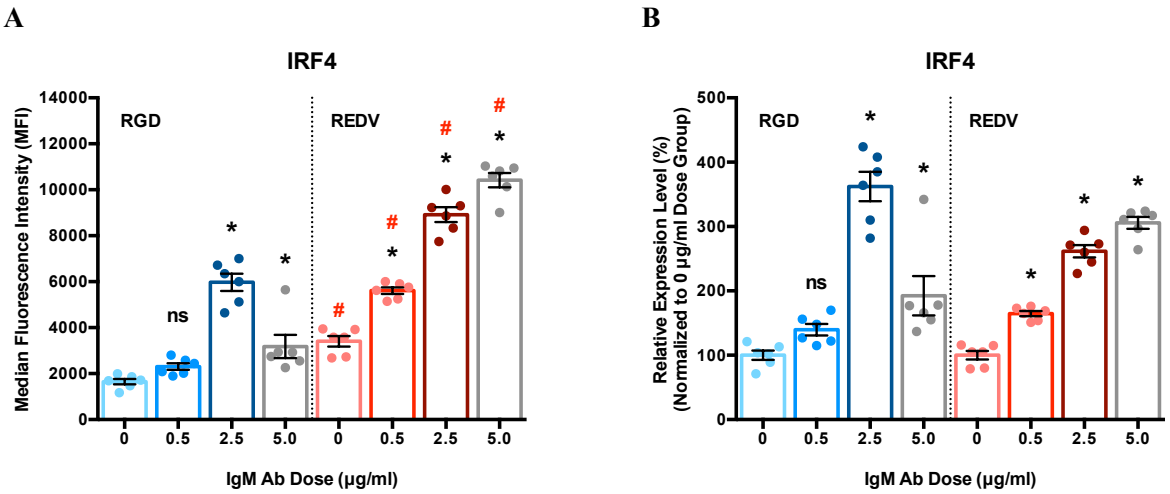

Figure 5-4: IRF4 intracellular expression in 3D immune organoids and BCR crosslinking
IRF4 (A) intracellular MFI expression level and (B) percent change in expression level normalized to 0 µg/ml dose group in CD19+ B cells was assessed for both RGD- and REDV-functionalized immune organoids with varying amount of soluble anti-IgM antibody added to induce BCR crosslinking. Statistical significance (*) with regard to 0 µg/ml dose group was based on $p < 0.05$. Red statistical significance sign indicates comparison with the corresponding dose group from another peptide (RGD). Values are shown as mean ± SEM (n = 6).

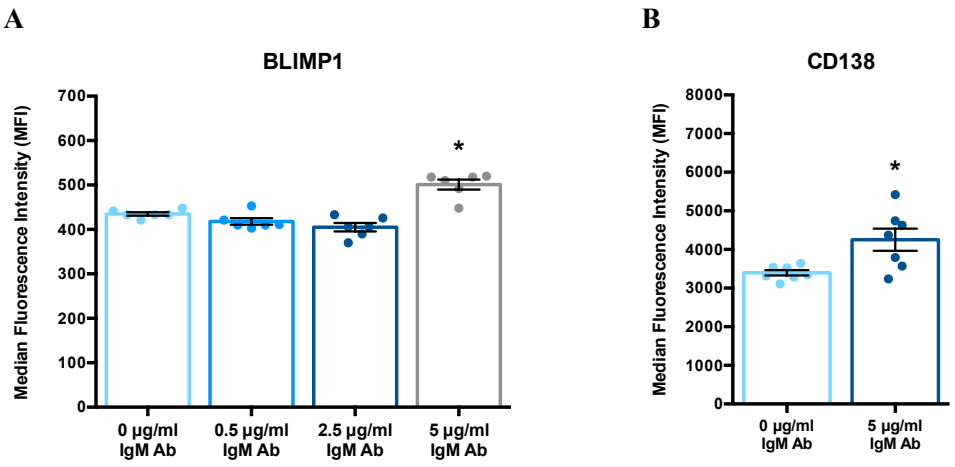

Figure 5-5: ASC marker expression in 3D immune organoids and BCR crosslinking
(A) BLIMP1 intracellular MFI expression level with varying amount of soluble IgM antibody added to induce BCR crosslinking. (B) CD138 surface MFI expression level with 0 or 5 µg/ml anti-IgM antibody. Statistical significance (*) with regard to 0 µg/ml dose group was based on $p < 0.05$. Values are shown as mean ± SEM (n = 6 for A and n = 7 for B).

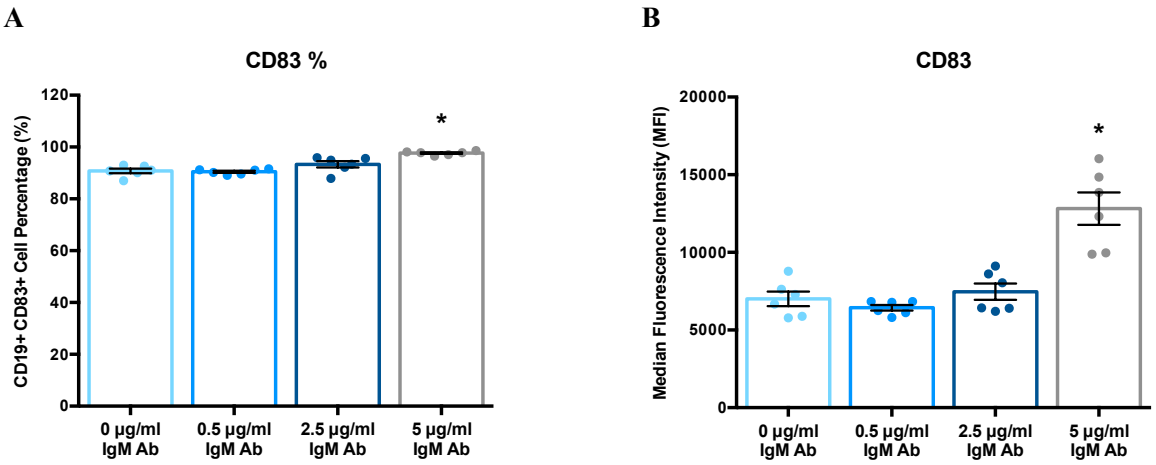

Figure 5-6: CD83 expression in 3D immune organoids and BCR crosslinking
(A) Percentage of CD83+ B cells and (B) CD83 surface MFI expression level in CD83+ B cells with varying amount of soluble anti-IgM antibody added to induce BCR crosslinking. Statistical significance (*) with regard to 0 µg/ml dose group was based on $p < 0.05$. Values are shown as mean ± SEM (n = 6).

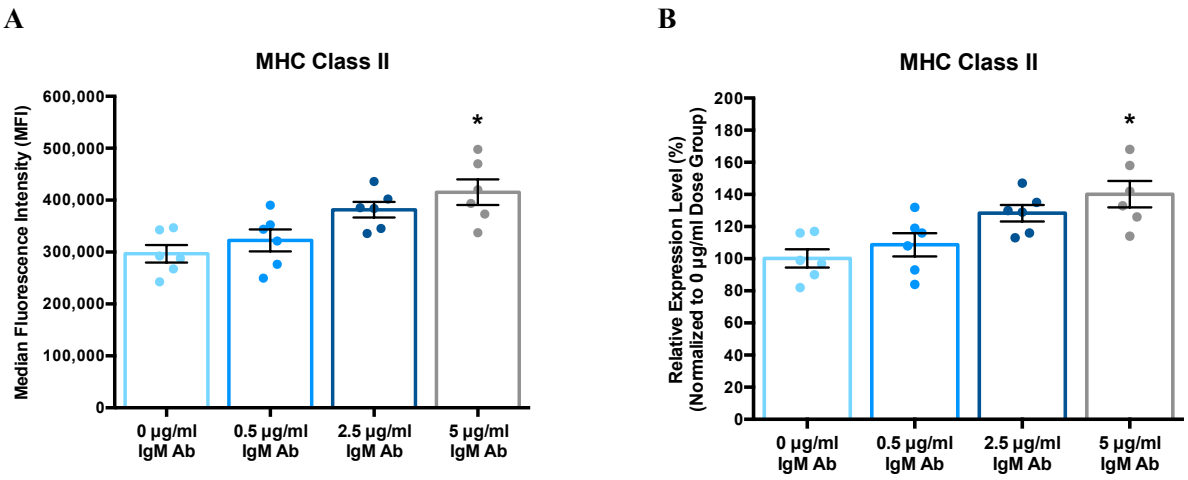

Figure 5-7: MHC Class II surface expression in 3D immune organoids and BCR crosslinking
MHC Class II (A) surface MFI expression level and (B) percent change in expression level normalized to 0 µg/ml dose group in CD19+ B cells with varying amount of soluble anti-IgM antibody added to induce BCR crosslinking. Statistical significance (*) with regard to 0 µg/ml dose group was determined on $p < 0.05$. Values are shown as mean ± SEM (n = 6).

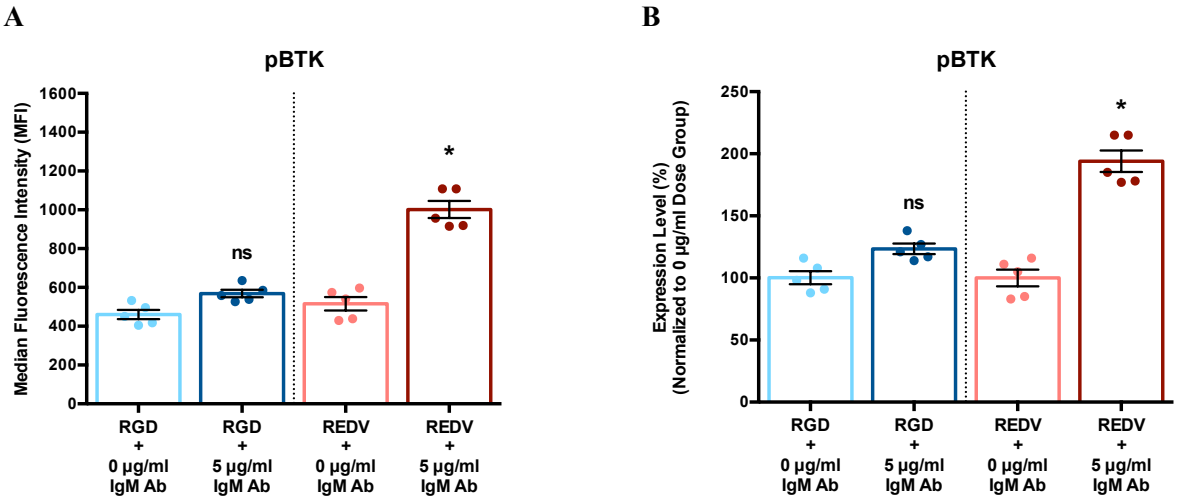

Figure 5-8: pBTK intracellular expression in 3D immune organoids and BCR crosslinking
pBTK (A) intracellular MFI expression level and (B) percent change in expression level normalized to 0 µg/ml dose group in CD19+ B cells was assessed for both RGD- and REDV-functionalized immune organoids with varying amount of soluble anti-IgM antibody added to induce BCR crosslinking. Statistical significance (*) with regard to 0 µg/ml dose group was determined on $p < 0.05$. Values are shown as mean ± SEM (n = 5).

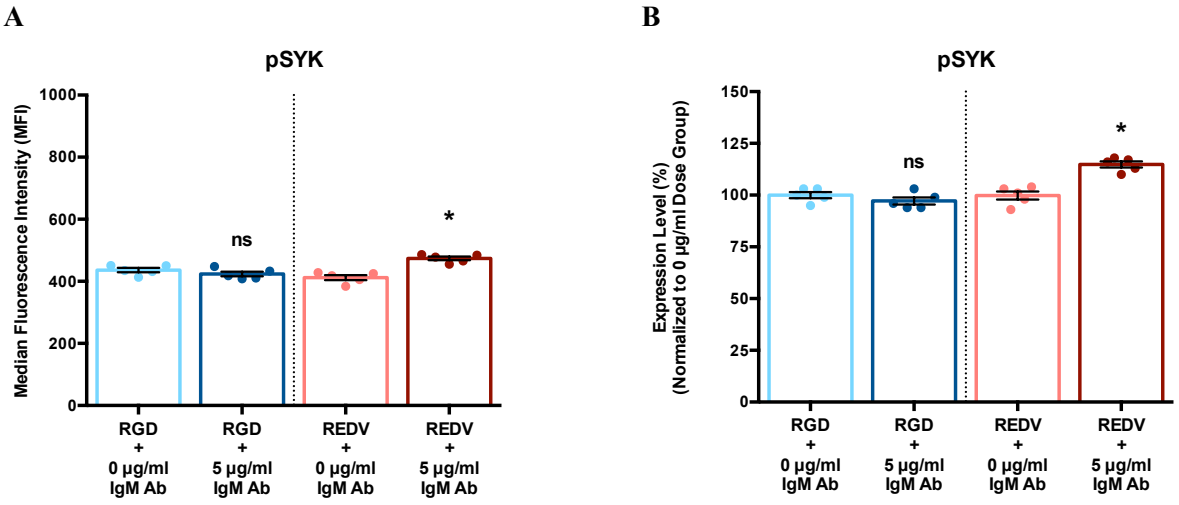

Figure 5-9: pSYK intracellular expression in 3D immune organoids and BCR crosslinking
pSYK (A) intracellular MFI expression level and (B) percent change in expression level normalized to 0 µg/ml dose group in CD19+ B cells was assessed for both RGD- and REDV-functionalized immune organoids with varying amount of soluble anti-IgM antibody added to induce BCR crosslinking. Statistical significance (*) with regard to 0 µg/ml dose group was determined on $p < 0.05$. Values are shown as mean ± SEM (n = 5).

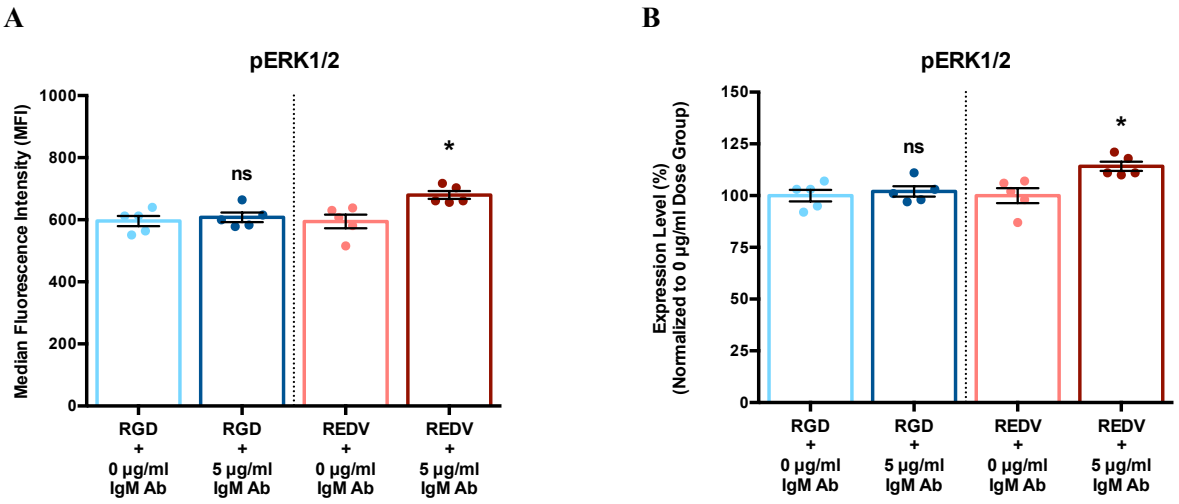

Figure 5-10: pERK1/2 intracellular expression in 3D immune organoids and BCR crosslinking
pERK1/2 (A) intracellular MFI expression level and (B) percent change in expression level normalized to 0 µg/ml dose group in CD19+ B cells was assessed for both RGD- and REDV-functionalized immune organoids with varying amount of soluble anti-IgM antibody added to induce BCR crosslinking. Statistical significance (*) with regard to 0 µg/ml dose group was determined on $p < 0.05$. Values are shown as mean ± SEM (n = 5).

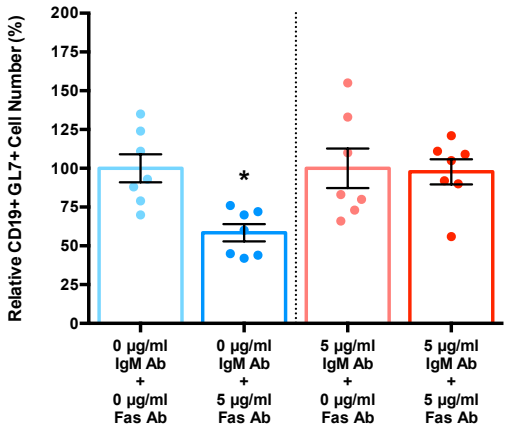

Figure 5-11: Relative GC-like B cell number with BCR crosslinking and Fas stimulation
Analysis was conducted on GC-like B cells in the presence of 5 µg/ml anti-IgM antibody with or without 5 µg/ml soluble Fas antibody. Statistical significance (*) with regard to 0 µg/ml dose group was determined on $p < 0.05$. Values are shown as mean ± SEM (n = 7).

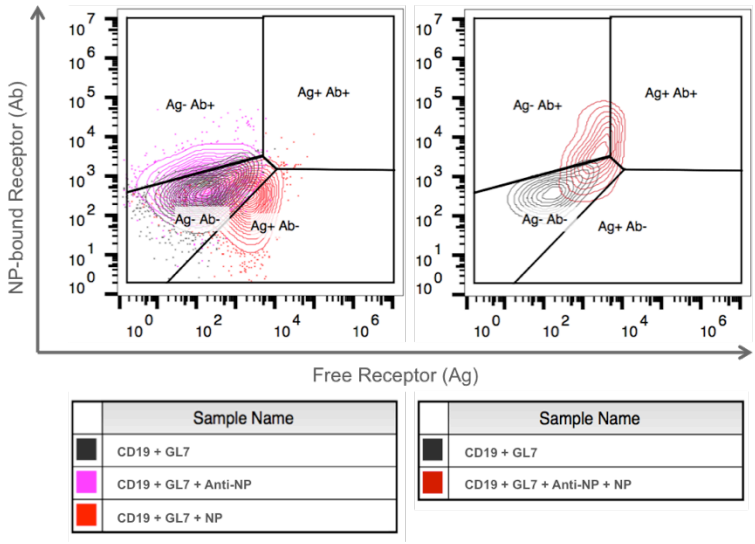

Figure 5-12: Gating schematic for antigen-specific GC-like B cell analysis
Gating schematic was prepared to analyze NP-specific and non-specific GC-like B cells. Gate was prepared based on the binding of fluorophore-conjugated NP and/or antibody against NP (left). Gating approach was demonstrated for GC-like B cells left unstained or stained with both fluorophore-conjugated NP and antibody against NP (right).

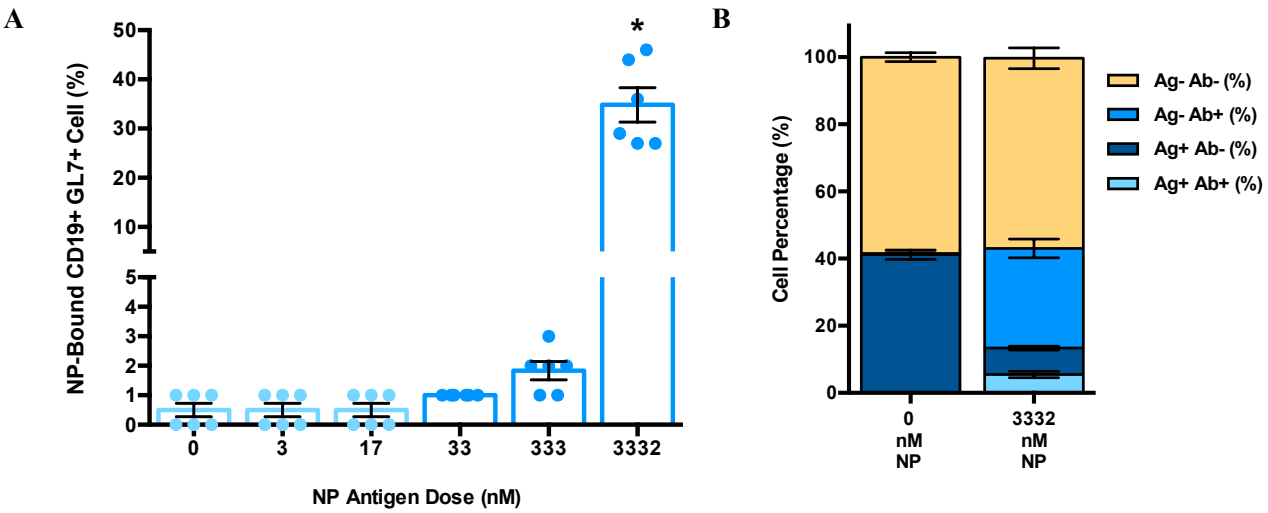

Figure 5-13: Antigen-bound GC-like B cell percentage with soluble NP antigen addition
(A) Quantification of NP-bound CD19+ GL7+ GC-like B cells with varying amount of soluble NP antigen. (B) Visualization of CD19+ GL7+ GC-like B cell composition at both 0 and 3332 nM soluble NP antigen dose. Statistical significance (*) with regard to 0 nM dose group was determined on $p < 0.05$. Values are shown as mean ± SEM (n = 7).

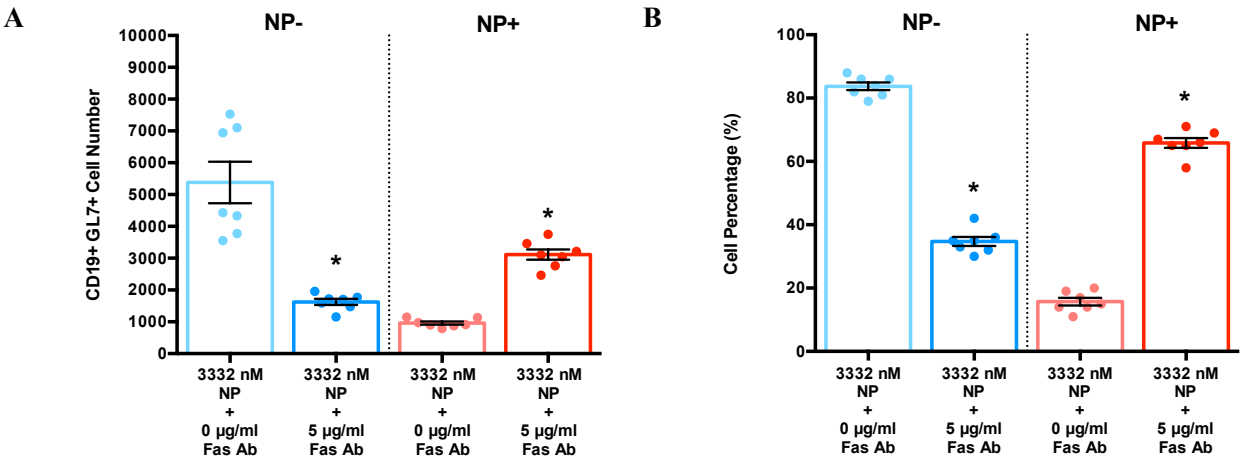

Figure 5-14: GC-like B cells with soluble NP addition and/or Fas stimulation
GC-like B cell analysis in (A) absolute number and (B) relative composition percentage in the presence of soluble NP antigen with or without soluble Fas antibody. Analysis was conducted on both antigen-specific (NP+) and non-specific (NP-) groups. Statistical significance (*) with regard to 0 µg/ml anti-Fas antibody dose group was determined on $p < 0.05$. Values are shown as mean ± SEM (n = 7).

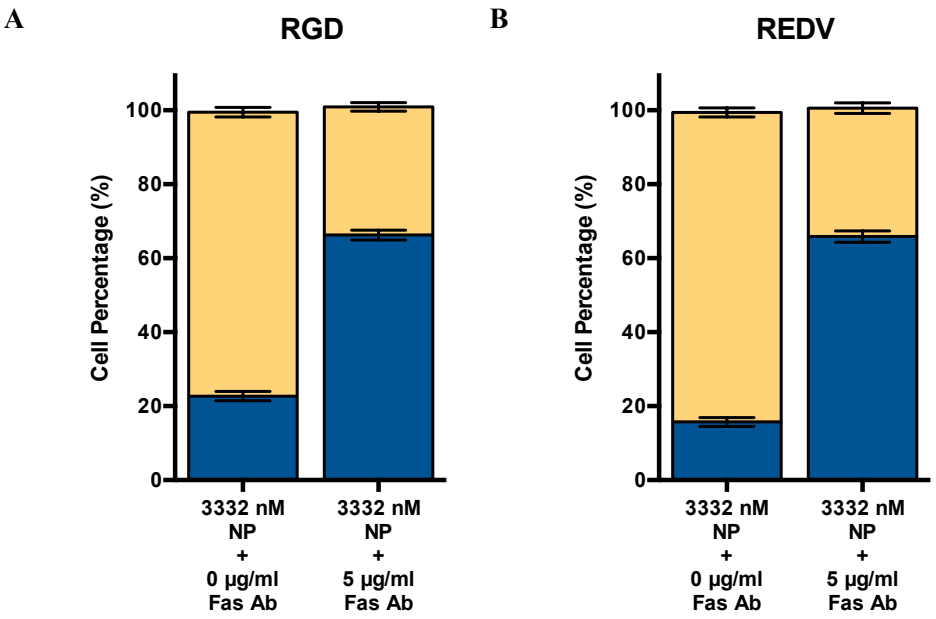

Figure 5-15: Simplified GC-like B cell composition with soluble NP antigen and Fas stimulation
GC-like B cell composition in (A) RGD- and (B) REDV-functionalized immune organoids in the presence of soluble NP antigen with or without soluble anti-Fas antibody. Analysis was done on antigen-specific (blue) and non-specific (yellow) GC-like B cells. Values are shown as mean ± SEM (n = 7).

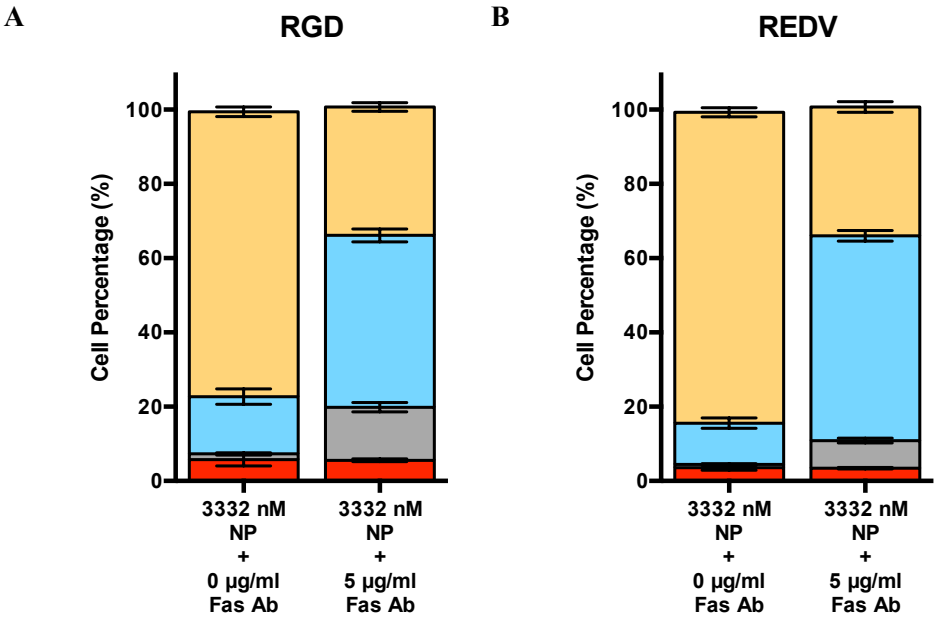

Figure 5-16: Detailed GC-like B cell composition with soluble NP antigen and Fas stimulation
Detailed GC-like B cell composition in (A) RGD- and (B) REDV-functionalized immune organoids in the presence of soluble NP antigen with or without soluble anti-Fas antibody. Analysis was done on partially bound (grey), fully bound (blue), unbound (red), and non-specific (yellow) GC-like B cells. Values are shown as mean ± SEM (n = 7).

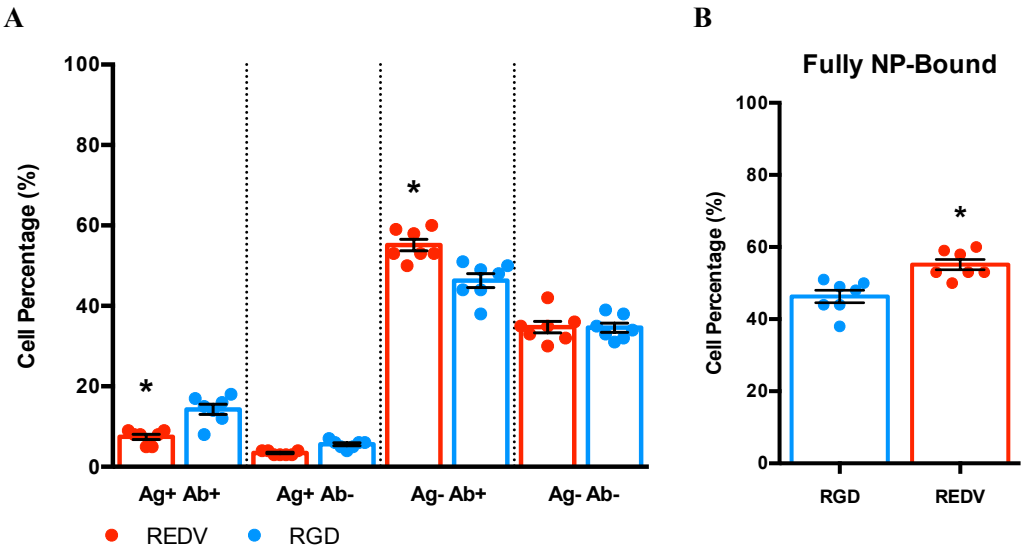

Figure 5-17: Quantification of GC-like B cell subtype with soluble NP antigen and Fas stimulation Quantified GC-like B cell subsets in RGD- and REDV-functionalized immune organoids in the presence of soluble NP antigen with or without soluble anti-Fas antibody. Analysis was conducted on partially bound (Ag+ Ab+), unbound (Ag+ Ab-), fully bound (Ag- Ab+), and non-specific (Ag- Ab-) groups. Statistical significance (*) with regard to the same subtype and another peptide (RGD) was determined on $p < 0.05$. Values are shown as mean ± SEM (n = 7).

CHAPTER 6

Research Discussion

6.1. Summary

We were initially motivated to develop an improved B cell culture system because existing *ex vivo* approaches have yet to capture the key aspects of lymphoid tissue microenvironment and/or be capable of functioning without live animal models. We expected that such approach could be used to model the GC reaction in order to better understand the signals that control GC induction, maintenance, and exit. In the long term, we hoped that the resulting technology could facilitate rapid *ex vivo* generation of antigen-specific antibodies. Such ability would greatly benefit studies on adaptive immune response generation, lymphoid transformation and therapeutic agents that can interact with the immune system.

With these goals in mind, we have developed the immune organoid technology and assessed the important design parameters. This assertion can be illustrated by highlighting several results that have been previously described in this dissertation. We first showed the ability of engineered immune organoids to improve GC induction in culture as indicated by the sustained B cell number and the enhanced expansion of GC-like B cells (Chapter 2). Our data indicated that the presence of RGD – the ligand for αvβ3 integrin subunits – was partially responsible for maintaining B cell number in culture. From further characterization on the immune organoids, we revealed that the organoid-derived GC-like B cells were comparable to *in vivo* GC B cells in terms of viability, acquisition of signature GC transcriptome, and somatic hypermutation (Chapter 3). Furthermore, the use of biomaterials-based scaffold provided better viability, proliferation, and representative GC transcriptome when compared to the conventional 2D co-culture system. In order to understand the role of integrin signaling, we utilized a modular immune organoid and showed that integrin ligand type could modulate GC-like B cell phenotype

(Chapter 4). We found that integrin ligand specificity could influence surface BCR clustering and expression on GC-like B cells. We then assessed the role of BCR stimulation in the presence of various integrin ligands toward GC-like B cell maintenance, differentiation, and selection (Chapter 5). We observed that BCR signaling could initiate the ASC differentiation program and facilitate the enrichment of antigen-specific GC-like B cells in the presence of Fas negative selection pressure. Summarizing these key points, we have shown our ability to expand GC reaction in culture using immune organoids, provide a comparable GC model relative to the *in vivo* counterpart, study the role of signals from the lymphoid microenvironment, and engineer specific GC processes in the immune organoids.

These results suggest that we are not only capable of inducing GC reaction to produce GC-like B cells but also controlling the phenotype of this cell population. The control could be illustrated by the enhanced generation of GC-like B cells in culture, the improved acquisition of key GC markers, the shift toward ASC differentiation program, and the enrichment of antigen-specific GC-like B cells. The potential application of this approach was also demonstrated in studying the EZH2-dependent mechanism of cell cycle regulation during GC reaction. Being able to produce these outcomes mean that we are indeed progressing toward an improved B cell culture system that can better model GC reaction. At the same time, it is important to reflect on our journey to gain insights about improving this system in the future.

In addition to highlighting the key findings above, this chapter is also meant to provide a reflection on the experience handling this project and a future outlook regarding the key next steps that can be done. By describing the approaches that work well and the steps that could have been taken in the past, we hope that the readers can learn important lessons about successfully completing a research project and avoiding pitfalls throughout the process. By providing a perspective about how this technology platform may evolve in the future, we wish that the readers could gain inspiration about potential research directions and improvements to the existing system.

6.2. Reflection

Throughout this project, several approaches have worked well in ensuring the completion of key milestones and the constant development of our B cell culture system. These recommended procedures could be distilled into three concrete steps: testing the main hypothesis, analyzing system sensitivity, and tracking changes throughout the proposed mechanism. We will describe the definition of each step and a short example of its implementation during this project.

First of all, developing a simple approach to quickly test the key hypothesis. Before we develop a sophisticated technology, we need to ensure that the underlying argument makes sense. We hypothesized that BCR stimulation in GC-like B cells would make them resistant to Fas-mediated apoptosis and therefore antigen-binding antigen-specific GC-like B cells could be enriched using this method. Nevertheless, we were using WT B cells and it was unclear how we can stimulate BCR signaling uniformly across B cells due to their heterogeneous BCR. We also learned that FasL is commonly used and yet it has to be immobilized for inducing an efficient Fas-mediated apoptosis. In order to quickly test the hypothesis before obtaining the antigen-specific transgenic mice and optimizing FasL conjugation into the organoid matrix, we first utilized an antibody against IgM to initiate BCR crosslinking and then introduced an antibody against Fas to trigger cytolytic activity. With the result showing that BCR stimulation maintained cell number following Fas signaling, we could quickly demonstrate the validity of our preliminary hypothesis and go forward with the antigen-specific system using B1-8^{hi} mouse model.

Secondly, systematically assessing the system sensitivity. We have to realize that the optimal dose for any particular stimulatory signal will be different depending on the system. In order to induce BCR crosslinking in the immune organoids using WT B cells, we utilized a soluble antibody against IgM and yet we found varying protocols for BCR stimulation in the literature. Since most works are done in 2D and the culture conditions can be very different, we used the published doses to prepare a guideline for

titrating the doses ourselves. For every experiment assessing the role of BCR stimulation, we always used 4 dose groups (including the negative control) to understand the dose response relationship and determine where the optimal response occurs.

Thirdly, running parallel experiments to validate multiple sub-hypotheses. Since any particular stimulation can result in several downstream effects, it is important to assess each factor from multiple outcomes. When we were analyzing how BCR signaling works in the modular immune organoid system, we conducted experiments to assess GC maintenance, ASC differentiation, BCR signaling, and Fas resistance. By being able to track changes across these metrics, we could increase our confidence that BCR stimulation was working in accordance with the proposed mechanism and using such knowledge as a benchmark before studying other variables (e.g. time points, specific antigens, presentation format, etc.)

At the same time, looking into past experiments has brought the realization that several things could have been done better. These proposed improvements could again be summarized with three concrete steps: balancing characterization and progression, thinking about the so what, and understanding the proper validation method. We will describe the definition of each step along with its relevance to this project.

First of all, it is important to ensure a good balance between characterizing the system and progressing with the next experiment. Throughout this project, we constantly asked ourselves how long we should spend our time understanding the system before going into our next aim. Since research proposal is often defined by three specific aims, we frequently want to quickly complete our current aim and move forward with the next aim. When we were trying to develop an immune organoid system for modeling GC reaction, we initially hoped that showing the presence of GC-like B cells would be enough and we could move toward generating antibody in culture. But then we realized the importance of assessing the presence/absence of each GC hallmark event, understanding the role of each design parameter, crafting a

strategy to induce differentiation toward ASC fate, and preparing a method to enrich antigen-specific cells such that antigen-specific antibodies could be produced in the future.

Secondly, we have to constantly think about the relevance of our result (i.e. the so what). Upon completing the study of integrin ligand specificity, it was unclear what was the next step for us. Such situation could be explained by the intense focus placed on running the previously planned experiments, analyzing the data, and writing the manuscript for submission. It would also be important to carefully think about the next study to be done. At the same time, having a good idea about the relevance of your current study would make it easier to plan the next ones. Realizing that integrin ligand specificity mostly modulated surface BCR on GC-like B cells and BCR stimulation could allow us to achieve our other goals (e.g. ASC terminal differentiation and antigen-based selection), we next studied how our immune organoids respond to BCR crosslinking in culture.

Thirdly, it is critical to understand the best way to validate your hypothesis. When we started with initiating GC reaction *ex vivo* using the immune organoid, we thought that validation was simply based on B cell number and expression of GC surface markers (e.g. GL7 and Fas). Our assumption originated from reading several papers on B cell activation and noticing that expansion of GL7+ Fas+ B cells was the main metric used in most of them. From further research and correspondence with our medical school collaborators, we learned the importance of supporting the earlier observations with sequencing data. The resulting information could notify us about things like gene expression profile and somatic hypermutation. Gene expression analysis would be important because the presence of signature GC transcriptome represents the gold standard for GC B cell identification, while somatic hypermutation signifies a GC-specific functional event. Conducting these studies to validate *ex vivo* GC reaction is truly important to demonstrate the comparability of our immune organoids with their *in vivo* counterparts.

6.3. Future Outlook

Having spent a large part of this dissertation discussing the observations made from past experiments, it is time to start considering the next steps of this project. While we have made great strides in achieving our initial goals, we realize that there is still room for further learning and improvements. From numerous discussions with my research advisor and lab colleagues, the next key steps could be distilled into four potential studies: understanding biomaterials-based signals, investigating the mechanism of integrin signaling, assessing the role of signal presentation format in selection efficiency, and studying antibody production in culture. For each study, we will discuss both the rationale and the expectations.

Studying the role of biomaterials-based signals will be important because we have shown the importance of gelatin matrix reinforced by silicate nanoparticles in not only improving GC-like B cell viability and proliferation but also ensuring the acquisition of signature GC transcriptome. But we have yet to fully understand how these outcomes were generated in terms of the specific signals and pathways. We thus need to learn what signals are being produced by the matrix and how they work in the immune organoids. Considering that GC-like B cells cluster next to *in vivo* GC B cells in the PCA space, we can also investigate what signal and/or pathway has to be added to bring the two cell clusters closer together.

While integrin signaling has been well studied in other cells and systems, we are just starting to appreciate the role of integrin in B cell activation and differentiation. We are thus still lacking a complete picture about how integrin activation works in GC B cells throughout GC reaction. While we observed integrin co-localization with BCR, we have yet to know how such process happens. We then need to determine the signaling pathways that occur following the binding of integrin ligand and develop a mechanistic understanding of integrin signaling during humoral immune response generation.

We need to understand the role of signal presentation format because we have been using soluble antigen and/or activating antibodies and yet some signals are found to be membrane-bound in the lymphoid tissue microenvironment. The literature has also indicated that presenting a signal in soluble form (vs. immobilized or membrane-bound) can either produce an opposite effect or modulate its potency. Signals such as FasL have also been known to require aggregation for improved function. As we are trying to improve the efficiency of our antigen-specific GC-like B cell enrichment process, we have to consider the importance of signal presentation format inside the modular immune organoids.

Since our long-term goal is to produce antigen-specific class-switched antibody in culture, we have to optimize the protocol for inducing terminal differentiation of GC-like B cells toward ASC fate and ensuring rapid antibody secretion from the differentiated cells. Our results indicate the induction of CSR upon IL-4 addition, but we need to optimize the process to produce an efficient class switching. While we have shown the induction of ASC differentiation program, we still need to ensure that the cells are turned into long-lived plasma cells instead of short-lived plasmablasts. We also need to confirm that antigen-specific class-switched antibodies are secreted at a sustained level over time in culture.

Having described the potential studies that can be done to bring our technology platform closer to our initial goal, we hope that the rationales provided will inspire the readers to continue the work for improving the immune organoids. While there is a still a long journey ahead, we believe that the reflection provided earlier in this chapter and the future outlook described above will the readers to achieve the goals of designing a fully functional B cell culture system. Reaching such objective will enable us to better model GC reaction and help fellow researchers answer open questions in GC research. From the translational standpoint, we believe that this capability will accelerate the development of antibody-based therapies and other therapeutic agents that interact with the immune system.

REFERENCES

1. Victora, G.D. and M.C. Nussenzweig, *Germinal centers.* Annual review of immunology, 2012. **30**: p. 429-457.
2. Allen, C.D., T. Okada, and J.G. Cyster, *Germinal-center organization and cellular dynamics.* Immunity, 2007. **27**(2): p. 190-202.
3. De Silva, N.S. and U. Klein, *Dynamics of B cells in germinal centres.* Nature Reviews Immunology, 2015. **15**(3): p. 137-148.
4. Klein, U. and R. Dalla-Favera, *Germinal centres: role in B-cell physiology and malignancy.* Nature Reviews Immunology, 2008. **8**(1): p. 22-33.
5. Batista, F.D. and N.E. Harwood, *The who, how and where of antigen presentation to B cells.* Nature Reviews Immunology, 2009. **9**(1): p. 15-27.
6. Paus, D., et al., *Antigen recognition strength regulates the choice between extrafollicular plasma cell and germinal center B cell differentiation.* The Journal of experimental medicine, 2006. **203**(4): p. 1081-1091.
7. Kouskoff, V., et al., *Antigens varying in affinity for the B cell receptor induce differential B lymphocyte responses.* Journal of Experimental Medicine, 1998. **188**(8): p. 1453-1464.
8. Jegerlehner, A., et al., *Regulation of IgG antibody responses by epitope density and CD21‐mediated costimulation.* European journal of immunology, 2002. **32**(11): p. 3305-3314.
9. Liu, W. and Y.H. Chen, *High epitope density in a single protein molecule significantly enhances antigenicity as well as immunogenicity: a novel strategy for modern vaccine development and a preliminary investigation about B cell discrimination of monomeric proteins.* European journal of immunology, 2005. **35**(2): p. 505-514.
10. Moon, J.J., et al., *Enhancing humoral responses to a malaria antigen with nanoparticle vaccines that expand Tfh cells and promote germinal center induction.* Proceedings of the National Academy of Sciences, 2012. **109**(4): p. 1080-1085.
11. Young, L.S. and A.B. Rickinson, *Epstein–Barr virus: 40 years on.* Nature Reviews Cancer, 2004. **4**(10): p. 757-768.
12. Tosato, G. and J.I. Cohen, *Generation of Epstein‐Barr Virus (EBV)–Immortalized B Cell Lines.* Current protocols in immunology, 2007: p. 7.22. 1-7.22. 4.
13. Kempkes, B., et al., *Immortalization of human primary B lymphocytes in vitro with DNA.* Proceedings of the National Academy of Sciences, 1995. **92**(13): p. 5875-5879.
14. Sugden, B., M. Phelps, and J. Domoradzki, *Epstein-Barr virus DNA is amplified in transformed lymphocytes.* Journal of virology, 1979. **31**(3): p. 590-595.
15. Chaganti, S., et al., *Epstein-Barr virus infection in vitro can rescue germinal center B cells with inactivated immunoglobulin genes.* Blood, 2005. **106**(13): p. 4249-4252.
16. Cerutti, A., et al., *CD40 ligand and appropriate cytokines induce switching to IgG, IgA, and IgE and coordinated germinal center and plasmacytoid phenotypic differentiation in a human monoclonal IgM+ IgD+ B cell line.* The Journal of Immunology, 1998. **160**(5): p. 2145-2157.
17. Avery, D.T., et al., *IL-21-induced isotype switching to IgG and IgA by human naive B cells is differentially regulated by IL-4.* The Journal of Immunology, 2008. **181**(3): p. 1767-1779.
18. Batten, M., et al., *BAFF mediates survival of peripheral immature B lymphocytes.* Journal of Experimental Medicine, 2000. **192**(10): p. 1453-1466.
19. Justement, L., J. Kreiger, and J. Cambier, *Production of multiple lymphokines by the A20. 1 B cell lymphoma after cross-linking of membrane Ig by immobilized anti-Ig.* The Journal of Immunology, 1989. **143**(3): p. 881-889.
20. Roberts, T. and E.C. Snow, *Cutting edge: recruitment of the CD19/CD21 coreceptor to B cell antigen receptor is required for antigen-mediated expression of Bcl-2 by resting and cycling hen egg lysozyme transgenic B cells.* The Journal of Immunology, 1999. **162**(8): p. 4377-4380.
21. Zamorano, J., et al., *Soluble, but not immobilized, anti-IgM antibody inhibits post-activation events leading to T-cell-dependent B-cell differentiation.* Immunology, 1995. **85**(2): p. 241.
22. Parry, S.L., et al., *Hypercross-linking surface IgM or IgD receptors on mature B cells induces apoptosis that is reversed by costimulation with IL-4 and anti-CD40.* The Journal of Immunology, 1994. **152**(6): p. 2821-2829.

23. Crotty, S., *Follicular helper CD4 T cells (Tfh).* Annual review of immunology, 2011. **29**: p. 621-663.
24. Shulman, Z., et al., *T follicular helper cell dynamics in germinal centers.* Science, 2013. **341**(6146): p. 673-677.
25. Shulman, Z., et al., *Dynamic signaling by T follicular helper cells during germinal center B cell selection.* Science, 2014. **345**(6200): p. 1058-1062.
26. Lahvis, G.P. and J. Cerny, *Induction of germinal center B cell markers in vitro by activated CD4+ T lymphocytes: the role of CD40 ligand, soluble factors, and B cell antigen receptor cross-linking.* The Journal of Immunology, 1997. **159**(4): p. 1783-1793.
27. Huang, S., et al., *Human B cells accumulate immunoglobulin V gene somatic mutations in a cell contact-dependent manner in cultures supported by activated T cells but not in cultures supported by CD40 ligand.* Clinical and experimental immunology, 1999. **116**(3): p. 441-448.
28. Zan, H., et al., *Induction of Ig somatic hypermutation and class switching in a human monoclonal IgM+ IgD+ B cell line in vitro: definition of the requirements and modalities of hypermutation.* The Journal of Immunology, 1999. **162**(6): p. 3437-3447.
29. Cannons, J.L., et al., *Optimal germinal center responses require a multistage T cell: B cell adhesion process involving integrins, SLAM-associated protein, and CD84.* Immunity, 2010. **32**(2): p. 253-265.
30. Lu, K.T., et al., *Functional and epigenetic studies reveal multistep differentiation and plasticity of in vitro-generated and in vivo-derived follicular T helper cells.* Immunity, 2011. **35**(4): p. 622-632.
31. Suto, A., et al., *Development and characterization of IL-21–producing CD4+ T cells.* Journal of Experimental Medicine, 2008. **205**(6): p. 1369-1379.
32. Nurieva, R.I., et al., *Bcl6 mediates the development of T follicular helper cells.* Science, 2009. **325**(5943): p. 1001-1005.
33. Yuseff, M.-I., et al., *How B cells capture, process and present antigens: a crucial role for cell polarity.* Nature Reviews Immunology, 2013. **13**(7): p. 475-486.
34. Kosco, M., E. Pflugfelder, and D. Gray, *Follicular dendritic cell-dependent adhesion and proliferation of B cells in vitro.* The Journal of Immunology, 1992. **148**(8): p. 2331-2339.
35. Aydar, Y., et al., *The influence of immune complex-bearing follicular dendritic cells on the IgM response, Ig class switching, and production of high affinity IgG.* The Journal of Immunology, 2005. **174**(9): p. 5358-5366.
36. Wu, Y., et al., *Immune complex-bearing follicular dendritic cells deliver a late antigenic signal that promotes somatic hypermutation.* The Journal of Immunology, 2008. **180**(1): p. 281-290.
37. Freedman, A.S., et al., *Adhesion of human B cells to germinal centers in vitro involves VLA-4 and INCAM-110.* Science, 1990. **249**(4972): p. 1030-1034.
38. Koopman, G., et al., *Adhesion of human B cells to follicular dendritic cells involves both the lymphocyte function-associated antigen 1/intercellular adhesion molecule 1 and very late antigen 4/vascular cell adhesion molecule 1 pathways.* Journal of Experimental Medicine, 1991. **173**(6): p. 1297-1304.
39. Koopman, G., et al., *Adhesion through the LFA-1 (CD11a/CD18)-ICAM-1 (CD54) and the VLA-4 (CD49d)-VCAM-1 (CD106) pathways prevents apoptosis of germinal center B cells.* The Journal of Immunology, 1994. **152**(8): p. 3760-3767.
40. Usui, K., et al., *Isolation and characterization of naïve follicular dendritic cells.* Molecular immunology, 2012. **50**(3): p. 172-176.
41. Schriever, F., et al., *Isolated human follicular dendritic cells display a unique antigenic phenotype.* Journal of Experimental Medicine, 1989. **169**(6): p. 2043-2058.
42. Han, S., et al., *Cellular interaction in germinal centers. Roles of CD40 ligand and B7-2 in established germinal centers.* The Journal of Immunology, 1995. **155**(2): p. 556-567.
43. Oxenius, A., et al., *CD40-CD40 ligand interactions are critical in TB cooperation but not for other anti-viral CD4+ T cell functions.* Journal of Experimental Medicine, 1996. **183**(5): p. 2209-2218.
44. Mazzei, G.J., et al., *Recombinant soluble trimeric CD40 ligand is biologically active.* Journal of Biological Chemistry, 1995. **270**(13): p. 7025-7028.
45. Fanslow, W.C., et al. *Structural characteristics of CD40 ligand that determine biological function*. in *Seminars in immunology*. 1994. Elsevier.
46. Pound, J.D. and J. Gordon, *Maintenance of human germinal center B cells in vitro.* Blood, 1997. **89**(3): p. 919-928.
47. Arpin, C., et al., *Generation of memory B cells and plasma cells in vitro.* Science, 1995. **268**(5211): p. 720-722.

48. Nojima, T., et al., *In-vitro derived germinal centre B cells differentially generate memory B or plasma cells in vivo.* Nature communications, 2011. **2**: p. 465.
49. Moutai, T., et al., *A Novel and Effective Cancer Immunotherapy Mouse Model Using Antigen-Specific B Cells Selected In Vitro.* PloS one, 2014. **9**(3): p. e92732.
50. Yamamura, S., et al., *Single-cell microarray for analyzing cellular response.* Analytical chemistry, 2005. **77**(24): p. 8050-8056.
51. Kim, H., et al., *Live lymphocyte arrays for biosensing.* Advanced functional materials, 2006. **16**(10): p. 1313-1323.
52. Kim, H., et al., *Large area two-dimensional B cell arrays for sensing and cell-sorting applications.* Biomacromolecules, 2004. **5**(3): p. 822-827.
53. Li, N. and C.-M. Ho, *Photolithographic patterning of organosilane monolayer for generating large area two-dimensional B lymphocyte arrays.* Lab on a Chip, 2008. **8**(12): p. 2105-2112.
54. Love, J.C., et al., *A microengraving method for rapid selection of single cells producing antigen-specific antibodies.* Nature biotechnology, 2006. **24**(6): p. 703-707.
55. Vasconcellos, F.C., et al., *Bioactive polyelectrolyte multilayers: Hyaluronic acid mediated B lymphocyte adhesion.* Biomacromolecules, 2010. **11**(9): p. 2407-2414.
56. Natkanski, E., et al., *B cells use mechanical energy to discriminate antigen affinities.* Science, 2013. **340**(6140): p. 1587-1590.
57. Nowosad, C.R., K.M. Spillane, and P. Tolar, *Germinal center B cells recognize antigen through a specialized immune synapse architecture.* Nature immunology, 2016. **17**(7): p. 870-877.
58. Spillane, K.M. and P. Tolar, *B cell antigen extraction is regulated by physical properties of antigen-presenting cells.* J Cell Biol, 2016: p. jcb. 201607064.
59. Depoil, D., et al., *CD19 is essential for B cell activation by promoting B cell receptor–antigen microcluster formation in response to membrane-bound ligand.* Nature immunology, 2008. **9**(1): p. 63-72.
60. Wan, Z., et al., *B cell activation is regulated by the stiffness properties of the substrate presenting the antigens.* The Journal of Immunology, 2013. **190**(9): p. 4661-4675.
61. Suematsu, S. and T. Watanabe, *Generation of a synthetic lymphoid tissue–like organoid in mice.* Nature biotechnology, 2004. **22**(12): p. 1539-1545.
62. Okamoto, N., et al., *Artificial lymph nodes induce potent secondary immune responses in naive and immunodeficient mice.* The Journal of clinical investigation, 2007. **117**(4): p. 997-1007.
63. Banerjee, P., et al., *A novel and simple cell-based detection system with a collagen-encapsulated B-lymphocyte cell line as a biosensor for rapid detection of pathogens and toxins.* Laboratory Investigation, 2008. **88**(2): p. 196-206.
64. Rider, T.H., et al., *AB cell-based sensor for rapid identification of pathogens.* Science, 2003. **301**(5630): p. 213-215.
65. Nichols, J.E., et al., *In vitro analog of human bone marrow from 3D scaffolds with biomimetic inverted colloidal crystal geometry.* Biomaterials, 2009. **30**(6): p. 1071-1079.
66. Feng, Q., et al., *Expansion of engrafting human hematopoietic stem/progenitor cells in three‐dimensional scaffolds with surface‐immobilized fibronectin.* Journal of Biomedical Materials Research Part A, 2006. **78**(4): p. 781-791.
67. Abbott, R.K., et al., *Germinal Center Hypoxia Potentiates Immunoglobulin Class Switch Recombination.* The Journal of Immunology, 2016. **197**(10): p. 4014-4020.
68. Schioppa, T., et al., *Regulation of the chemokine receptor CXCR4 by hypoxia.* Journal of Experimental Medicine, 2003. **198**(9): p. 1391-1402.
69. Piovan, E., et al., *Differential regulation of hypoxia-induced CXCR4 triggering during B-cell development and lymphomagenesis.* Cancer research, 2007. **67**(18): p. 8605-8614.
70. Carpenter, L., et al., *Human induced pluripotent stem cells are capable of B-cell lymphopoiesis.* Blood, 2011. **117**(15): p. 4008-4011.
71. Cho, S.K., et al., *Functional characterization of B lymphocytes generated in vitro from embryonic stem cells.* Proceedings of the National Academy of Sciences, 1999. **96**(17): p. 9797-9802.
72. Hunte, B.E., et al., *flk2/flt3 ligand is a potent cofactor for the growth of primitive B cell progenitors.* The Journal of Immunology, 1996. **156**(2): p. 489-496.
73. Veiby, O.P., S.D. Lyman, and S. Jacobsen, *Combined signaling through interleukin-7 receptors and flt3 but not c-kit potently and selectively promotes B-cell commitment and differentiation from uncommitted murine bone marrow progenitor cells.* Blood, 1996. **88**(4): p. 1256-1265.

74. Vieira, P. and A. Cumano, *Differentiation of B lymphocytes from hematopoietic stem cells.* B Cell Protocols, 2004: p. 67-76.
75. Vodyanik, M.A., et al., *Human embryonic stem cell–derived CD34+ cells: efficient production in the coculture with OP9 stromal cells and analysis of lymphohematopoietic potential.* Blood, 2005. **105**(2): p. 617-626.
76. Dallas, M.H., et al., *Density of the Notch ligand Delta1 determines generation of B and T cell precursors from hematopoietic stem cells.* Journal of Experimental Medicine, 2005. **201**(9): p. 1361-1366.
77. Schmitt, T.M. and J.C. Zúñiga-Pflücker, *Induction of T cell development from hematopoietic progenitor cells by delta-like-1 in vitro.* Immunity, 2002. **17**(6): p. 749-756.
78. Schmitt, T.M., et al., *Induction of T cell development and establishment of T cell competence from embryonic stem cells differentiated in vitro.* Nature immunology, 2004. **5**(4): p. 410-417.
79. La Motte-Mohs, R.N., E. Herer, and J.C. Zúñiga-Pflücker, *Induction of T-cell development from human cord blood hematopoietic stem cells by Delta-like 1 in vitro.* Blood, 2005. **105**(4): p. 1431-1439.
80. De Smedt, M., I. Hoebeke, and J. Plum, *Human bone marrow CD34+ progenitor cells mature to T cells on OP9-DL1 stromal cell line without thymus microenvironment.* Blood Cells, Molecules, and Diseases, 2004. **33**(3): p. 227-232.
81. Mohtashami, M. and J.C. Zúñiga-Pflücker, *Cutting edge: three-dimensional architecture of the thymus is required to maintain delta-like expression necessary for inducing T cell development.* The Journal of Immunology, 2006. **176**(2): p. 730-734.
82. Dallas, M.H., et al., *Enhanced T-cell reconstitution by hematopoietic progenitors expanded ex vivo using the Notch ligand Delta1.* Blood, 2007. **109**(8): p. 3579-3587.
83. Varnum-Finney, B., et al., *Immobilization of Notch ligand, Delta-1, is required for induction of notch signaling.* Journal of cell science, 2000. **113**(23): p. 4313-4318.
84. Poznansky, M.C., et al., *Efficient generation of human T cells from a tissue-engineered thymic organoid.* Nature biotechnology, 2000. **18**(7): p. 729-734.
85. Lee, J. and N.A. Kotov, *Notch Ligand Presenting Acellular 3D Microenvironments for ex vivo Human Hematopoietic Stem‐Cell Culture made by Layer‐By‐Layer Assembly.* Small, 2009. **5**(9): p. 1008-1013.
86. Lin, J., et al., *Controlled major histocompatibility complex-T cell receptor signaling allows efficient generation of functional, antigen-specific CD8+ T cells from embryonic stem cells and thymic progenitors.* Tissue engineering Part A, 2010. **16**(9): p. 2709-2720.
87. Taqvi, S., L. Dixit, and K. Roy, *Biomaterial‐based notch signaling for the differentiation of hematopoietic stem cells into T cells.* Journal of biomedical materials research Part A, 2006. **79**(3): p. 689-697.
88. Levine, B.L., et al., *Antiviral effect and Ex Vivo CD4positive T cell proliferation in HIV-positive patients as a result of CD28 costimulation.* Science, 1996. **272**(5270): p. 1939.
89. Levine, B.L., et al., *Effects of CD28 costimulation on long-term proliferation of CD4+ T cells in the absence of exogenous feeder cells.* The Journal of Immunology, 1997. **159**(12): p. 5921-5930.
90. Tham, E.L., P.L. Jensen, and M.F. Mescher, *Activation of antigen-specific T cells by artificial cell constructs having immobilized multimeric peptide–class I complexes and recombinant B7–Fc proteins.* Journal of immunological methods, 2001. **249**(1): p. 111-119.
91. Oelke, M., et al., *Ex vivo induction and expansion of antigen-specific cytotoxic T cells by HLA-Ig–coated artificial antigen-presenting cells.* Nature medicine, 2003. **9**(5): p. 619-625.
92. Matic, J., et al., *Fine tuning and efficient T cell activation with stimulatory aCD3 nanoarrays.* Nano letters, 2013. **13**(11): p. 5090-5097.
93. Stephan, S.B., et al., *Biopolymer implants enhance the efficacy of adoptive T-cell therapy.* Nature biotechnology, 2015. **33**(1): p. 97-101.
94. Alizadeh, A.A., et al., *Distinct types of diffuse large B-cell lymphoma identified by gene expression profiling.* Nature, 2000. **403**(6769): p. 503-511.
95. Allman, D., et al., *BCL-6 expression during B-cell activation.* Blood, 1996. **87**(12): p. 5257-5268.
96. Song, J., et al., *Extracellular matrix of secondary lymphoid organs impacts on B-cell fate and survival.* Proceedings of the National Academy of Sciences, 2013. **110**(31): p. E2915-E2924.
97. Wang, X., et al., *Integrin-mediated interactions between B cells and follicular dendritic cells influence germinal center B cell fitness.* The Journal of Immunology, 2014. **192**(10): p. 4601-4609.
98. Nichol, J.W., et al., *Cell-laden microengineered gelatin methacrylate hydrogels.* Biomaterials, 2010. **31**(21): p. 5536-5544.

99. Patel, R.G., et al., *Microscale Bioadhesive Hydrogel Arrays for Cell Engineering Applications.* Cellular and Molecular Bioengineering, 2014. **7**(3): p. 394-408.
100. Peak, C.W., et al., *Elastomeric cell-laden nanocomposite microfibers for engineering complex tissues.* Cellular and Molecular Bioengineering, 2015. **8**(3): p. 404-415.
101. Xavier, J.R., et al., *Bioactive nanoengineered hydrogels for bone tissue engineering: a growth-factor-free approach.* ACS nano, 2015. **9**(3): p. 3109-3118.
102. Phelps, E.A., et al., *Maleimide cross‐linked bioactive peg hydrogel exhibits improved reaction kinetics and cross‐linking for cell encapsulation and in situ delivery.* Advanced materials, 2012. **24**(1): p. 64-70.
103. Phelps, E.A., et al., *Bioartificial matrices for therapeutic vascularization.* Proceedings of the National Academy of Sciences, 2010. **107**(8): p. 3323-3328.
104. Swartz, M.A., S. Hirosue, and J.A. Hubbell, *Engineering approaches to immunotherapy.* Science translational medicine, 2012. **4**(148): p. 148rv9-148rv9.
105. Hubbell, J.A., S.N. Thomas, and M.A. Swartz, *Materials engineering for immunomodulation.* Nature, 2009. **462**(7272): p. 449-460.
106. Dominguez, P.M., et al., *DNA methylation dynamics of germinal center B cells are mediated by AID.* Cell reports, 2015. **12**(12): p. 2086-2098.
107. Benton, J.A., et al., *Photocrosslinking of gelatin macromers to synthesize porous hydrogels that promote valvular interstitial cell function.* Tissue Engineering Part A, 2009. **15**(11): p. 3221-3230.
108. Lin, R.-Z., et al., *Transdermal regulation of vascular network bioengineering using a photopolymerizable methacrylated gelatin hydrogel.* Biomaterials, 2013. **34**(28): p. 6785-6796.
109. Gaharwar, A.K., et al., *Shear-thinning nanocomposite hydrogels for the treatment of hemorrhage.* ACS nano, 2014. **8**(10): p. 9833-9842.
110. Fujita, T. and M. Kashimura, *Scanning electron microscope studies of human spleen.* Immunologic Research, 1983. **2**(4): p. 375-384.
111. Hirsch, S., et al., *MR Elastography of the Liver and the Spleen Using a Piezoelectric Driver, Single‐Shot Wave‐Field Acquisition, and Multifrequency Dual Parameter Reconstruction.* Magnetic resonance in medicine, 2014. **71**(1): p. 267-277.
112. Mas-Moruno, C., F. Rechenmacher, and H. Kessler, *Cilengitide: the first anti-angiogenic small molecule drug candidate. Design, synthesis and clinical evaluation.* Anti-Cancer Agents in Medicinal Chemistry (Formerly Current Medicinal Chemistry-Anti-Cancer Agents), 2010. **10**(10): p. 753-768.
113. Stupp, R., et al., *Cilengitide combined with standard treatment for patients with newly diagnosed glioblastoma with methylated MGMT promoter (CENTRIC EORTC 26071-22072 study): a multicentre, randomised, open-label, phase 3 trial.* The lancet oncology, 2014. **15**(10): p. 1100-1108.
114. Vuong, B.Q., et al., *Specific recruitment of protein kinase A to the immunoglobulin locus regulates class-switch recombination.* Nature immunology, 2009. **10**(4): p. 420-426.
115. Shinkura, R., et al., *Separate domains of AID are required for somatic hypermutation and class-switch recombination.* Nature immunology, 2004. **5**(7): p. 707-712.
116. Hatzi, K., et al., *A hybrid mechanism of action for BCL6 in B cells defined by formation of functionally distinct complexes at enhancers and promoters.* Cell reports, 2013. **4**(3): p. 578-588.
117. Gorbet, M.B. and M.V. Sefton, *Endotoxin: the uninvited guest.* Biomaterials, 2005. **26**(34): p. 6811-6817.
118. Hatzi, K. and A. Melnick, *Breaking bad in the germinal center: how deregulation of BCL6 contributes to lymphomagenesis.* Trends in molecular medicine, 2014. **20**(6): p. 343-352.
119. Basso, K. and R. Dalla-Favera, *Germinal centres and B cell lymphomagenesis.* Nature Reviews Immunology, 2015. **15**(3): p. 172-184.
120. Evan, G.I. and K.H. Vousden, *Proliferation, cell cycle and apoptosis in cancer.* Nature, 2001. **411**(6835): p. 342-348.
121. Minucci, S. and P.G. Pelicci, *Histone deacetylase inhibitors and the promise of epigenetic (and more) treatments for cancer.* Nature Reviews Cancer, 2006. **6**(1): p. 38-51.
122. Raaphorst, F.M., et al., *Coexpression of BMI-1 and EZH2 polycomb group genes in Reed-Sternberg cells of Hodgkin's disease.* The American journal of pathology, 2000. **157**(3): p. 709-715.
123. Velichutina, I., et al., *EZH2-mediated epigenetic silencing in germinal center B cells contributes to proliferation and lymphomagenesis.* Blood, 2010. **116**(24): p. 5247-5255.
124. Caganova, M., et al., *Germinal center dysregulation by histone methyltransferase EZH2 promotes lymphomagenesis.* The Journal of clinical investigation, 2013. **123**(12): p. 5009-5022.

125. Béguelin, W., et al., *EZH2 is required for germinal center formation and somatic EZH2 mutations promote lymphoid transformation.* Cancer cell, 2013. **23**(5): p. 677-692.
126. Su, I.-h., et al., *Ezh2 controls B cell development through histone H3 methylation and Igh rearrangement.* Nature immunology, 2003. **4**(2): p. 124-131.
127. Dobin, A., et al., *STAR: ultrafast universal RNA-seq aligner.* Bioinformatics, 2013. **29**(1): p. 15-21.
128. Liao, Y., G.K. Smyth, and W. Shi, *featureCounts: an efficient general purpose program for assigning sequence reads to genomic features.* Bioinformatics, 2013. **30**(7): p. 923-930.
129. Robinson, M.D., D.J. McCarthy, and G.K. Smyth, *edgeR: a Bioconductor package for differential expression analysis of digital gene expression data.* Bioinformatics, 2010. **26**(1): p. 139-140.
130. Paradis, E., J. Claude, and K. Strimmer, *APE: analyses of phylogenetics and evolution in R language.* Bioinformatics, 2004. **20**(2): p. 289-290.
131. Subramanian, A., et al., *Gene set enrichment analysis: a knowledge-based approach for interpreting genome-wide expression profiles.* Proceedings of the National Academy of Sciences, 2005. **102**(43): p. 15545-15550.
132. Chang, Y., C. Paige, and G. Wu, *Enumeration and characterization of DJH structures in mouse fetal liver.* The EMBO journal, 1992. **11**(5): p. 1891.
133. Cobaleda, C., W. Jochum, and M. Busslinger, *Conversion of mature B cells into T cells by dedifferentiation to uncommitted progenitors.* Nature, 2007. **449**(7161): p. 473-477.
134. Schlissel, M.S., L.M. Corcoran, and D. Baltimore, *Virus-transformed pre-B cells show ordered activation but not inactivation of immunoglobulin gene rearrangement and transcription.* J. Exp. Med, 1991. **173**(3): p. 711-720.
135. Hanna, J., et al., *Direct reprogramming of terminally differentiated mature B lymphocytes to pluripotency.* Cell, 2008. **133**(2): p. 250-264.
136. Koboldt, D.C., et al., *VarScan: variant detection in massively parallel sequencing of individual and pooled samples.* Bioinformatics, 2009. **25**(17): p. 2283-2285.
137. Goodnow, C.C., et al., *Control systems and decision making for antibody production.* Nature immunology, 2010. **11**(8): p. 681-688.
138. Acharya, M., et al., *[alpha] v Integrins combine with LC3 and atg5 to regulate Toll-like receptor signalling in B cells.* Nature communications, 2016. **7**.
139. Tian, Y.F., et al., *Integrin-specific hydrogels as adaptable tumor organoids for malignant B and T cells.* Biomaterials, 2015. **73**: p. 110-119.
140. Metters, A. and J. Hubbell, *Network formation and degradation behavior of hydrogels formed by Michael-type addition reactions.* Biomacromolecules, 2005. **6**(1): p. 290-301.
141. Weinstein, J.S., et al., *TFH cells progressively differentiate to regulate the germinal center response.* Nat Immunol, 2016. **17**(10): p. 1197-205.
142. Ma, C.S., et al., *The origins, function, and regulation of T follicular helper cells.* J Exp Med, 2012. **209**(7): p. 1241-53.
143. Purwada, A., et al., *Ex vivo engineered immune organoids for controlled germinal center reactions.* Biomaterials, 2015. **63**: p. 24-34.
144. Purwada, A. and A. Singh, *Immuno-engineered organoids for regulating the kinetics of B-cell development and antibody production.* Nature protocols, 2017. **12**(1): p. 168-182.
145. Lee, T.T., et al., *Light-triggered in vivo activation of adhesive peptides regulates cell adhesion, inflammation and vascularization of biomaterials.* Nature materials, 2014.
146. Phelps, E.A., et al., *Vasculogenic bio-synthetic hydrogel for enhancement of pancreatic islet engraftment and function in type 1 diabetes.* Biomaterials, 2013. **34**(19): p. 4602-11.
147. Lutolf, M.P., P.M. Gilbert, and H.M. Blau, *Designing materials to direct stem-cell fate.* Nature, 2009. **462**(7272): p. 433-441.
148. Lutolf, M.P., et al., *Synthetic matrix metalloproteinase-sensitive hydrogels for the conduction of tissue regeneration: engineering cell-invasion characteristics.* Proc Natl Acad Sci U S A, 2003. **100**(9): p. 5413-8.
149. Anderson, S.B., et al., *The performance of human mesenchymal stem cells encapsulated in cell-degradable polymer-peptide hydrogels.* Biomaterials, 2011. **32**(14): p. 3564-74.
150. Wang, I.K., S.Y. Lin-Shiau, and J.K. Lin, *Suppression of invasion and MMP-9 expression in NIH 3T3 and v-H-Ras 3T3 fibroblasts by lovastatin through inhibition of ras isoprenylation.* Oncology, 2000. **59**(3): p. 245-54.

151. Melamed, D., et al., *Modulation of matrix metalloproteinase-9 (MMP-9) secretion in B lymphopoiesis.* Int Immunol, 2006. **18**(9): p. 1355-62.
152. Turqueti-Neves, A., et al., *B-cell-intrinsic STAT6 signaling controls germinal center formation.* European journal of immunology, 2014. **44**(7): p. 2130-8.
153. Hathcock, K.S., et al., *Analysis of thymic subpopulations expressing the activation antigen GL7. Expression, genetics, and function.* J Immunol, 1995. **155**(10): p. 4575-81.
154. Han, S., et al., *Neoteny in lymphocytes: Rag1 and Rag2 expression in germinal center B cells.* Science, 1996. **274**(5295): p. 2094-7.
155. Pasare, C. and R. Medzhitov, *Control of B-cell responses by Toll-like receptors.* Nature, 2005. **438**(7066): p. 364-8.
156. Shapiro-Shelef, M., et al., *Blimp-1 is required for the formation of immunoglobulin secreting plasma cells and pre-plasma memory B cells.* Immunity, 2003. **19**(4): p. 607-20.
157. Lagresle, C., et al., *Concurrent engagement of CD40 and the antigen receptor protects naive and memory human B cells from APO-1/Fas-mediated apoptosis.* J Exp Med, 1996. **183**(4): p. 1377-88.
158. Hao, Z., et al., *Fas receptor expression in germinal-center B cells is essential for T and B lymphocyte homeostasis.* Immunity, 2008. **29**(4): p. 615-27.
159. Allen, C.D. and J.G. Cyster, *Follicular dendritic cell networks of primary follicles and germinal centers: phenotype and function.* Seminars in immunology, 2008. **20**(1): p. 14-25.
160. Khalil, A.M., J.C. Cambier, and M.J. Shlomchik, *B cell receptor signal transduction in the GC is short-circuited by high phosphatase activity.* Science, 2012. **336**(6085): p. 1178-81.
161. Danhier, F., A.L. Breton, and V.r. Préat, *RGD-based strategies to target alpha (v) beta (3) integrin in cancer therapy and diagnosis.* Molecular pharmaceutics, 2012. **9**(11): p. 2961-2973.
162. Lucie, S., et al., *Clustering and internalization of integrin αvβ3 with a tetrameric RGD-synthetic peptide.* Molecular therapy, 2009. **17**(5): p. 837-843.
163. Mould, A., et al., *The CS5 peptide is a second site in the IIICS region of fibronectin recognized by the integrin alpha 4 beta 1. Inhibition of alpha 4 beta 1 function by RGD peptide homologues.* Journal of Biological Chemistry, 1991. **266**(6): p. 3579-3585.
164. Purwada, A., et al., *Modular Immune Organoids with Integrin Ligand Specificity Differentially Regulate Ex Vivo B Cell Activation.* ACS Biomaterials Science & Engineering, 2017. **3**(2): p. 214-225.
165. Rathmell, J.C., et al., *CD95 (Fas)-dependent elimination of self-reactive B cells upon interaction with CD4positive T cells.* Nature, 1995. **376**(6536): p. 181.
166. Rothstein, T.L., et al., *Protection against Fas-dependent Th1-mediated apoptosis by antigen receptor engagement in B cells.* Nature, 1995. **374**(6518): p. 163.
167. Strasser, A., et al., *Bcl-2 and Fas/APO-1 regulate distinct pathways to lymphocyte apoptosis.* The EMBO journal, 1995. **14**(24): p. 6136.
168. Memon, S.A., et al., *Bcl-2 blocks glucocorticoid-but not Fas-or activation-induced apoptosis in a T cell hybridoma.* The Journal of Immunology, 1995. **155**(10): p. 4644-4652.
169. Daburon, S., et al., *Functional characterization of a chimeric soluble Fas ligand polymer with in vivo anti-tumor activity.* PloS one, 2013. **8**(1): p. e54000.
170. Schneider, P., et al., *Conversion of membrane-bound Fas (CD95) ligand to its soluble form is associated with downregulation of its proapoptotic activity and loss of liver toxicity.* Journal of Experimental Medicine, 1998. **187**(8): p. 1205-1213.
171. Shih, T.-A.Y., M. Roederer, and M.C. Nussenzweig, *Role of antigen receptor affinity in T cell–independent antibody responses in vivo.* Nature immunology, 2002. **3**(4): p. 399-406.
172. Niu, H., H.Y. Bihui, and R. Dalla-Favera, *Antigen receptor signaling induces MAP kinase-mediated phosphorylation and degradation of the BCL-6 transcription factor.* Genes & development, 1998. **12**(13): p. 1953-1961.
173. Sciammas, R., et al., *An incoherent regulatory network architecture that orchestrates B cell diversification in response to antigen signaling.* Molecular systems biology, 2011. **7**(1): p. 495.
174. Victora, G.D., et al., *Identification of human germinal center light and dark zone cells and their relationship to human B-cell lymphomas.* Blood, 2012. **120**(11): p. 2240-2248.
175. Bannard, O., et al., *Ubiquitin-mediated fluctuations in MHC class II facilitate efficient germinal center B cell responses.* Journal of Experimental Medicine, 2016: p. jem. 20151682.
176. Krzyzak, L., et al., *CD83 modulates B cell activation and germinal center responses.* The Journal of Immunology, 2016. **196**(9): p. 3581-3594.

177. Kurosaki, T. and M. Kurosaki, *Transphosphorylation of Bruton's tyrosine kinase on tyrosine 551 is critical for B cell antigen receptor function.* Journal of Biological Chemistry, 1997. **272**(25): p. 15595-15598.
178. Yamanashi, Y., et al., *Role of the rasGAP-associated docking protein p62 dok in negative regulation of B cell receptor-mediated signaling.* Genes & Development, 2000. **14**(1): p. 11-16.
179. Aiba, Y., et al., *Preferential localization of IgG memory B cells adjacent to contracted germinal centers.* Proceedings of the National Academy of Sciences, 2010. **107**(27): p. 12192-12197.